Australian Government
Geoscience Australia

Solubility of uranium in hydrothermal fluids at 25° to 300°C

Implications for the formation of uranium deposits

Evgeniy N. Bastrakov, Subhash Jaireth and Terrence P. Mernagh

Record
2010/29

GeoCat #
70633

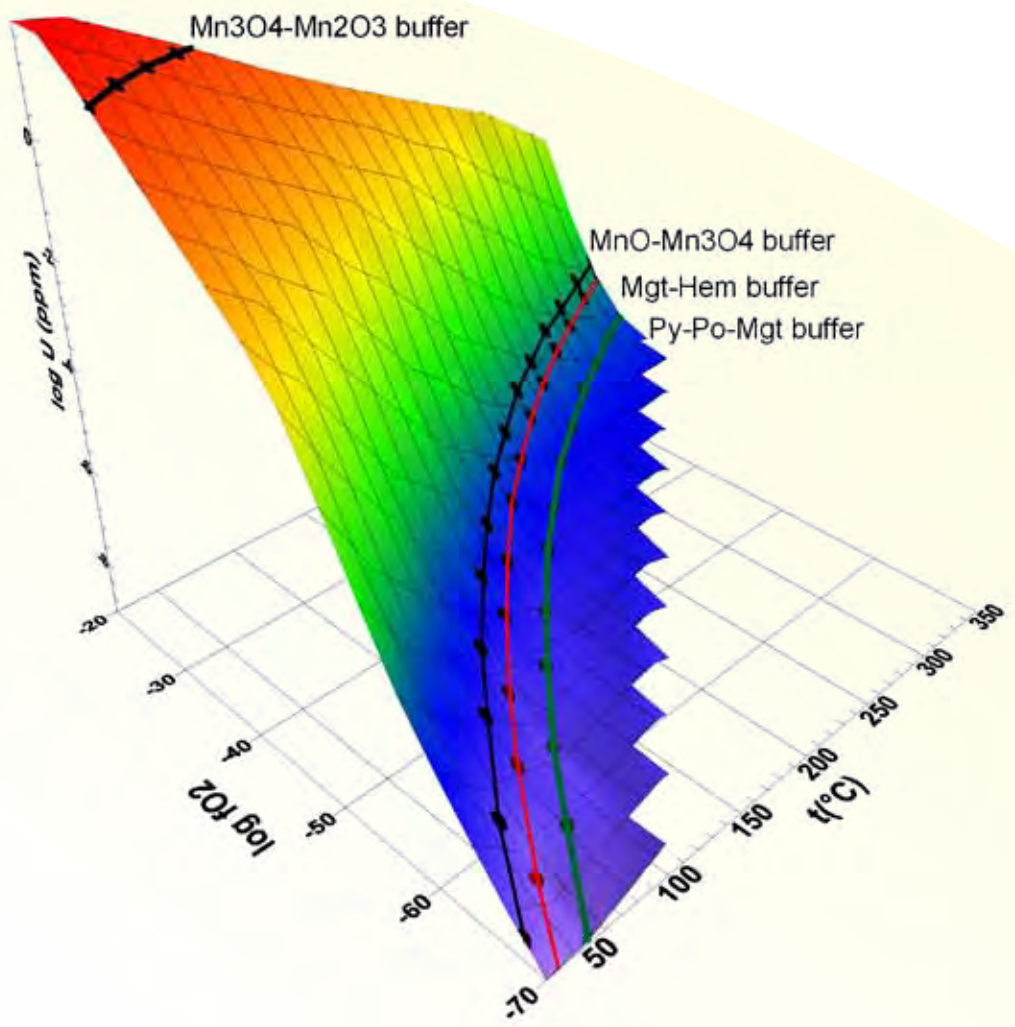

Solubility of uranium in hydrothermal fluids at 25° to 300°C: Implications for the formation of uranium deposits

GEOSCIENCE AUSTRALIA
RECORD 2010/29

by

Evgeniy N. Bastrakov[1*], Subhash Jaireth[1] and Terrence P. Mernagh[1]

Australian Government
Geoscience Australia

[1]Onshore Energy and Minerals Division. Geoscience Australia, GPO Box 378, Canberra, ACT, Australia 2601
[*] Corresponding author: evgeniy.bastrakov@ga.gov.au

Department of Resources, Energy and Tourism
Minister for Resources and Energy: The Hon. Martin Ferguson, AM MP
Secretary: Mr Drew Clarke

Geoscience Australia
Chief Executive Officer: Dr Chris Pigram

ISSN 1448-2177
ISBN 978-1-921781-27-8 Web
ISBN 978-1-921781-28-5 Hardcopy

GeoCat # 70633

Bibliographic reference: Bastrakov, E.N., Jaireth, S., Mernagh, T.P., 2010. Solubility of uranium in hydrothermal fluids at 25° to 300°C: Implications for the formation of uranium deposits. Geoscience Australia Record 2010/29. 91p.

Contents

Executive Summary

The geochemistry of uranium in hydrothermal fluids at temperatures between 25° and 300°C can provide significant geochemical constraints on the transport and deposition of uranium in most types of hydrothermal uranium systems. These constraints can assist in identifying mappable features of fertile uranium systems such as association of uranium with oxidation-reduction fronts, alteration zones and other chemical gradients useful for regional- and deposit-scale targeting. Geochemical modelling, underpinned by thermodynamic data for aqueous uranium species and uranium minerals, enables geologists to understand and predict these constraints in a rigorous quantitative way.

Recent reviews on thermodynamics of uranium species provide a basis for re-evaluation of the behaviour of uranium in hydrothermal fluids. This report presents an up-to-date compilation of thermodynamic data for inorganic uranium species suitable for geochemical equilibrium calculations from low to moderate temperatures (up to 300°C).

The report has several parts. First, we briefly review the fundamental geochemical properties of uranium that are pertinent to its mobilisation and transport by groundwaters and hydrothermal fluids. Second, we review the current state of thermodynamic data of uranium minerals and aqueous species and list a thermodynamic dataset used to calculate speciation and stability of uranium complexes and minerals. Further, using these data, we discuss speciation and solubility of important uranium ore minerals at temperatures ≤ 200°C and 200° to 300°C, respectively, including the analysis of fO_2-pH diagrams. Finally, these data and information are used for geochemical modelling of fluids in sedimentary basins recharged by oxidised meteoric waters.

The presented thermodynamic data for aqueous uranium species are based on the equations-of-state that enable geochemical calculations at elevated temperatures and pressures (the modified Helgeson-Kirkham-Flowers model; the modified Ryzhenko-Bryzgalin equation). The data are freely downloadable from the Geoscience Australia website in a format suitable for modern-day software package HCh, and suitable for a ready conversion to other popular geochemical packages (e.g., Geochemist's Workbench) via an HCh add-on utility, UT2K.

For temperatures ≤ 200°C, we discuss the speciation and solubility of important uranium ore minerals: uranium oxides, coffinite and carnotite. The main factors which control the stability of carnotite are pH and concentrations of potassium, carbonate, and sulphate in the fluids. In specific conditions, mixing of oxidised (carrying uranium) and reduced (carrying vanadium) fluids can be an important process for formation of many calcrete-uranium deposits. Another process that affects these chemical parameters and can result in precipitation of carnotite, is evaporation.

At temperatures 200° to 300°C, solubility of uranium in hydrothermal systems partially buffered by host rock assemblages (dominance of the U (IV) aqueous species) is generally orders of magnitude lower than in highly oxidised near-surficial environments (dominance of the U (VI) aqueous species). In consistency with previous findings published elswhere, uranium transport in hydrothermal systems requires either acidic solutions or very stable complexes of U(IV), properties of which are currently poorly constrained. The present review emphasises the need for experimental data on uranium speciation at temperatures >200°C.

The report presents results of geochemical modelling of fluids in sedimentary basins recharged by oxidised meteoric waters. The modelling results suggest that a fluid-flow regime similar to the regime responsible the formation of red-bed copper deposits, can transport geologically realistic

concentrations of uranium in sediment-hosted stratiform copper and unconformity-related uranium deposits. For a generic mineral system, the calculations show that one of the controlling factors in this fluid-flow regime can be the episodic nature of the fluid-flow, which controls the uranium to base metal ratio of the fluid and the composition of ores formed when this fluid reacts with chemical reductants. A similar model is used to explain the uranium and base metal zoning of mineral deposits in the Westmoreland uranium field.

1. Introduction

Comprehensive reviews of geochemistry of uranium in low to moderate temperatures were done in the late 1970s and early 1980s (Rich et al., 1977; De Voto, 1978; Kimberley, 1979; Langmuir, 1979; Romberger, 1984). These reviews were preceded by papers on theoretical and experimental solubility of uranium oxides, the most notable of which are Rafalsky and Sidorov (1958) and Garrels and Christ (1965). These studies provided a geochemical framework to understand the behaviour of uranium in low-temperature hydrothermal fluids relevant for uranium systems associated with basinal fluid flow (sandstone-hosted uranium, calcrete uranium, oxidation of primary high-temperature uranium ores, etc). In the 1970s thermodynamic data on uranium complexes in fluids at temperatures ≥200-250°C were limited and of questionable quality.

In recent years, with thorough review and compilation of new experimental results (Grenthe et al., 1992; Guillaumont et al., 2003), the development of new correlation algorithms for predicting thermodynamic data (e.g., (Shock et al., 1997)), and the renewed interest in the geochemistry of uranium, new studies and reviews started to be published (e.g., Shock et al., 1997; Murphy and Shock, 1999; Barsukov and Borisov, 2003). These studies now provide a basis for re-evaluation of the behaviour of uranium in hydrothermal fluids.

The geochemistry of uranium in hydrothermal fluids at temperatures between 25° and 300°C can provide significant geochemical constraints on the transport and deposition of uranium in most significant types of hydrothermal uranium systems. The constraints can assist in identifying mappable features of fertile uranium systems such as oxidation-reduction fronts, alteration zones and other chemical gradients useful for regional- and deposit-scale targeting.

The present report provides an up-to-date compilation of thermodynamic data suitable for geochemical equilibrium calculations from low to moderate temperatures (up to 300°C). It also reports a set of diagrams displaying the solubility of uranium minerals (uraninite, coffinite and carnotite) and the stability of uranium and vanadium complexes at temperatures between 25 and 300°C. Some of these results have been summarised by Skirrow et al. (2009), whereas here we present a more comprehensive review. Further, we discuss mass-balance calculations of fluid-rock reactions at temperatures up to 200°C relevant to understanding the behaviour of uranium in unconformity-related uranium and sediment-hosted stratiform copper-uranium deposits.

Chapter 1 reviews basic geochemical information about uranium, its valency state and abundance in major rock types and in primary and accessory minerals. A summary of available data on the leachability of uranium from minerals is also presented.

Chapter 2 reviews the current state of thermodynamic data of uranium minerals and aqueous species and lists the internally consistent thermodynamic dataset used to calculate speciation and stability of uranium complexes and minerals.

Chapter 3 discusses the speciation and solubility of uranium oxides, coffinite and carnotite at temperatures ≤ 200°C. The solubility is represented in the form of $\log fO_2$-pH diagrams relevant for uranium systems associated with basinal fluid flow. The chapter examines the metastability of coffinite and outlines processes which can form coffinite in sandstone-hosted uranium deposits. The speciation of vanadium and solubility and stability of carnotite is important to understand the geochemical conditions of its formation in surface-related-uranium deposits, including “calcrete” types. The stability of carnotite is shown on a set of $\log fO_2$-pH diagrams.

Chapter 4 discusses the speciation and stability of uranium at temperatures between 200° and 300°C, relevant to moderate temperature uranium ore-forming systems such as unconformity-related uranium.

Chapter 5 presents results of geochemical modelling of fluids in sedimentary basins recharged by oxidised meteoric waters. This model has been proposed to explain the formation of red-bed copper deposits, some of which contain uranium-enriched zones. The main aim of the modelling is to test whether a similar fluid-flow regime can transport geologically realistic concentrations of uranium in both unconformity-related and sediment-hosted stratiform copper deposits.

The present review emphasises the need for experimental data on uranium speciation at temperatures >200°C to support numerical modelling beneficial to mineral exploration.

2. Uranium: basic geochemical data

This chapter presents a summary of basic geochemical data on uranium, relevant for determining speciation and solubility of uranium in hydrothermal fluids. More detailed information can be found in reviews by De Voto (1978), Steacy and Kiaman (1978), Smith (1984), and Dahlkamp (1993).

2.1 IONIC SIZE, VALENCE STATE AND AQUEOUS SPECIES

Uranium occurs in four oxidation states out of which only two, tetravalent (U^{+4}), and hexavalent (U^{+6}) uranium are geologically important. The ionic radius of uranium ions depends on the coordination state (Table 2.1). The large size of U^{+4} and U^{+6} in 6 and 8 fold coordination largely determines the geochemical behaviour of uranium in geological systems.

Table 2.1: Ionic size of uranium ions

VALENCE STATE	COORDINATION NUMBER	IONIC RADIUS (Å)
U	4	1.43
U^{+3}	6	1.12
U^{+3}	8	1.16
U^{+4}	6	0.97
U^{+4}	8	1.01
U^{+5}	6	0.90
U^{+6}	4	0.66
U^{+6}	6	0.8
U^{+6}	8	1.0

After Dahlkamp (1993); http://www.webelements.com/uranium/atom_sizes.html.

The high charge and large size of the tetravalent (U^{+4}) ion makes it chemically highly reactive. It forms oxides and silicates and enters into the crystal structure of rock-forming and accessory minerals. Extensive substitution of thorium is due to the similarity in charge and ionic size of Th^{+4} and U^{+4}. Because of charge discrepancy between uranium and major rock-forming cations (+4 compared to +2), little uranium is found in major rock-forming silicates (such as pyroxenes and amphiboles), however limited U^{+4} substitution for Ca^{+2} occurs in common accessory minerals such as apatite, titanite and fluorite (Table 2.2). The similar charge and radius of U^{+4}, and Zr^{+4}, Th^{+4}, and Ce^{+4} allow high uranium concentrations in allanite, monazite, xenotime and zircon. Limited substitution by uranium is also observed in oxides of Mo, W, Nb and Ta. In addition to uranium-bearing rock-forming minerals, accessory minerals can serve as important sources of uranium in rocks that may be leached by fluids.

According to Pearson's (1963) classification of metal ions and ligands into acids (those which accept electrons) and bases (those which donate electrons), U^{+4}, and U^{+6} are hard acids and hence tend to complex more readily with hard bases such as F^-, OH^-, NO_3^-, CO_3^{-2}, HCO_3^-, SO_4^{-2}, HSO_4^-, PO_4^{-3}, HPO_4^{-2}, and $H_2PO_4^-$ (Table 2.3). In highly saline fluids with an excess of chloride ion U also may form chloro complexes. A common association of uranium with manganese, cobalt, arsenic, vanadium, platinum group elements, rhenium and rare earth elements observed in many uranium ore deposits is possibly related to the fact that these elements also behave as hard acids complexing easily with hard bases.

Table 2.2: Uranium content of rock-forming and accessory minerals. Data after De Voto (1978)

MINERAL	COMMON RANGE U (PPM)
ROCK FORMING MINERALS	
Quartz	0.1-10
Feldspar	0.1-10
Muscovite	2-8
Biotite	1-60
Hornblende	0.2-60
Pyroxene	0.01-50
Olivine	~0.05
ACCESSORY MINERALS	
Allanite $(Ca,Ce)_2(Fe^{+2},Fe^{+3})Al_2O.OH[Si_2O_7][SiO_4]$	30-1000
Apatite $Ca_5(PO_4)_3(OH,F,Cl)$	5-100
Epidote $(CaFe^{+3})Al_2O.OH[Si_2O_7][SiO_4]$	20-200
Garnet $Ca_3Al_2Si_3O_{12}$	6-30
Ilmenite FeTiO3	1-50
Magnetite Fe_3O_4	1-30
Monazite $(Ce,La,Th)PO_4$	500-3000
Titanite $CaTi[SiO_4](O,OH,F)$	10-700
Xenotime YPO_4	300-35,000
Zircon $ZrSiO_4$	100-6000

Under relatively reduced conditions, characteristic of most magmatic and metamorphic environments, and in deep basinal fluid settings, ionic complexes of tetravalent uranium (uranous) predominate. In oxidised conditions typical of surficial and shallow ground water conditions, uranium forms a reactive complex ion containing hexavalent uranium called uranyl. This linear polar uranyl ion $(U^{+6}O_2)^{+2}$ readily complexes with anions and anionic complexes to create soluble complexes (Table 2.4).

Uranium is also known to form organic complexes but their role in the formation of uranium deposits is not clear. The close association observed between bitumens and uranium in some basins is generally explained by the mixing of uranium-rich fluids with a relatively mobile organic reductant (Landais, 1993). The suggestion by Capus (1979) (cited in Landais, 1993) of transporting uranium by oil to explain uranium mineralisation in the Lodeve Basin (France) is considered highly unlikely (Landais, 1993), although partial remobilisation of uranium mineralisation by an organic fluid has been observed (Leventhal et al., 1987).

2.2 URANIUM MINERALS

In reducing conditions characteristic of magmatic, metamorphic and deep basinal environments, uranium forms simple and complex oxide minerals (Steacy and Kiaman, 1978; Smith, 1984; Dahlkamp, 1993). The most common uranium ore minerals in these environments are uraninite (UO_2(cr)), pitchblende (roughly UO_2(am)), and coffinite (uranium silicate of variable composition, $U(SiO_4)_{1-x}(OH)_{4x}$ (cr)). In nature, the pure $U^{+4}O_2$ phase does not exist because of self oxidation caused by radioactive decay (Dahlkamp, 1993).

Table 2.3: Classification of metals and ligands in terms of Pearson's (1963) HSAB principle

HARD	BORDERLINE	SOFT
Acids H^+ $Li^+ > Na^+ > K^+ > Rb^+ > Cs^+$ $Be^{+2} > Mg^{+2} > Ca^{+2} > Sr^{+2} > Ba^{+2}$ $Al^{+3} > Ga^{+3}$ $Sc^{+3} > Y^{+3}$; REE^{+3} ($Lu^{+3} > La^{+3}$) $Ce^{+4} > Sn^{+4}$ $Ti^{+4} > Ti^{+3} > Zr^{+4} \sim Hf^{+4}$ $Cr^{+6} > Cr^{+3}$; $Mo^{+6} > Mo^{+5} > Mo^{+4}$; $W^{+6} > W^{+4}$; Nb^{+5}, Ta^{+5}, Re^{+4}>; $Re^{+6} > Re^{+4}$; $V^{+6} > V^{+5} > V^{+4}$ Mn^{+4}; Fe^{+3}; Co^{+3}; $As^{+5} \sim Sb^{+5}$ Th^{+4}; **U^{+6}; U^{+4}** $PGE^{+5} > PGE^{+4}$	**Acids** $Fe^{+2} > Mn^{+2} > Co^{+2} > Ni^{+2} > Cu^{+2}$, Zn^{+2}> , Pb^{+2} , Sn^{+2}, As^{+3} , Sb^{+3} , Bi^{+3}	**Acids** $Au^+ > Ag^+ > Cu^+ > Hg^{+2} > Cd^{+2}$ $Pt^{+2} > Pd^{+2}$ > other PGE^{+2} , $Tl^{+3} > Tl^+$
Bases $F^- > H_2O$, OH^-, O^{-2}; $NH_3 > NO_3^-$; $CO_3^{-2} > HCO_3^{-2} > SO_4^{-2} > HSO_4^{-1}$; $PO_4^{-3} > HPO_4^{-2} > H_2PO_4^-$; Carboxylates (acetate, oxalate, etc) $MoO_4^{-2} > WO_4^{-2}$	**Bases** Cl^-	**Bases** $I^- > Br^-$, CN^-; CO; $S^{-2} > HS^{-1} > H_2S$; Organic phosphines (R_3P), organic thiols (RP); polysulphide, thiosulphate, sulphite HSe^- , Se^{-2}, HTe^- , Te^{-2}; AsS_2^-; SbS_2^-

Note : In the case of hard species, the symbol > "denotes "harder than" and in the case of soft species it denotes "softer than". The symbol "R" denotes an organic carbon chain

Table 2.4: Uranous and uranyl aqueous complexes of uranium compiled from literature (e.g., Barsukov and Borisov, 2003; Guillaumont et al., 2003)

Simple, oxy and hydroxy	U^{+4}, $U(OH)^{+3}$, $U(OH)_2^{+2}$, $U(OH)_3^{+1}$, $U(OH)_4$, $U(OH)_5^{-1}$, $U_2(OH)_5^{+3}$, UO_2^{+1}, UO_2^{+2},$UO_2(OH^)^{+1}$, $UO_2(OH)_2$, $UO_2(OH)_3^-$, $(UO_2)_2(OH)_2^{+2}$, $(UO_2)_3(OH)_5^+$
Carbonate	UO_2CO_3, $UO_2(CO_3)_2^{-2}$, $UO_2(CO_3)_3^{-4}$
Phosphate	$UHPO_4^{+2}$, $U(HPO_4)_2$, $U(HPO_4)_3^{-2}$,$U(HPO_4)_4^{-4}$, $UO_2(HPO_4)$, $UO_2(HPO_4)_2^{-2}$, $UO_2(H_2PO_4)^+$, $UO_2(H_2PO_4)_2$, $UO_2(H_2PO_4)_3^-$
Sulfate	$U(SO_4)_2$, $UO_2(SO_4)$, $UO_2(SO_4)_2^{+2}$, USO_4^{+2}
Fluoride	UF^{+3}, UF_2^{+2}, UF_3^+, UF_4, UF_6^{-2}, UO_2F^+,UO_2F_2, $UO_2F_3^-$, $UO_2F_4^{-2}$
Chloride	UCl_4, UCl_5, UCl_6, UCl^{+3}, UO_2Cl^+

Uranium also forms a large number of minerals containing U^{+6} in the form of the uranyl (UO_2^{+2}) ion. The uranyl minerals have the following general formula:

$A(UO_2)(RO_4).xH_2O$ and $B(UO_2)(RO_4)$ x H_2O,

where A is K or Na; R is V^{+5}, P^{+5}, or As^{+5} and B is Ba, Ca, Cu, Fe^{+2}, Mg or Pb. Economically the most important mineral in this group is carnotite with the formula $K(UO_2)(VO_4).xH_2O$ in which uranium is hexavalent and vanadium is pentavalent. The uranyl ion also commonly forms minerals containing complex ions such as $(MoO_4)^{-2}$, $(SO_4)^{-2}$,$(CO_3)^{-2}$, $(SiO_3)^{-2}$, $(SeO_3)^{-2}$, and $(TeO_3)^{-2}$.

Due to their large size and high charge density, U^{+4} and U^{+6} ions are readily adsorbed by many organic and inorganic substances. The common adsorbents suggested are hydroxides of Fe, Mn,

Ti, Zr, Si, Al, and Mo. Zeolites, clays, and humic material can also adsorb significant amounts of uranium (Rozhkova et al., 1958; Dahlkamp, 1991). The efficiency of adsorption depends on the pH (maximal for pH ranges of 3.5 to 6.0 for humic material and 4.5 to 7.5 for inorganic material). The precise role of adsorption in the transport of uranium and in uranium deposition is not clear but can be very significant in low temperature surficial conditions. For example, at a pH between 4 and 5 a gel of Fe_2O_3 can adsorb up to 30 ppb uranium (Langmuir, 1978). It has been suggested that reduction of uranyl ions to uranium oxide (in low temperature surficial conditions) may involve adsorption of uranyl ions as an intermediat step, followed by reduction of the uranyl ions by mobile reductants. According to (Boyle, 1982) the precipitation of uranium minerals in pyrite-rich portions of the host sands of the Blizzard deposit, Canada, may have been preceded by sorption of uranyl ions on Fe(III) oxyhydroxides during oxidation of pyrite by uranium-bearing fluids.

2.3 LABILE URANIUM IN SOURCE ROCK

The total concentration of uranium in rocks is only a rough guide to their potential as sources of uranium in hydrothermal fluids. If uranium in the source rock is present as uranium oxide it can be easily leached by oxidised fluids. However in rocks lacking uranium oxides, uranium is present in various rock-forming and accessory minerals (Table 2.2). Experimental leaching studies provide some information on the amount of labile uranium present in potential source rocks (Larsen and Gottfried, 1961; Boyle, 1982). Acid-soluble leaching of quartz monzonite (containing 4.6 ppm uranium) showed that more that 60% of the uranium tied up in the rock and accessory minerals can be mobilised (Table 2.5). However, leaching studies of felsic intrusive and volcanic rocks in proximity to the Blizzard deposit by Boyle (1982) demonstrated that less than 3% of uranium was labile.

Table 2.5: Leachable (acid-soluble) uranium content of minerals from the quartz monzonite containing an average of 4.6 ppm uranium (Larsen and Gottfried, 1961)

MINERAL	ABUNDANCE (WT%)	URANIUM (ORIGINAL, PPM)	URANIUM (INSOLUBLE, PPM)	PERCENT DISSOLVED (SAMPLE)	PERCENT DISSOLVED (URANIUM)
Quartz	34	5.6	2.0	< 3	64
Orthoclase	36	2.2	0.38	9	84
Plagioclase	26	1.5	0.47	3	69
Biotite	2	13	1.9	66	85
Hornblende	0.5	60	13	47	78
Allanite	0.005	540	100	90	81

3. Thermodynamic dataset of uranium species

3.1 REVIEW OF AVAILABLE DATASETS FOR URANIUM SPECIES

Major datasets of the thermodynamic properties of aqueous, gaseous, and solid uranium species are available in publications by the international Nuclear Energy Agency, NEA (Grenthe et al., 1992; Guillaumont et al., 2003). The Thermochemical Database Project by the NEA provides a comprehensive, internally consistent, internationally recognised and quality-assured chemical thermodynamic database of selected chemical elements, including radionuclides The uranium data of Guillaumont et al. (2003) or at least the initial compilation by (Grenthe et al., 1992) are currently the core components of the available geochemical databases, including databases for Chess (Common Thermodynamic Database Project (van der Lee and Lomenech, 2003)) and Geochemist's Workbench (thermo.com.v8.r6+.dat file, Bethke (2007)). The latest compilations by the NEA (Guillaumont et al., 2003; datafiles available from the NEA website) comprise stability data for 86 aqueous uranium ions and complexes at 25°C.

Unfortunately, the NEA database provides temperature dependencies only for a limited number of uranium species, fitted to a simple polynomial with restricted predictive capabilities in terms of temperature and pressure relevant to many hydrothermal uranium systems (see Table 3.1 for details; (up to 100°C, at saturated vapour pressures, Psat). This major deficiency stems largely from the limited number of high temperature hydrothermal experiments. As a result, the prediction of uranium solubility and speciation at elevated temperature and pressure still heavily relies on theoretical estimation and extrapolations.

Shock et al. (1997) used available experimental data combined with empirical correlation algorithms to provide estimates of parameters for the modified Helgeson-Kirkham-Flowers (MHKF) equation of state for aqueous uranium species in the U–O–H system. They compiled the initial dataset for uranium ions and hydroxo-complexes suitable for high-temperature calculations. Based on these estimates, Shock et al. (1997) and Murphy and Shock (1999) predicted that U(IV) and U(VI) species predominate in aqueous solution in the U–O–H system over the temperature range of 25° to 350°C. Increasing temperature stabilizes U (VI) and U (III) species relative to U (IV) species, but U (IV) species dominate at oxidation states consistent with mineral-buffer assemblages (with fO_2 values equal to or below that of hematite-magnetite) and near-neutral pH. At low pH, U(VI) is stabilized relative to U (IV). Shock et al. (1997) concluded that uranium transport in hydrothermal systems requires either acidic solutions or potent complexes of U(IV).

Langmuir (2001) pointed out that Shock et al. (1997) reproduced errors introduced by Grenthe et al. (1992) by grossly overestimating the stability of the complexes $UO_2(OH)_2^{\ 0}$, $U(OH)_4^0$, and $U(OH)_5^-$ (those correspond to $UO_3^{\ 0}$ (aq), $UO_2^{\ 0}$ (aq), and HUO_3^- species of Shock et al. (1997), Table 3.1). These errors were acknowledged by Grenthe et al. (1995), and were admitted by the authors in their appendix. Based on this fact Langmuir (2001) concluded that phase diagrams and discussion provided by Shock et al. (1997) for these species are of questionable value.

Following prediction algorithms developed by Shock and Helgeson (1988), Shock et al. (1989), and Sverjensky et al. (1997), Thoenen and Kulik (2003) provided a set of MHKF parameters for numerous aqueous uranium complexes included in the dataset for the GEM-Selektor (V.2-PSI) geochemical modelling code (Nagra/PSI TDB 01/01). The authors have not provided comparisons with the temperature dependencies of uranium species stabilities provided by the NEA (or with any experimental results). However, the comparison of these data with data from the NEA shows dramatic differences in the predicted stabilities of uranium complexes (Figure 3.1; stability of UCl^{+3} and UO_2CO_3 (aq)). In a note to their report, Thoenen and Kulik (2003) stressed that their

dataset contains numerous thermodynamic data that were taken from the literature without being critically reviewed. Thus we preferred to omit their dataset from our compilation.

One of the most extensive datasets for aqueous uranium species suitable for calculations of geochemical equilibria within the range of 25° to 150°C was published by Barsukov and Borisov (2003). The data came from miscellaneous sources, including the original dataset of Shock et al. (1997). Barsukov and Borisov (2003) did not provide discussion of self-consistency of the compiled data; however, their compilation included a number of species with data at elevated temperatures not available elsewhere (some of them are re-used in the present compilation, Table 3.1). Barsukov and Borisov (2003) did not supply equations-of-state and parameters to calculate thermodynamic properties of uranium species at elevated temperatures; instead, they tabulated apparent free energies of their formation between 25° to 150°C at 25° increments.

Bearing in mind the consistency limitations, the speciation model of Barsukov and Borisov (2003) provides a good starting point for refining thermodynamic properties of uranium species for which high-temperature predictions are possible.

3.2 SPECIATION MODEL FOR CALCULATIONS OF HYDROTHERMAL EQUILIBRIA

To compile our dataset of aqueous uranium species (Table 3.1), we used the following approach

1. To facilitate calculations of hydrothermal equilibria et elevated (>25°C) temperatures, we considered only species with published temperature dependencies of their stabilities (Table 3.1).
2. Whenever available, we used species with MHKF parameters and low-temperature stabilities consistent with recommendations by the NEA. These species include those provided by Shock et al. (1997), with the exclusion of UO_3^0 (aq), UO_2^0 (aq), and HUO_3^- (written as $UO_2(OH)_2^0$, $U(OH)_4^0$, and $U(OH)_5^-$ in conventional notation; see the discussion above):

   – The stabilities of UO_3^0 (aq) and UO_2^0 (aq) at 25°C were adjusted to account for values recommended by the NEA (ΔG^0_{298} values).

   – HUO_3^- (or, conventionally, $U(OH)_5^-$) is excluded from dataset as it is not recommended by the NEA.
3. Whenever there are temperature dependences for other uranium complexes provided by the NEA (Grenthe et al., 1992; Guillaumont et al., 2003), they were recast in terms of the modified Ryzhenko-Bryzgalin equation (thereafter referred to as MRB; see below).
4. Whenever there were temperature dependences for additional uranium complexes provided by sources other than the NEA (e.g., Barsukov and Borisov, 2003 or Plyasunov and Grenthe, 1994), they were recast in therms of the MRB equation.

The final dataset, still largely based on the NEA data, comprised 64 aqueous uranium species. Data based on (1) to (3) (and those of Plyasunov and Grenthe, 1994) are internally consistent at 25°C.

Table 3.1: Aqueous uranium species used in calculations. For hydroxide complexes, conventional hydroxide complex representation is shown in the second column.

SPECIES		VALENCY	MODEL	REFERENCE
U^{+3}		III	MHKF	Shock,97a
UOH^{+2}		III	MHKF	Shock,97b
UO^{+}	$U(OH)_2^{+}$	III	MHKF	Shock,97b
HUO_2 (aq)	$U(OH)_3$ (aq)	III	MHKF	Shock,97b
UO_2^{-}	$U(OH)_4^{-}$	III	MHKF	Shock,97b
U^{+4}		IV	MHKF	Shock,97a
UOH^{+3}		IV	MHKF	Shock,97b
UO^{+2}	$U(OH)_2^{+2}$	IV	MHKF	Shock,97b
HUO_2^{+}	$U(OH)_3^{+}$	IV	MHKF	Shock,97b
UO_2 (aq)	$U(OH)_4$ (aq)	IV	MHKF	NEA; Shock,97b; *
HUO_3^{-}	$U(OH)_5^{-}$	IV	MHKF	Shock,97b; †
UF^{+3}		IV	MRB	NEA; *
UF_2^{+2}		IV	MRB	NEA; *
UF_3^{+}		IV	MRB	NEA; *
UF_4		IV	MRB	NEA; *
UF_5^{-}		IV	MRB	BB2003
UF_6^{-2}		IV	MRB	BB2003
UCl^{+3}		IV	MHKF	NEA; *
UCl_2^{+2}		IV	MHKF	BB2003; †
$UHCO_3^{+3}$		IV	MHKF	BB2003; *
$U(HCO_3)_2^{+2}$		IV	MHKF	BB2003; *
$U(CO_3)_5^{-6}$		IV	MHKF	NEA; *
$UHPO_4^{+2}$		IV	MHKF	BB2003; *
$U(HPO_4)_2$		IV	MHKF	BB2003; *
$U(HPO_4)_3^{-2}$		IV	MHKF	BB2003; *
$U(HPO_4)_4^{-4}$		IV	MHKF	BB2003; *
USO_4^{+2}		IV	MHKF	NEA; *
$U(SO_4)_2$ (aq)		IV	MHKF	NEA; *
$UO2^{+}$		V	MHKF	Shock,97a
UO_2OH (aq)		V	MHKF	Shock,97b
UO_3^{-}	$UO_2(OH)_2^{-}$	V	MHKF	Shock,97b
UO_2Cl (aq)		V	MHKF	BB2003; *
$UO_2Cl_2^{-}$		V	MHKF	BB2003; *
UO_2HCO_3		V	MHKF	BB2003; *
$UO_2(HCO_3)_2^{-}$		V	MHKF	BB2003; *
UO_2^{+2}		VI	MHKF	Shock,97a
UO_2OH^{+}		VI	MHKF	Shock,97b
UO_3 (aq)	$UO_2(OH)_2$ (aq)	VI	MHKF	NEA; Shock,97b; *
HUO_4^{-}	$UO_2(OH)_3^{-}$	VI	MHKF	Shock,97b
UO_4^{-2}	$UO_2(OH)_4^{-2}$	VI	MHKF	Shock,97b
$(UO_2)_2OH^{+3}$		VI	MRB	PG1994; * †
$(UO_2)_2(OH)_2^{+2}$		VI	MRB	PG1994; * †
$(UO_2)_3(OH)_4^{+2}$		VI	MRB	PG1994; * †
$(UO_2)3(OH)_5^{+}$		VI	MRB	PG1994; *
$(UO_2)3(OH)_7^{-}$		VI	MRB	PG1994; *
$(UO_2)4(OH)_7^{+}$		VI	MRB	PG1994; *
UO_2F^{+}		VI	MRB	NEA; *
UO_2F_2		VI	MRB	NEA; *

$UO_2F_3^-$		VI	MRB	NEA; *
$UO_2F_4^{-2}$		VI	MRB	NEA; *
UO+Cl+		VI	MRB	NEA; *
UO_2Cl_2		VI	MRB	NEA; *
UO_2CO_3		VI	MRB	NEA; *
$UO_2(CO_3)_2^{-2}$		VI	MRB	NEA; *
$UO_2(CO_3)_3^{-4}$		VI	MRB	NEA; *
$(UO_2)_3(CO_3)_6^{-6}$		VI	MRB	NEA; *
$UO_2H_2PO_4^+$		VI	MRB	BB2003; *
$UO_2(H_2PO_4)_2$		VI	MRB	BB2003; *
$UO_2(H_2PO_4)_3^-$		VI	MRB	BB2003; *
UO_2HPO_4		VI	MRB	BB2003; *
$UO_2(HPO_4)_2^{-2}$		VI	MRB	BB2003; *
UO_2SO_4		VI	MRB	NEA; *
$UO_2(SO_4)_2^{-2}$		VI	MRB	NEA; *

Models: MHKF – modified Helgeson-Kirkham-Flowers (Helgeson, 1981); MRB–modified Rhyzhenko-Bryzgalin model (Borisov, 1992). References: BB2003 – Barsukov and Borisov, 2003; NEA – Guillaumont et al., 2003; PG1994 – Plyasunov and Grenthe, 1994; SSB97 – Shock et al., 1997; SSWS97 – (Shock et al., 1997); * Data re-fitted in the present study; †species excluded from high-temperature calculations (~300°C).

3.3 RECASTING OF AVAILABLE DATA IN FORMATS SUITABLE FOR CALCULATIONS AT HIGH TEMPERATURES AND PRESSURES

Neither data provided by the NEA (Grenthe et al., 1992; Guillaumont et al., 2003) nor by Barsukov and Borisov (2003) can be readily incorporated in the modelling software employed in the present study (HCh, Shvarov, 1999; Shvarov and Bastrakov, 1999); Geochemist's Workbench, Bethke, 2007). Moreover, even the original data by the NEA cannot be extrapolated to high temperatures or used to calculate equilibria at elevated pressures. Thus, these data were recast in terms of the modified Rhyzhenko-Bryzgalin equation (Borisov and Shvarov, 1992; Shvarov and Bastrakov, 1999), one of the data formats implemented in the HCh software. This two-parameter equation provides a simple but efficient tool for interpolation and extrapolation of stability constants and free energies of formation of aqueous complexes, arguably up to 300°C (Borisov and Shvarov, 1992). According to this model, apparent Gibbs free energies of aqueous complexes, *g(T,P)*, are calculated from their dissociation constants (more precisely, $pK_{diss}(T,P) = -\log K_{diss}(T,P)$ values) as follows:

$$\Delta g(T,P) = \sum n_i \cdot \Delta g_i(T,P) - R \cdot T \cdot \ln(10) \cdot pK_{diss}(T,P),$$

where $\Delta g_i(T,P)$ are apparent Gibbs free energies of constituent ions (including H_2O, H^+, and OH^-), and n_i are stoichiometric coefficients. The temperature and pressure dependences of $pK_{diss}(T,P)$ values are represented by the equation

$$pK_{diss}(T,P) = \frac{T_r}{T} \cdot pK_{diss}(T_r,P_r) + B(T,P) \cdot (zz/a)_{eff},$$

where $(zz/a)_{eff}$ is the effective property of the complex which depends on temperature:

$$(zz/a)_{eff} = A + \frac{B}{T} \quad .$$

The parameter B(T,P) does not depend on the complex type and is computed from the dissociation constant of water from Marshall and Franck (1981). It is assumed that for H_2O $(zz/a)_{eff} = 1.0107$

(Borisov and Shvarov, 1992). Complex-specific A and B parameters can be fitted based on experimental data or known temperature dependencies.

To complete the recasting task we used the UT-RYZ utility included in the HCh package.

3.3.1 Recasting of NEA data in terms of the MRB format

The NEA databank provides data for 86 reactions involving aqueous uranium species. From these, the temperature dependencies of their values are reported only for 31 reactions, for which the databank tabulates log K_r, ΔG_r, ΔH_r, and ΔS_r values at 298.15K. Accordingly, the log K_r(T) values can be calculated according to the Vant Hoff equation recast in terms of ΔH_r, and ΔS_r:

$$\ln K_r = -\Delta H_r^0/(R*T) + \Delta S_r^0/R),$$

where K_r is the equilibrium constant at absolute temperature T, ΔH_r^0 is the standard enthalpy change, ΔS_r^0 is the standard entropy change, and R is the gas constant.

The appropriate digital data were imported directly from a NEA flat-text reaction datafile.

The log K_r values calculated for the temperature array of 25, 50, 75, and 100°C were fitted to the MRB equation by solving for its A(zz/a) parameter. For each complex, we adopted the pK(298) value recommended by the NEA (Guillaumont et al., 2003) and assumed B(zz/a) equal to zero.

3.3.2 Recasting of Barsukov and Borisov (2003) data in terms of the MRB format

The apparent Gibbs free energies of aqueous uranium complexes tabulated by Barsukov and Borisov (2003) were used to calculate free energies of their complete dissociation and the appropriate pK_{diss} vaues. The latter, tabulated for the range of 25° to 150°C in 25° increments, were fitted to the MRB equation by solving for its A parameter assuming the B(zz/a) parameter equal to zero and fixing the pK(298) value.

3.3.3 Recasting of Plyasunov and Grenthe (1994) data in terms of the MRB format

Plyasunov and Grenthe (1994) provided temperature dependencies of stability constants for the formation of polynuclear uranium complexes (e.g., $(UO_2)_2OH^{+3}$;Table 3.1) in terms of the conventional Rhyzhenko-Bryzgalin equation. Once more, their data were refitted with the MRB equation with trivial differences compared to the original values by Plyasunov and Grenthe (1994).

3.3.4 Overview of the temperature dependencies

Figure 3.1 summarises the quality of our fits versus the data provided by the NEA.

Some of the aqueous species listed in Table 3.1 were excluded from calculations above 200°C. The reasons are specified in Chapters 4 to 5, and include overestimation of stabilities of less-reliable complexes (other than NEA-derived, see Table 3.1).

3.3.5 Uranium minerals used in calculations

Based on the discussion provided in Chapter 2, Table 3.2 summarises minerals considered in our calculations (Table 3.2):

Table 3.2: Uranium solid phases used in calculations.

SPECIES	FORMULA	REFERENCE	COMMENT
Uranium	U	SBGB99	
Uraninite	UO_2	NEA	
UO_3 (cr)	UO_3	SBGB99	
U_3O_8 (cr)	U_3O_8	SBGB99	
U_4O_9 (cr)	U_4O_9	SBGB99	
Schoepite	$UO_2(OH)_2*H_2O$	L1978	†
Metaschoepite	$UO_2(OH)_2*H_2O$	GL2008	
K-autinite	$K_2(UO_2)_2(PO_4)_2$	L1978	†
Autinite	$Ca(UO_2)_2(PO_4)_2$	L1978	†
Carnotite	$K_2(UO_2)_2(VO_4)_2$	L1978	†
Tyuyamunite	$Ca(UO_2)_2(VO_4)_2$	L1978	†
Rutherfordine	UO_2CO_3(cr)	H1982 *	
Coffinite	$USiO_4$	R1995 *	

References: NEA – Guillaumont et al. (2003); SBGB99 – Shvarov et al. (1999); L1978 – Langmuir (1978); GL2008 – Gorman-Lewis et al. (2008); H1982 – Hemingway (1982); R1995 – Robie and Hemingway (1995); * This study. † Data for 25°C only.

Only uranium oxides, rutherfordine and coffinite were used in high temperature calculations (Chapters 3 to 5).

From the set of listed minerals, missing thermodynamic properties of rutherfordine and coffinite were estimated as follows: heat capacity of rutherfordine was taken from Hemingway (1982), and combined with free energy of formation quoted by the NEA; heat capacity of coffinite was estimated assuming ΔCp_r of the exchange reactio $ZrSiO_4 + UO_2 = USiO_4 + ZrO_2$ equal to zero using heat capacities of the reactants from Robie and Hemingway (1995).

The compiled dataset for the uranium species is available as electronic attachments to the present report available from the Geoscience Australia web site.

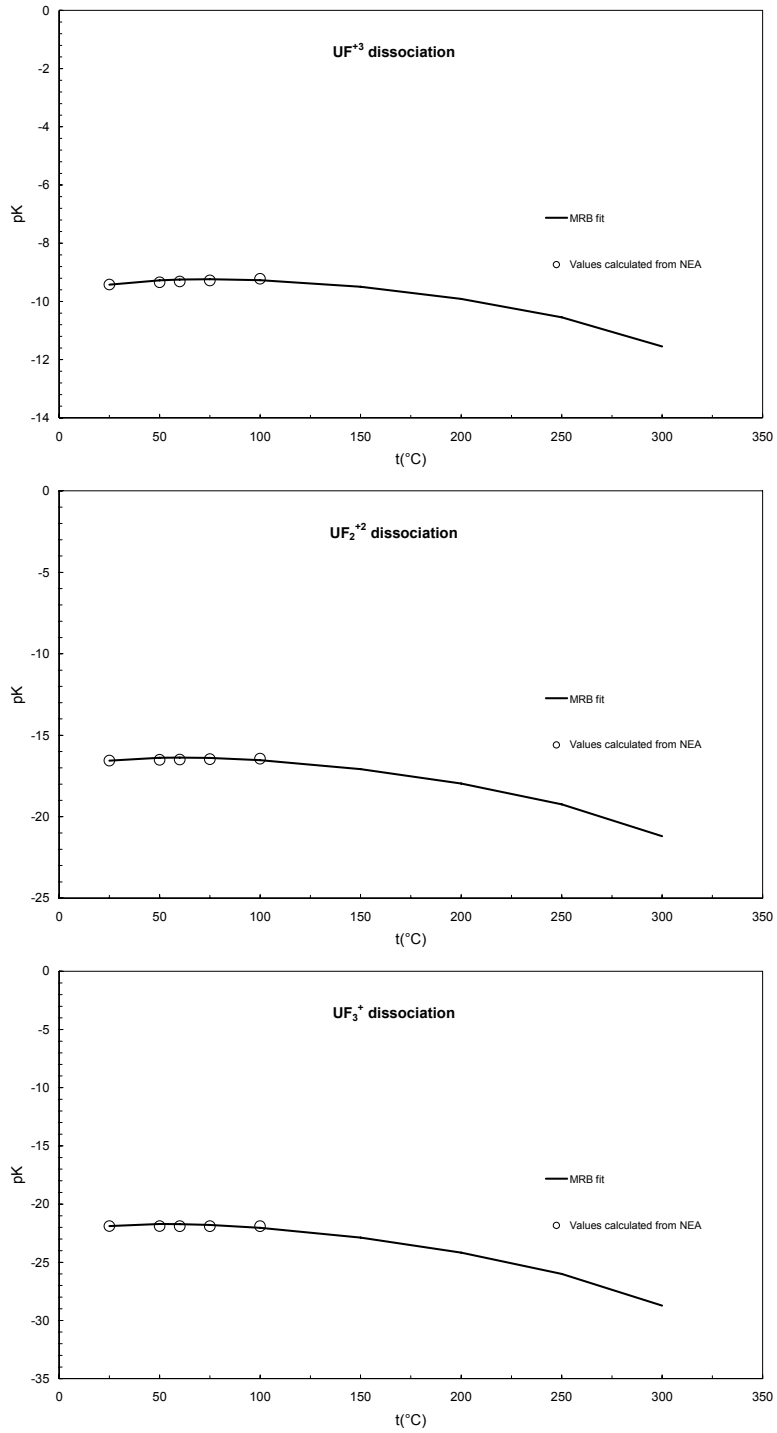

Figure 3.1: *Temperature dependencies of pK values (–log K values) of complete dissociation of aqueous uranium complexes fitted to the modified Ryzhenko-Bryzgalin equation based on the NEA data.*

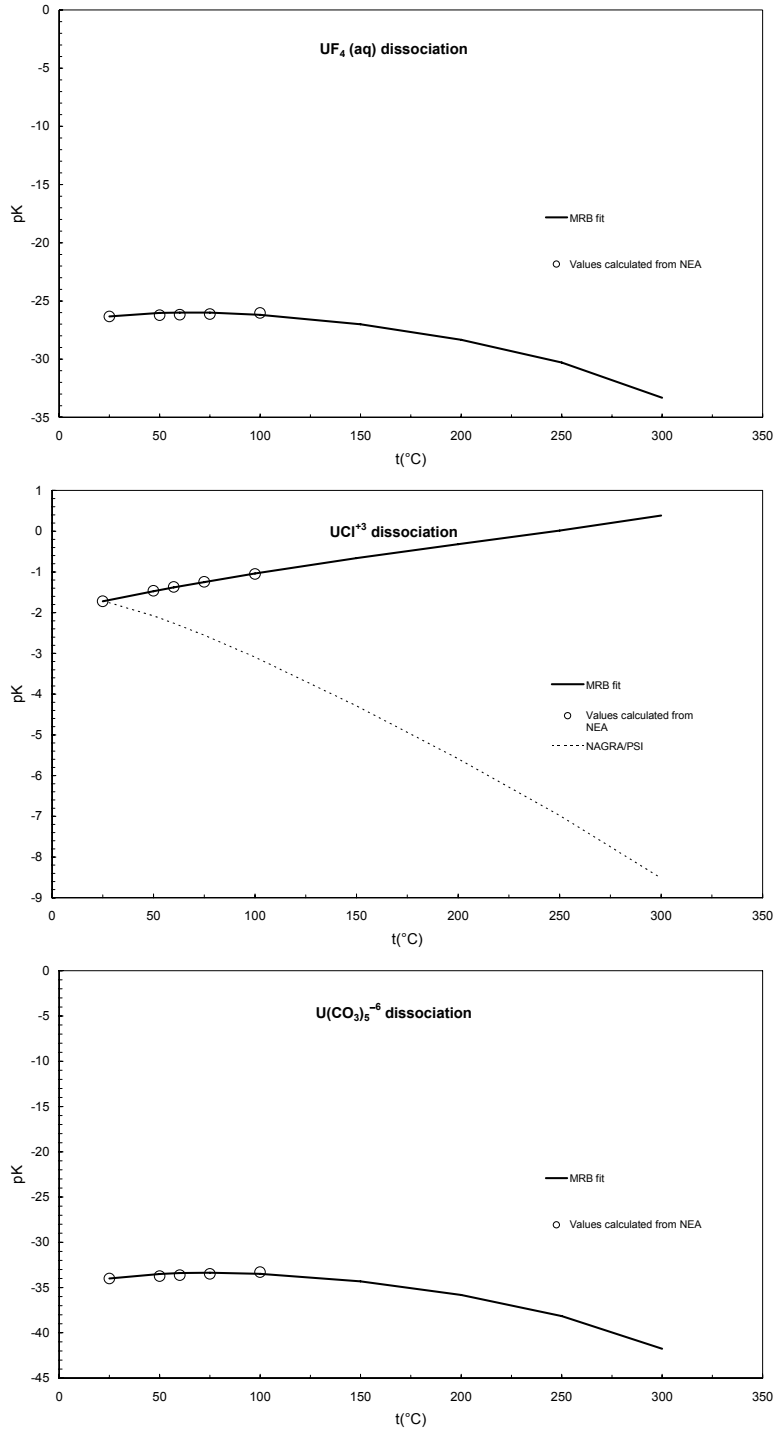

Figure 3.1 (continued): *Temperature dependencies of pK values (–log K values) of complete dissociation of aqueous uranium complexes fitted to the modified Ryzhenko-Bryzgalin equation based on the NEA data.*

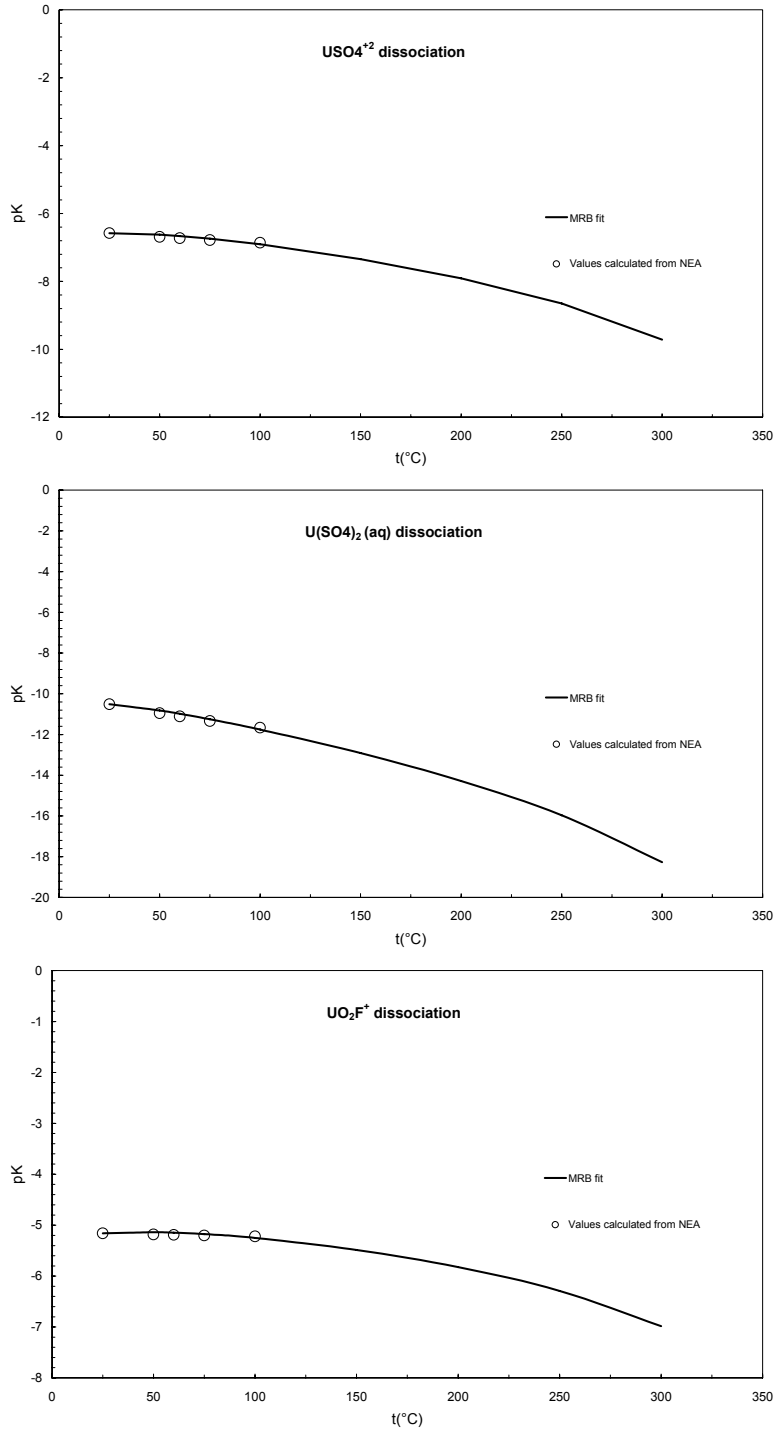

Figure 3.1 (continued): *Temperature dependencies of pK values (–log K values) of complete dissociation of aqueous uranium complexes fitted to the modified Ryzhenko-Bryzgalin equation based on the NEA data.*

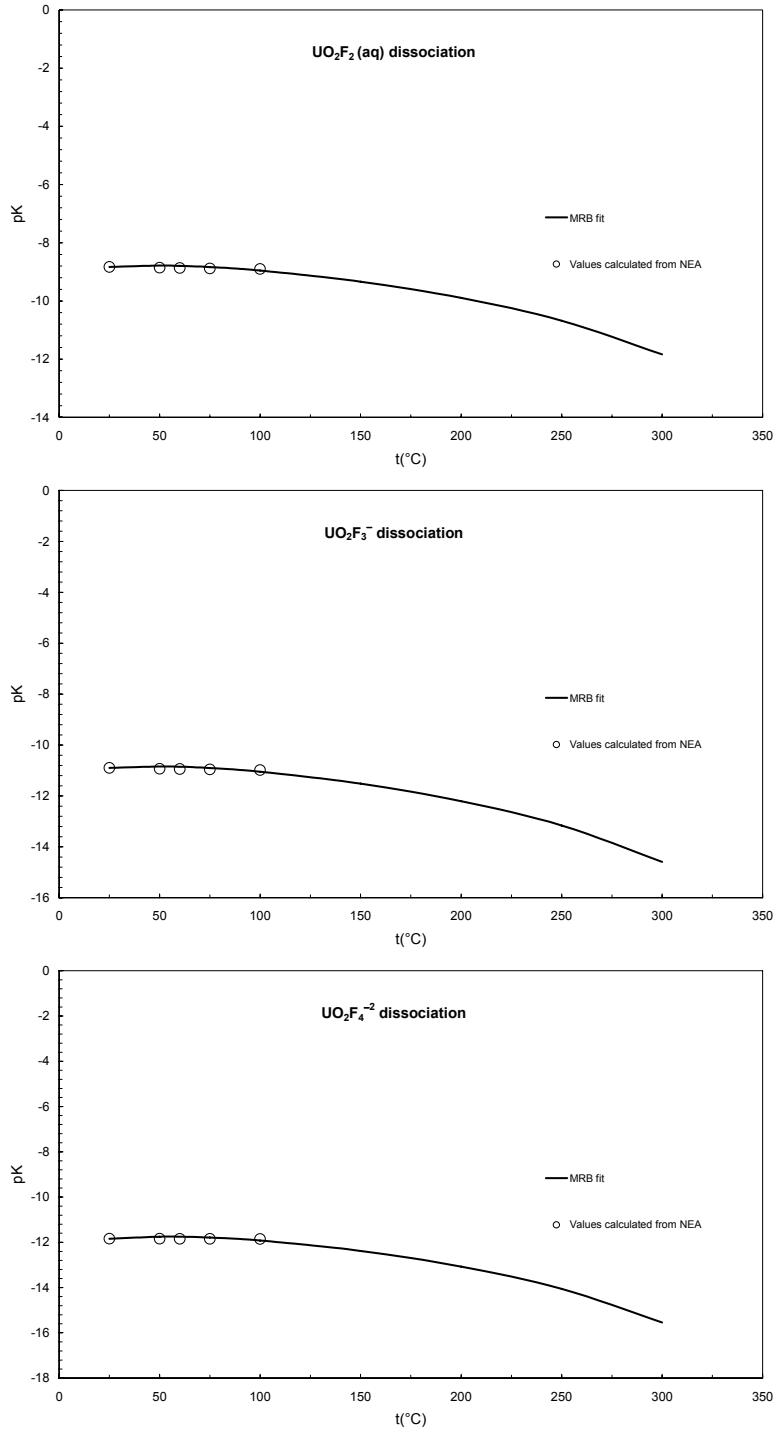

Figure 3.1 (continued): *Temperature dependencies of pK values (–log K values) of complete dissociation of aqueous uranium complexes fitted to the modified Ryzhenko-Bryzgalin equation based on the NEA data.*

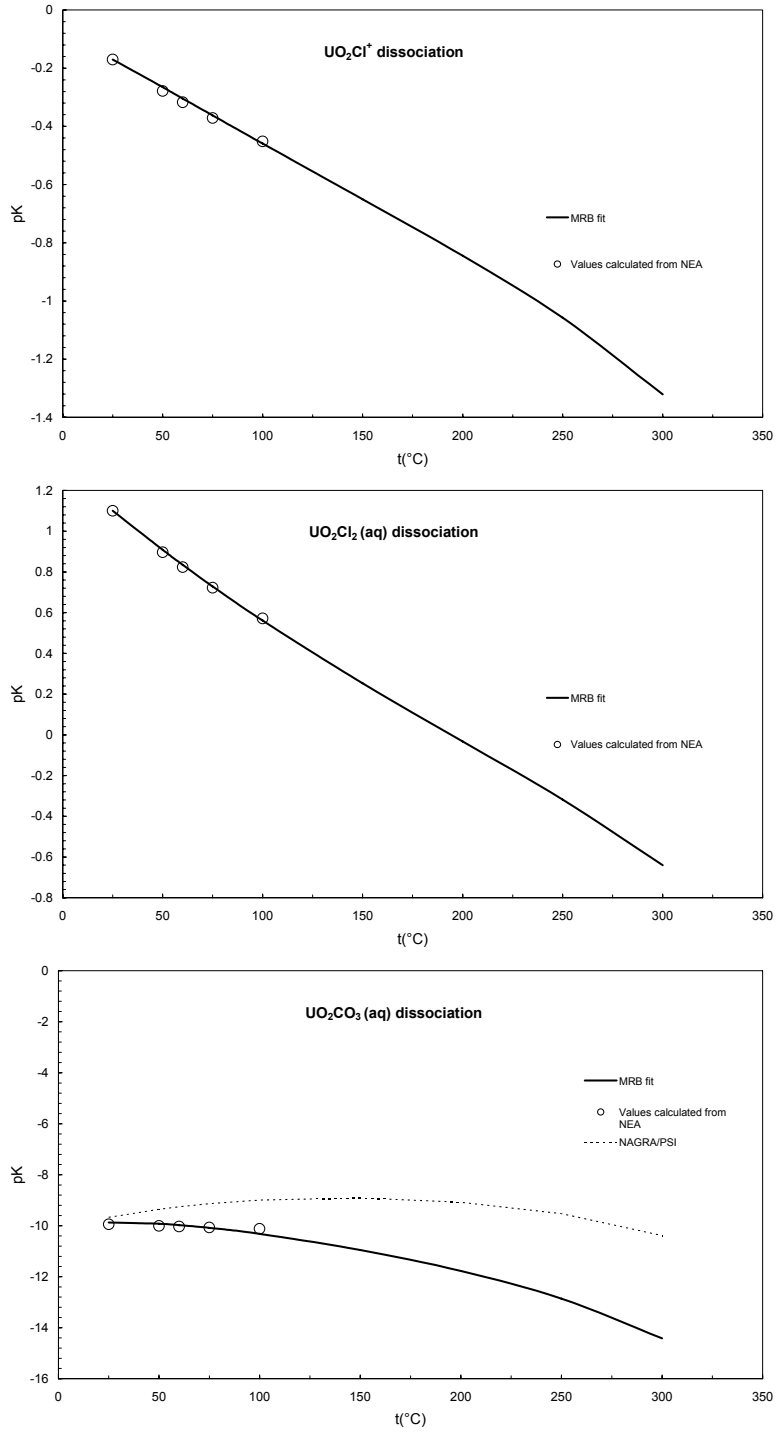

Figure 3.1 (continued): *Temperature dependencies of pK values (–log K values) of complete dissociation of aqueous uranium complexes fitted to the modified Ryzhenko-Bryzgalin equation based on the NEA data.*

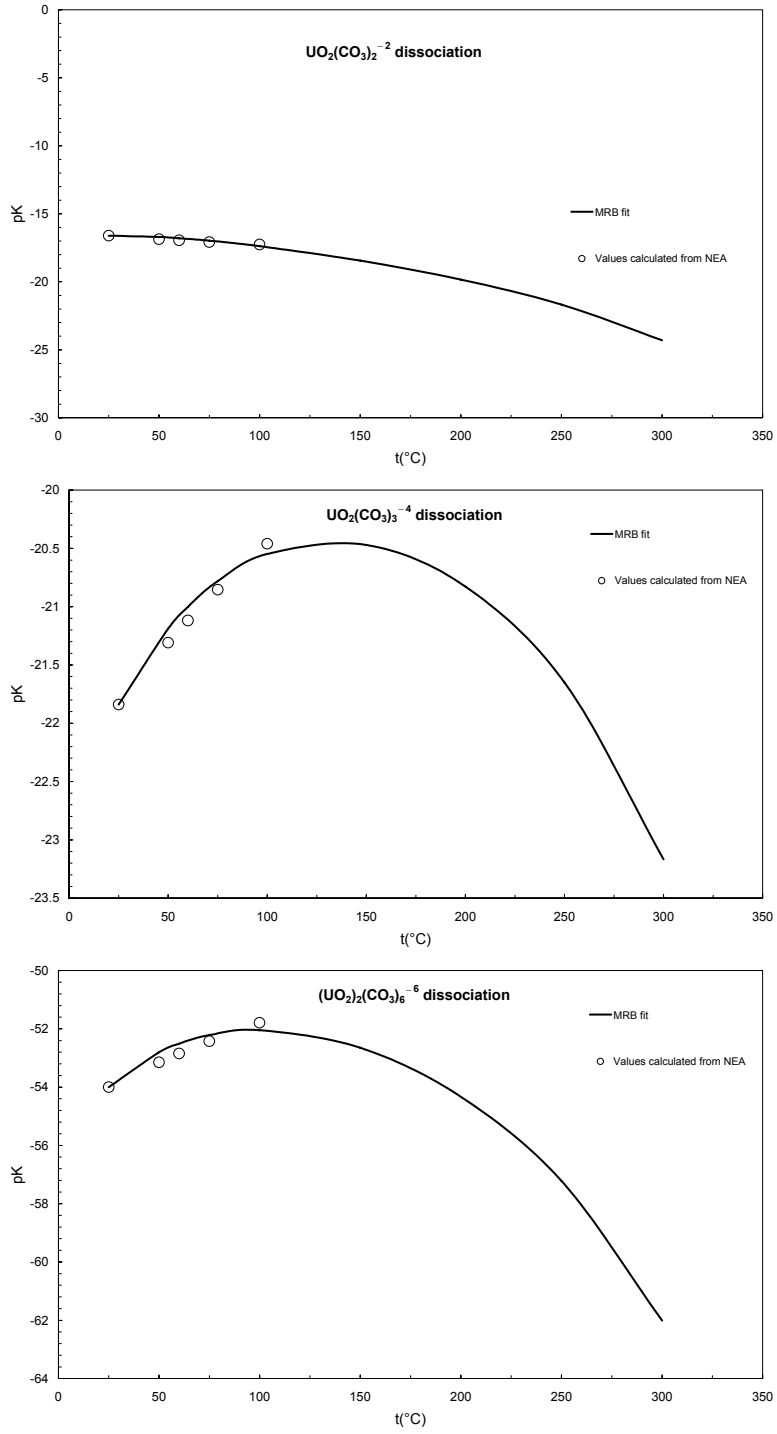

Figure 3.1 (continued): *Temperature dependencies of pK values (–log K values) of complete dissociation of aqueous uranium complexes fitted to the modified Ryzhenko-Bryzgalin equation based on the NEA data.*

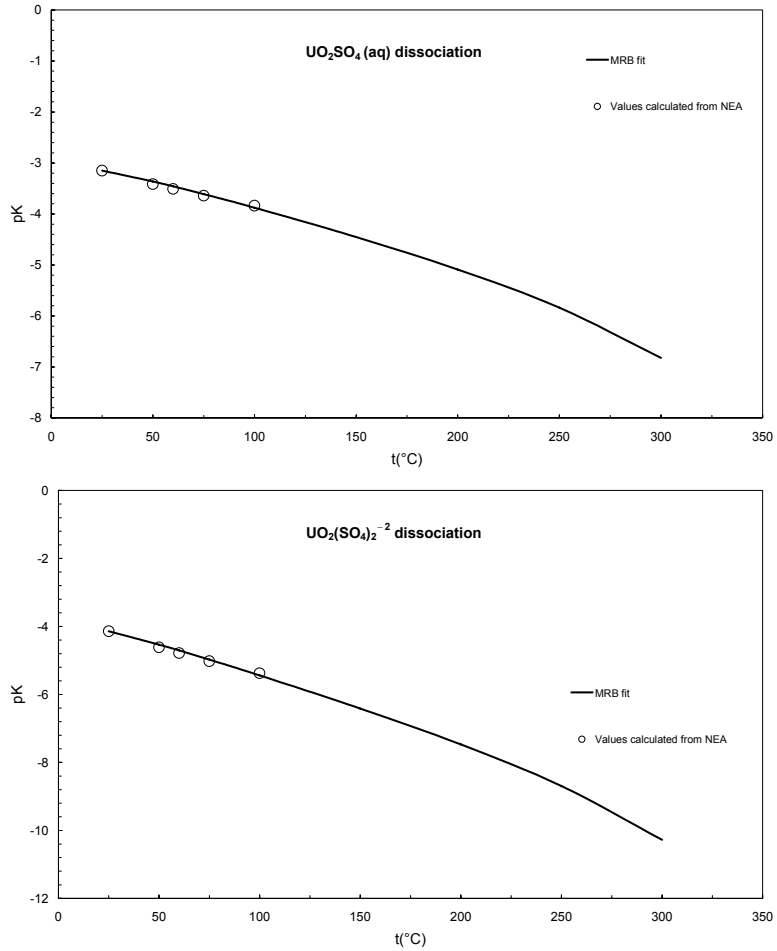

Figure 3.1 (continued): *Temperature dependencies of pK values (–log K values) of complete dissociation of aqueous uranium complexes fitted to the modified Ryzhenko-Bryzgalin equation based on the NEA data.*

4. Speciation and solubility of uranium at low to moderate temperatures (≤ 200°C)

In low-temperature surficial and basin fluid flow systems, the behaviour of uranium is determined predominantly by the oxidation state of the system. This chapter summarises the speciation and solubility of uranium at temperatures ≤ 200°C. The first section presents a series of logfO_2-pH diagrams at low to moderate temperatures and the second section discusses the solubility of uranium in fluids with their pH buffered by mineral assemblages.

4.1 SPECIATION AND SOLUBILITY OF URANIUM AT TEMPERATURES BETWEEN 25° AND 50°C

The speciation of uranium in fluids undersaturated with uranium minerals and a total salinity of ~5000 ppm is shown in Figs. 4.1a (at 25°C) and 4.1b (at 50°C). This fluid is more saline than average surface and rain water but is very similar to the shallow groundwaters sampled in the aquifers at the Honeymoon uranium deposit in South Australia (Southern Cross Resources, 2000). The calculations show that in reduced conditions (logfO_2 < −65) uranous complexes are stable, replaced by uranyl complexes in oxidising conditions (logfO_2 > −65). Under these conditions fluoro complexes of U^{+4} are confined to very acidic pHs (<3 to 4).

In oxidising conditions, the type of dominant uranyl complex depends on the pH. Under the conditions specified, uranyl sulphate complexes dominate under acidic conditions and are replaced by phosphate, carbonate and hydroxy with increasing pH. In general at a given pH, the concentration of ligands determines the type of dominant uranium complex. For instance, uranyl phosphate complexes may be more stable than the uranyl carbonate complexes at intermediate pH, but if the concentration of carbonate ($\sum CO_3^{-2}$) is high, the uranyl carbonate complexes may become dominant. The concentration of chloride in the fluid is too low to stabilise chloro-complexes. In fluids with higher concentrations of chloride, chloro-complexes will occupy a similar pH-logfO_2 space to the fluoro complexes. The activities of some important ligands in the fluid are determined by the solubility of major minerals such as fluorite for fluorine, apatite for phosphate, calcite and other carbonates for carbonate. Hence the presence or absence of these minerals in the system can be significant in the transport and deposition of uranium.

The solubility of uranium at 25°C and 50°C is shown in Figures 4.2a and 4.2b. The conditions are appropriate for low temperature near-surface environments of uranium mineralisation involving meteoric waters or shallow groundwaters, such as sandstone and calcrete uranium systems. Key implications of uranium solubility at low temperatures are as follows.

- For the conditions shown, the solubility of uranium depends primarily on the oxidation state (fO_2) of the fluid and on the availability of appropriate ligands. In alkaline and very alkaline fluids (pH > 8) where uranyl phosphate, carbonate and hydroxy complexes are dominant, the solubility depends both on pH and fO_2.
- At oxidation states corresponding to the hematite-magnetite buffer (logfO_2 = −71.8 at 25°C and −65.3 at 50°C) the solubility of uranium is very low (far less than 0.01 ppm). However a fluid saturated with air or buffered at the level of Mn_2O_3-Mn_3O_4 buffer (logfO_2 = −28.5 at 25°C and −25.6 at 50°C) can dissolve more than 100 ppm uranium.
- Reducing reactions provide the most effective way of depositing uranium from uranium-rich oxidised fluids.
- The role of chloro and fluoro complexes is insignificant unless pH values are <3 and Cl^- or F^- concentrations are high (see discussion of solubility at 100°C below).

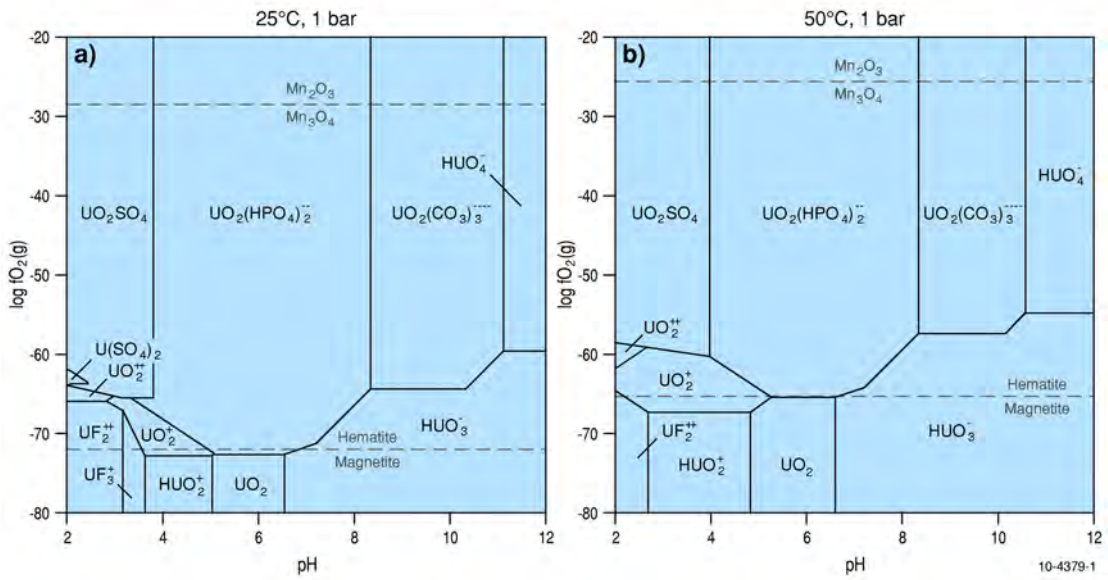

Figure 4.1: *LogfO$_2$-pH diagrams calculated at Σ[Cl] = 0.15m, Σ[C] = 0.003m, Σ[S] = 0.016m, Σ[P] = 4x10^{-6}m, Σ[F]= 4x10^{-6}m, Σ[SiO2]= 8x10^{-5}m for 25° and 50°C, respectively. The fluid is undersaturated with respect to uranium oxides. The diagrams show dominant aqueous species of uranium. Dashed lines marked Mn$_3$O$_4$/Mn$_2$O$_3$ and Hematite/Magnetite show the position of fO$_2$ buffers. In this and all subsequent diagrams an activity coefficient of 1 is assumed for all ionic species.*

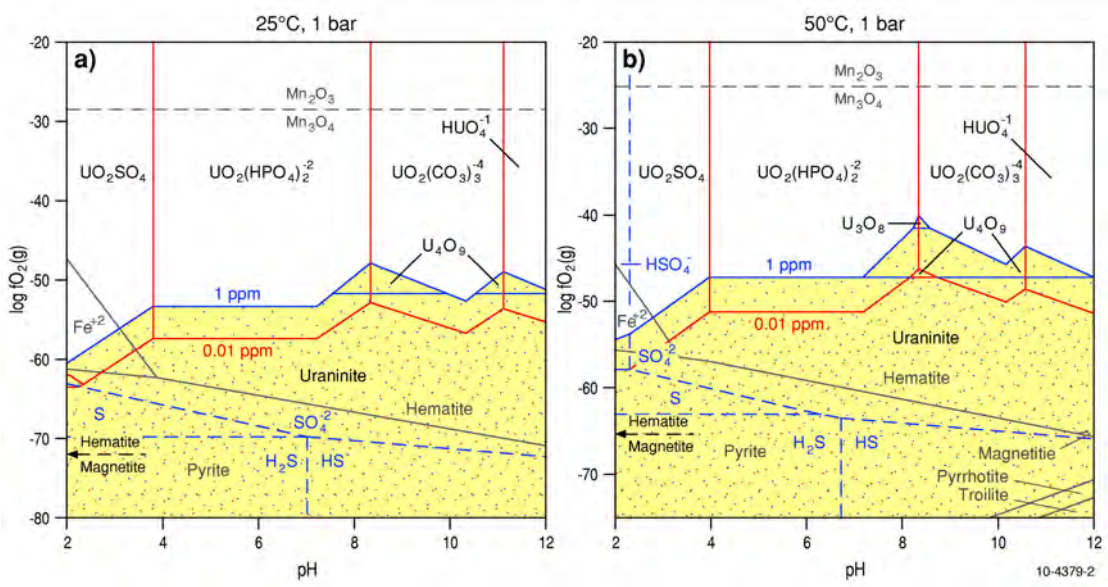

Figure 4.2*: LogfO$_2$-pH diagrams showing solubility of uraninite in fluids with 0.01 ppm (red line) and 1 ppm (blue line uranium. The diagrams are calculated at 25^{o}C and 50^{o}C for fluids containing Σ[Cl] = 0.15m, Σ[C] = 0.003m, Σ[S] = 0.016m, Σ[P] = 4x10^{-6}m, Σ[F]= 4x10^{-6}m, Σ[SiO2]= 8x10^{-5}. Stability fields of minerals in Fe-S-O system are shown in grey lines, and stability fields of sulphur species in blue dashed lines. The stability field of uraninite with 1 ppm dissolved uranium (stipple) moves to relatively more oxidising conditions. fO$_2$ buffers shown by dashed line marked Mn$_3$O$_4$/Mn$_2$O$_3$ and by a dashed arrow marked Hematite/Magnetite.*

4.2 URANINITE/COFFINITE STABILITY

Although coffinite is the dominant primary uranium oxide in ores of most sandstone hosted uranium deposits, the problem of its stability with respect to uraninite remains unresolved. This is because of two important reasons; the variation in the composition of natural coffinite, $U(SiO_4)_{1-x}(OH)_{4x}$ and uraninite $UO_{2-2.6}$ and the uncertainty in the thermodynamic data for coffinite. A detailed discussion on the problem can be found in Brookins (1975), Langmuir (1978), and Hemingway (1982).

The relative stability of uraninite and coffinite is expressed by the reaction:

$$UO_2 + H_4SiO_4\ (aq) = USiO_4 + 2H_2O$$

It shows that at a certain activity/concentration of dissolved silica uraninite will become unstable with respect to coffinite. Silica concentrations in ground waters average about $10^{-3.45}$mol/l (17 ppm dissolved silica). This concentration is less than the equilibrium concentration of dissolved silica ($10^{-3.25}$ at 25°C, Fig. 4.3a) determined using thermodynamic data for coffinite estimated by (Robie et al., 1979). According to Hemingway (1982) this means that natural coffinite coexisting with quartz and uraninite is in a metastable state. Langmuir (1978) noted that waters in the Grants mineral belt in New Mexico, where both uraninite and coffinite coexist, contain $10^{-3.5}$ to $10^{-2.7}$mol/l or 19 to 120 ppm dissolved silica and suggested that coffinite became stable relative to uraninite at intermediate levels of dissolved silica; that is, at a level above those in average ground water but below the saturation with amorphous silica.

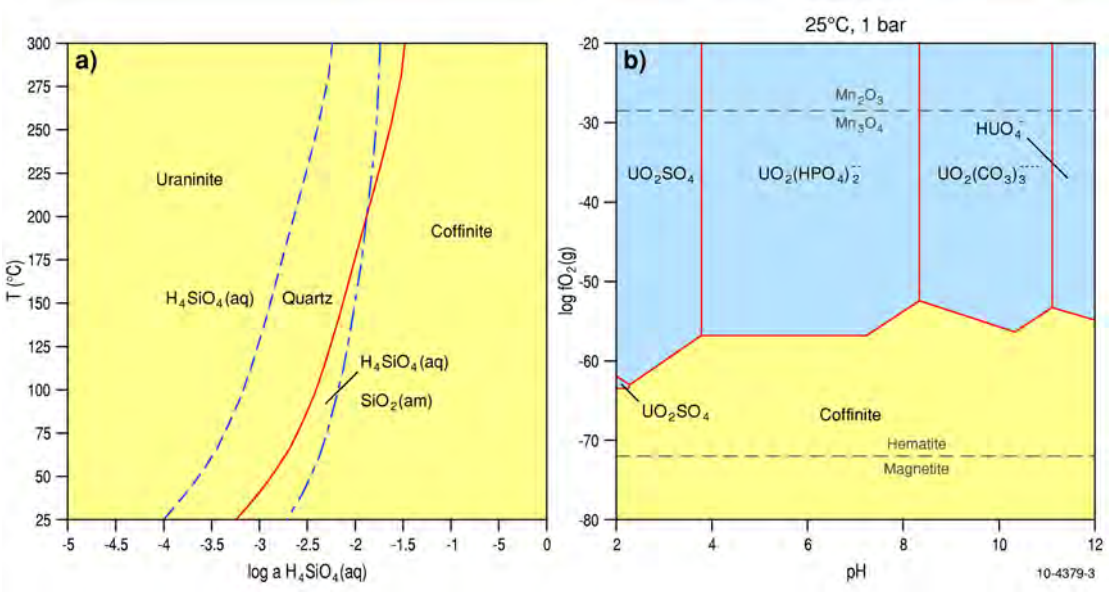

Figures 4.3*: Diagram showing relative stability of uraninite and coffinite. (a) T-log $a_{H4SiO4\ (aq)}$ diagram showing the stability fields of uraninite and coffinite as a function of dissolved silica. (b) Log fO_2-pH diagram at 25°C, calculated for a fluid containing Σ[Cl] = 0.15m, Σ[C] = 0.003m, Σ[S] = 0.016m, Σ[P] = $4x10^{-6}$m, Σ[F]= $4x10^{-6}$m, $a_{H4SiO4\ (aq)}$ = 0.001m (or log $a_{H4SiO4\ (aq)}$ = -3.0) The stability field of coffinite is drawn at total dissolved uranium = 0.01 ppm. Compare this diagram with Fig. 4.2a calculated for the same fluid but at low concentration of dissolved silica, [SiO2] = $8x10^{-5}$m.*

Coffinite, uraninite and quartz commonly coexist in many sandstone uranium deposits. In the uranium ores of the Wyoming deposits, uraninite and coffinite often form submicrospcopic intergrowths and concentric bands within colloform aggregates (Ludwig and Grauch, 1980). At the MI Vida Mine, San Juan (USA) coffinite replaces cellular textures of replaced wood whereas uraninite cements detrital grains adjacent to woody material (Gross, 1956). In contrast, in medium-temperature hydrothermal veins at Bois Noir, coffinite replaces pitchblende and forms concretionary overgrowths on crystalline quartz (Cuney, 1978).

The formation of coffinite thus requires fluids supersaturated with respect to quartz. This can be achieved by any of the following processes:

- Suppression of silica precipitation due to the high salinity, high concentration of dissolved aluminium and low pH of the fluid (Goldhaber et al., 1987).
- Formation of organo-silica complexes that generate higher concentrations of dissolved silica (Bennett and Siegel, 1987). The ubiquitous occurrence of organic material with coffinite in many deposit indicates a possible genetic link between them (see Spirakis, 1996 for discussion). The organo-silica complexes can produce the silica-rich waters needed to form coffinite (Spirakis, 1996). Bennett and Siegel (1987) record microbial oxidation of petroleum resulting in the formation of carbon dioxide and various mono- and multi-protic organic acids. Complexing of silica with these acids can account for the silica oversaturation observed in the groundwater sites contaminated by crude petroleum.
- Step-wise reduction of uranium in the presence of silica gel (Hemingway, 1982). It is suggested that reduction of UO_2^{+2} to U^{+4} occurs through an intermediate stage in which UO_2^{+2} is first reduced to UO_2^{+1}. The linear U-O-U molecule readily bonds to the surface of the silica gel and is further reduced to form coffinite. Excess silica or uranium in the gel can be excluded during the precipitation of coffinite to form quartz and/or uraninite. The absence of silica gel as an adsorbent can lead to formation of uraninite without coffinite. The alternating bands of uraninite and coffinite in many ores can form due to variation in the rate of adsorption of uranium on silica gel caused by changes in the oxidation state of the fluid or in the rate of mass and fluid-flow.

4.3 SPECIATION OF VANADIUM AND SOLUBILITY OF CARNOTITE

Carnotite (uranium-bearing potassium vanadate) is the dominant ore mineral in calcrete-hosted uranium deposits. The stability and solubility of carnotite and the geochemical conditions in which it is deposited in shallow groundwater systems depends on the speciation of vanadium and uranium in such fluids. The following sections give a brief discussion on the speciation and solubility of vanadium oxides and carnotite.

4.3.1 Speciation of vanadium and solubility of vanadium oxides at 25°C

Like uranium vanadium is a heterovalent element, occurring in nature in V^{+3}, V^{+4} and V^{+5} states. The average concentration of vanadium in the crust in 110 ppm. Mafic rocks contain an average of 250 ppm vanadium. The average abundance of vanadium in shales and granites is 130 ppm and 50 ppm respectively. Thus mafic rocks are the most effective sources of vanadium for calcrete related uranium and sandstone uranium deposits. Vanadium can also be sourced from Banded iron formations and ferricrete, which can contain up to 10 ppm and 800 ppm respectively (Horstmann and Halbich, 1995; Mann and Deutscher, 1978).

The speciation of vanadium in hydrothermal fluids depends on the oxidation state of the fluid (Figs. 4.4a). At oxidation states below the hematite-magnetite buffer ($\log fO_2 < -71.8$ at 25°C) hydroxy complexes of V^{+3} are more stable. However at pH > 8.5 the only stable complex of vanadium is the hydroxy complex containing V^{+5}. At oxidation states higher than the hematite-magnetite buffer, vanadium either forms a sulphate complex of V^{+4} in acidic to neutral conditions ($pH \leq 4$ to 7) or hydroxy complexes containing V^{+5} in neutral to alkaline conditions ($pH \geq 4$ to 7). Under very oxidising conditions ($fO_2 \geq Mn_3O_4$-Mn_2O_3 buffer) vanadium forms sulphate and hydroxy complexes of V^{+5}.

In relatively reducing conditions ($fO_2 \leq$ hematite-magnetite buffer) where vanadium forms complexes of V^{+3}, the solubility of karelianite (vanadium oxide with V^{+3}) is a function of pH, increasing with a decrease in pH. However in neutral to alkaline conditions, because vanadium forms complexes containing V^{+5}, the solubility of vanadium oxide increases with an increase in pH and oxygen fugacity (Fig. 4.4b). In more oxidised fluids (fO_2 > hematite-magnetite buffer), where vanadium forms complexes of containing V^{+4} and V^{+5} the solubility of vanadium oxides is both a function of pH and oxidation state. The solubility increases with an increase in the oxidation state and pH (in alkaline fluid) and increases with a decrease in pH (in acidic fluids). The calculations shows that an acidic fluid (pH $\leq$ 6) with its oxidation state buffered by the hematite-magnetite assemblage can dissolve up to 0.01 ppm vanadium. For such a fluid an increase in pH will initiate precipitation of vanadium oxide.

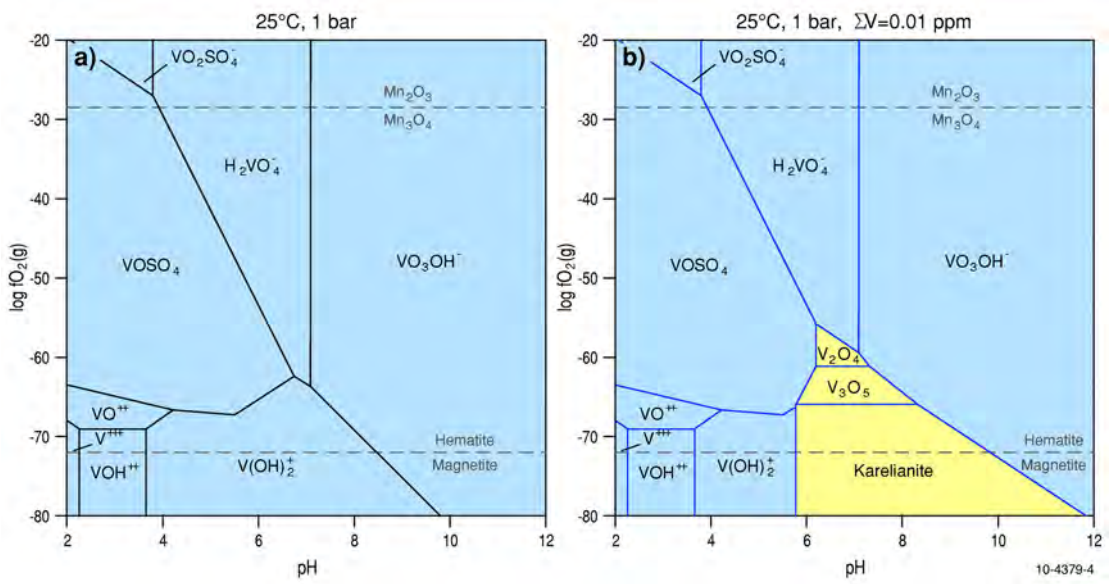

Figure 4.4: *LogfO2-pH diagrams calculated at Σ[Cl] = 2.68m, Σ[C] = 0.0017m, Σ[S] = 0.089m, Σ[P] = 1.05x10^{-5}m, Σ[F]= 5.3x10^{-5}m, Σ[SiO2]= 0.00014m, 25°C. The fluid composition is from the Lake Way area, Yilgarn Craton (Mann and Deutscher, 1978). (a) Fluid undersaturated with respect to vanadium oxides. The diagrams show dominant aqueous species of vanadium; (b) Fluid saturated with respect to vanadium oxides at 0.01 ppm total vandaium in the fluid. Karelianite is vanadium oxide (V_2O_3). Dashed lines marked Mn_3O_4/Mn_2O_3 and Hematite/Magnetite show the position of fO_2 buffers.*

In relatively reducing conditions ($fO_2 \leq$ hematite-magnetite buffer) where vanadium forms complexes of V^{+3}, the solubility of karelianite (vanadium oxide with V^{+3}) is a function of pH, increasing with a decrease in pH. However in neutral to alkaline conditions, because vanadium form complexes containing V^{+5}, the solubility of vanadium oxide increases with an increase in pH and oxygen fugacity (Fig. 4.4b). In more oxidised fluids (fO_2 > hematite-magnetite buffer), where vanadium forms complexes of containing V^{+4} and V^{+5} the solubility of vanadium oxides is both a function of pH and oxidation state. The solubility increases with an increase in the oxidation state and pH (in alkaline fluid) and increases with a decrease in pH (in acidic fluids). The calculations show that at near-neutral to an acidic fluid (pH $\leq$ 6) with its oxidation state buffered by the hematite-magnetite assemblage can dissolve up to 10 ppb vanadium. For such a fluid an increase in pH will initiate precipitation of vanadium oxide.

4.3.2 Solubility of carnotite

Carnotite is a uranium bearing potassium vanadate with the formula $K(U^{+6}O_2)(V^{+5}O_4)*H_2O$. Its solubility and precipitation depends on:

- The concentration/activity of potassium, uranium and vanadium in the fluid.
- The oxidation state of the fluid, because in oxygen-saturated low-temperature surficial fluids, uranium and vanadium form aqueous complexes of uranyl ($U^{+6}O_2$) and V^{+4} and V^{+5} respectively.
- The type of oxidation-reduction reaction: as the valence state of uranium and vanadium in carnotite is +6 and +5 respectively, oxidation-reduction reactions are only important with respect to vanadium only in conditions where vanadium forms complexes containing V^{+3} and V^{+4}. In such cases precipitation of carnotite will require oxidation and not reduction of the fluid (see discussion below).

At 25°C, the stability field of carnotite extends to a region of high oxidation, much higher than that buffered by hematite-magnetite assemblage ($\log fO_2 = -71.8$) and at pHs between 5 and 9 (Fig. 4.5a and 4.5b). Carnotite is soluble both in acidic or alkaline conditions (pH < 5 or pH > 9). In acidic fluids the solubility increases with a decrease in pH (increasing acidity) whereas in alkaline fluids it increases with pH (increasing alkalinity). This is because in acidic fluids of the composition used in these calculations, uranium is soluble as sulphate complexes of uranyl whereas in alkaline fluids it forms carbonate and hydroxy complexes.

These diagrams also show the effect on the stability of carnotite when uranium is added to a fluid carrying 0.01 ppm vanadium. As expected an addition of uranium makes carnotite less soluble (the stability field of carnotite expands). Fluids represented by points A and B are undersaturated with respect to carnotite for a uranium concentration of 0.01 ppm (Fig. 4.5a), but become saturated when the uranium concentration is increased to 1 ppm (Fig. 4.5b). Thus mixing of a fluid containing vanadium (0.01 ppm) with a fluid carrying 1 ppm uranium can cause precipitation of carnotite.

These diagrams also show that oxidation-reduction reactions are only important in a restricted zone of low pH where vanadium forms aqueous complexes of V^{+4}. Under such conditions precipitation of carnotite will require an increase in either pH or fO_2, i.e. the fluid will have to undergo oxidation and not reduction (see Fig. 4.5a). This is because under such conditions vanadium forms aqueous complexes of V^{+4} and not V^{+5} (Fig. 4.5a).

Both uraninite (including other uranium oxides) and carnotite are stable within most of the logfO_2-pH space of these diagrams with uraninite confined to more reducing conditions. The diagrams show that oxidation of uraninite in ores by fluids containing vanadium and potassium will replace it by carnotite. The presence of such secondary carnotite is recorded in many sandstone uranium deposits.

The stability of carnotite and vanadium oxides in fluids rich of differing vanadium content but poor in uranium (0.01 ppm) is represented in Fig. 4.6. These diagrams should be read in combination with the diagrams in Fig. 4.5. They show that the stability field of carnotite is limited to a zone of high logfO_2 (> -55) and pH between 5 and 8. The precipitation of carnotite can be caused by an increase in pH (under acidic conditions) and a decrease in pH (under alkaline conditions; Fig. 4.6b). At pH < 5, where vanadium forms a sulphate complex of V^{+4}, oxidation can cause precipitation of carnotite.

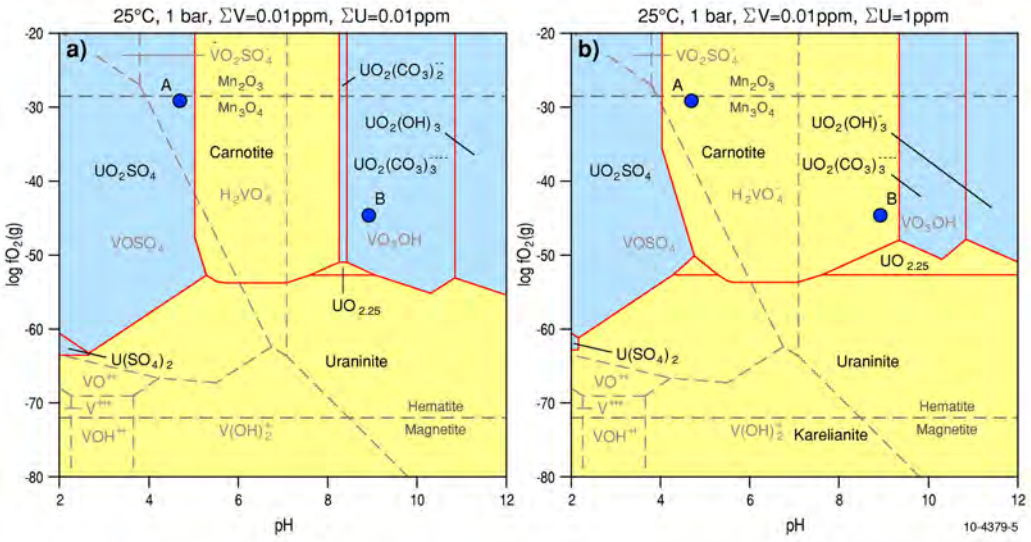

Figure 4.5: *LogfO_2-pH diagrams calculated at Σ[Cl] = 2.68m, Σ[C] = 0.0017m, Σ[S] = 0.089m, Σ[P] = 1.05x10^{-5}m, [F]= 5.3x10^{-5}m, [SiO_2]= 0.00014m, 25°C. The fluid composition is from the Lake Way area, Yilgarn Craton (Mann and Deutscher, 1978). Stability fields for carnotite and uraninite are drawn at 0.01 ppm vanadium and 0.01 ppm uranium (a), and at 0.01 ppm vanadium and 1 ppm U (b). With increase in the concentration of uranium in the fluid the stability field of carnotite expands and fluids of composition (points A and B) undersaturated with respect to carnotite (in Fig. 4.5a) become saturated with carnotite (Fig. 4.5b). Dashed lines marked Mn_3O_4/Mn_2O_3 and Hematite/Magnetite show the position of mineral fO_2 buffers*

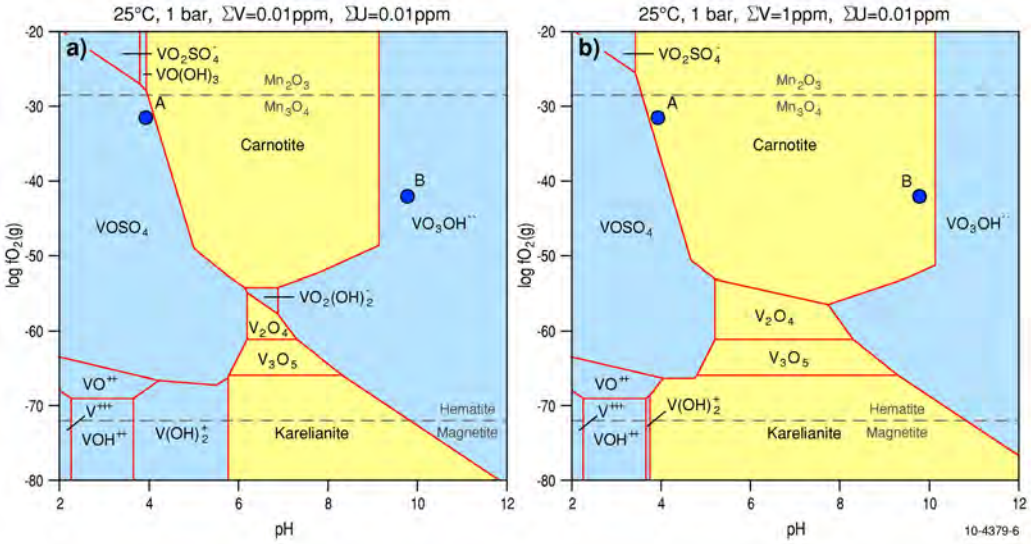

Figure 4.6: *LogfO_2-pH diagrams calculated at Σ[Cl] = 2.68m, Σ[C] = 0.0017m, Σ[S] = 0.089m, Σ[P] = 1.05x10^{-5}m, Σ[F]= 5.3x10^{-5}m, Σ[SiO_2]= 0.00014m, 25°C. The fluid composition is from the Lake Way area, Yilgarn Craton (Mann and Deutscher, 1978).Stability fields for carnotite and vanadium oxides are drawn at 0.01 ppm uranium and 0.01 ppm vanadium (a), and at 0.01 ppm uranium and 1 ppm vanadium (b), respectively. With increase in the concentration of vanadium in the fluid the stability field of carnotite expands and fluids of compositions A and B initially undersaturated with respect to carnotite (in Fig. 4.6a) become carnotite-saturated (Fig. 4.6b). Dashed lines marked Mn_3O_4/Mn_2O_3 and Hematite/Magnetite show the position of fO_2 buffers.*

Figures 4.7 to 4.9 show the effect of changes in the concentration of dissolved potassium, sulphur and carbonate in the fluid on the stability of carnotite. As expected, an increase in the concentration of dissolved potassium expands the stability field of carnotite, which means that adding more potassium to the fluid may trigger formation of carnotite (compare fluids represented by blue stars on Fig. 4.7a and 4.7b). The concentration of potassium in the fluid can change by reaction with potassium-rich felsic rocks or by mixing with a potassium-rich fluid. It is possible that precipitation of calcite, causing depletion of dissolved calcium can cause a concomitant increase in the relative concentration of potassium but more detailed mass-balance calculations are required to confirm this.

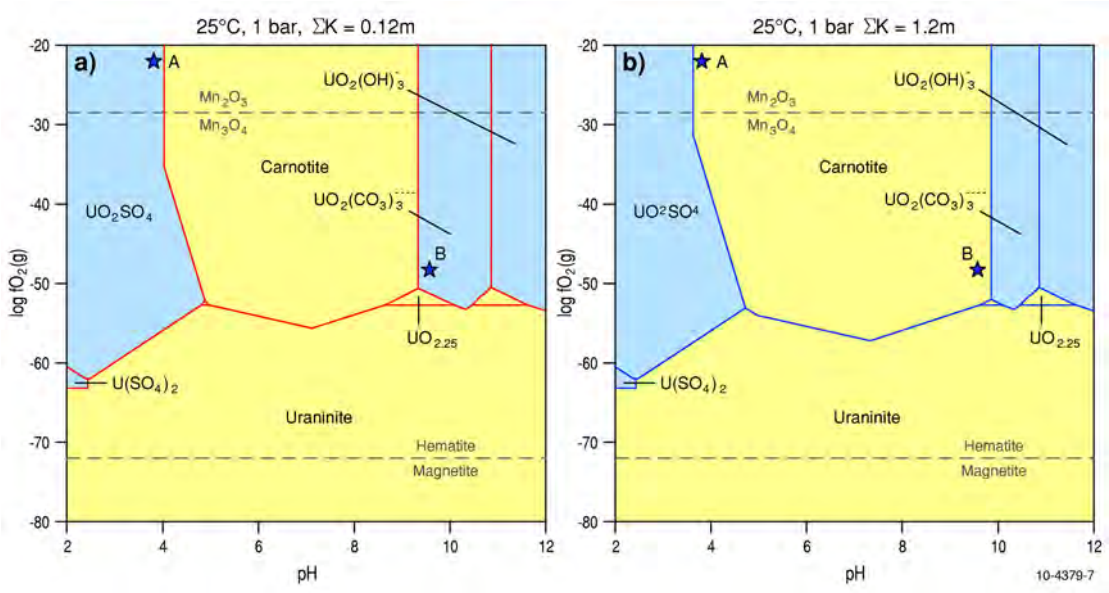

Figure 4.7: *LogfO$_2$-pH diagrams calculated at Σ[Cl] = 2.68m, Σ[C] = 0.0017m, Σ[S] = 0.089m, Σ[P] = 1.05x10^{-5}m, Σ[F]= 5.3x10^{-5}m, [SiO$_2$]= 0.00014m. The fluid composition is from the Lake Way area, Yilgarn Craton (Mann and Deutscher, 1978). Figures show the effect of increase in the concentration of dissolved potassium in the fluid. Fluid contains Σ[U] = 0.1 ppm and Σ[V] = 0.1 ppm. With an increase of potassium concentration from Σ[K] = 0.12m (4.7a) to Σ[K] = 1.2m (4.7b), carnotite becomes more stable. Its field expands both in low pH and high pH region and fluids of compositions A and B undersaturated with respect to carnotite (in Fig. 4.7a) become carnotite-saturated (Fig. 4.7b). Dashed lines marked Mn$_3$O$_4$/Mn$_2$O$_3$ and Hematite/Magnetite show the position of fO$_2$ buffers.*

Carnotite in calcretes within paleochannels often forms sheets or lenses near the fluctuating water table. It is possible that changes in the partial pressure of CO_2 in the seasonally fluctuating water table control deposition of carnotite in paleochannels.

The effect of changes in the concentration of sulphur in the fluid on the stability of carnotite is limited to relatively acidic fluids (pH < 5). An increase in the concentrations of sulfur as sulphates makes carnotite less stable because it increases the amount of uranium that can be dissolves as uranyl-sulphate complexes (compare the fluid represented by point A in Fig. 4.9). Hence a drop in the activity of sulphate ions, caused by the precipitation of sulphates such as barite and gypsum, can trigger precipitation of carnotite. The activity of sulphate can also be lowered by forming pyrite but its effect should be limited because it requires concomitant reduction of the fluid which generally inhibits deposition of carnotite.

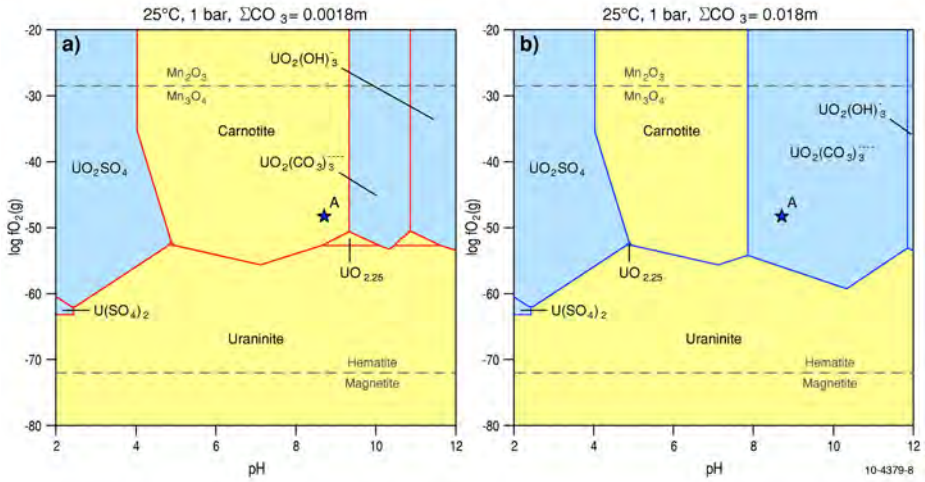

Figure 4.8: *LogfO$_2$-pH diagrams calculated at Σ[Cl] = 2.68m, Σ[C] = 0.0017m, Σ[S] = 0.089m, Σ[P] = 1.05x10^{-5}m, Σ[F]= 5.3x10^{-5}m, [SiO$_2$]= 0.00014m. The fluid composition is from the Lake Way area, Yilgarn Craton (Mann and Deutscher, 1978). Figures show the effect of increase in the concentration of dissolved carbonate in the fluid. Fluid contains Σ[U] = 0.1 ppm and Σ[V] = 0.1 ppm. With an increase in the concentration of dissolved carbonate from 0.00177m (4.8a) to 0.0177m (4.8b), carnotite becomes more soluble. The effect is only at pH > 7 where carbonate complexes of uranyl determine the solubility of uranium. The stability in the region of pH < 4 remains unchanged. Note that a fluid saturated with carnotite (point A in Fig. 4.8a) becomes undersaturated with respect to carnotite (point A in Fig. 4.8b). Dashed lines marked Mn$_3$O$_4$/Mn$_2$O$_3$ and Hematite/Magnetite show the position of fO$_2$ buffers.*

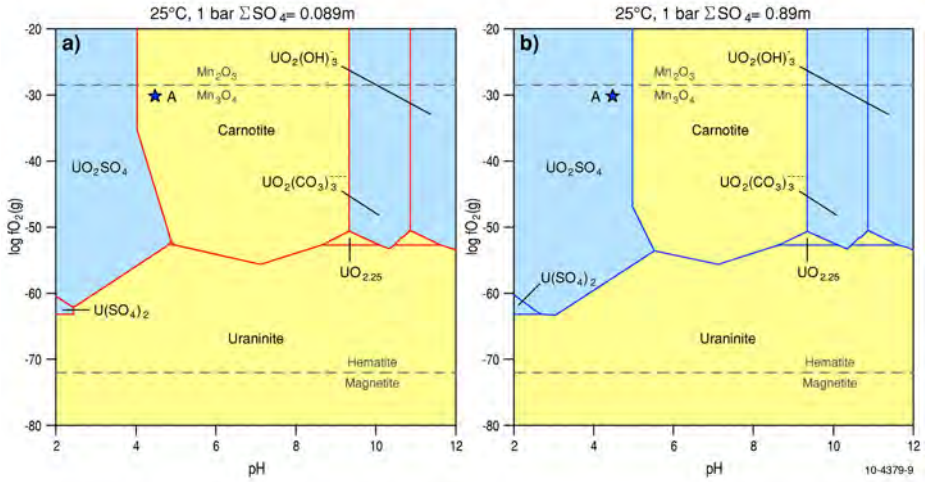

Figures 4.9: *LogfO$_2$-pH diagrams calculated at Σ[Cl] = 2.68m, Σ[C] = 0.0017m, Σ[S] = 0.089m, Σ[P] = 1.05x10^{-5}m, Σ[F]= 5.3x10^{-5}m, Σ[SiO2]= 0.00014m. The fluid composition is from the Lake Way area, Yilgarn Craton (Mann and Deutscher, 1978). Figures show the effect of increase in the concentration of dissolved sulphur in the fluid. Fluid contains Σ [U] = 0.1 ppm and Σ [V] = 0.1 ppm. With an increase in the concentration of dissolved sulphur from 0.089m (4.9a) to 0.89m (4.9b), carnotite becomes more soluble. The effect is only at pH < 4 where sulphate complexes of uranyl determine the solubility of uranium. The stability in the region of pH > 7 remains unchanged. Note that a fluid saturated with carnotite (point A in Fig. 4.9a) becomes undersaturated with respect to carnotite (point A in Fig. 4.9b). Dashed lines marked Mn$_3$O$_4$/Mn$_2$O$_3$ and Hematite/Magnetite show the position of fO$_2$ buffers*

.

4.3.3 Factors controlling precipitation of carnotite in calcrete-hosted uranium deposits

Butt et al. (1984) classified calcrete-hosted uranium deposits in Western Australia by their geomorphological setting into three main types: valley, playa, and terrace deposits. The valley deposits (such as Yeelirrie, Hinkler-Centipede, Lake Way and Lake Raeside in the Yilgarn Craton) occur in calcretes and associated sediments in the central channels of major drainages, and in the platforms and chemical deltas where the drainage enter playas. The calcretes generally change downwards into an alluvial clay-quartz unit. Uranium mineralisation is not limited to the calcretes but transgresses into underlying units, with the greatest concentration in the vicinity of the present-day groundwater table. Mineralisation occurs almost entirely as carnotite, generally as a late-stage precipitate in cavities, lined by thin coatings of minerals such as calcite, dolomite, silica and/or sepiolite. Carnotite may also form fine disseminations in clay-quartz units.

The playa deposits (such as Lake Maitland and Lake Austin deposits) occur in near-surface evaporitic and alluvial sediments. The calcretes near playas act as principle aquifers to the playas. In the Yilgarn, mineralised playas are usually closely associated with calcretes in the channels, often enriched in uranium. Mineralisation is generally concentrated near the groundwater table in sediments consisting of gypsiferous clays and muds. The sandy and silty clays, locally containing calcareous nodules. In some deposits such as Lake Maitland the mineralisation is in thin calcretes in the playa itself.

The terrace deposits are less common and occur in calcrete terraces in dissected valleys mainly in the Gascoyne Province of Western Australia.

The above discussion on the speciation of uranium and vanadium and of stability of carnotite shows that geologically important concentrations of uranium and vanadium (> 0.01 ppm each of uranium and vanadium) can be co-transported in oxidised fluids (Fig. 4.5). In such conditions uranium forms aqueous complexes of uranyl and vanadium forms complexes containing either V^{+4} or V^{+5}. The calculations also show that precipitation of carnotite can occur due to changes in any of the following:

1. pH; decrease in pH if the groundwater is alkaline (pH >8) or increase in pH if the groundwater is acidic
2. oxidation state; in very oxidised conditions (air-saturated ground water) where vanadium and uranium are present in their highest oxidation states (V^{+5} and U^{+6}) precipitation of carnotite does not require changes in the oxidation state. However, at relatively lower oxidation states where vanadium is transported as complexes of V^{+3} and/or V^{+4}, an oxidation of ground water can be important to form carnotite.
3. concentration of dissolved potassium, uranium and vanadium; an increase in their concentration can cause precipitation of carnotite
4. partial pressure of CO_2, which controls the concentration of carbonate complexes in the groundwater. As uranium in these conditions is transported as uranyl-carbonate complex, a decrease in the concentration of carbonate ions in groundwater will favour precipitation of carnotite
5. concentration of dissolved calcium in the groundwater; as addition of calcium to the groundwater can cause precipitation of carbonate, the associated decrease in the concentration of dissolved carbonate ion in the groundwater can cause precipitation of carnotite
6. concentration of dissolved sulphur in the groundwater; in oxidised groundwater sulphur is dissolved to form sulphate ions which control the solubility of uranium as uranium forms uranyl-sulphate complexes. A decrease in the concentrations of sulphate ions caused often by the deposition of gypsum and barite can thus favour precipitation of carnotite.

The geomorphological setting of both valley- and playa-type calcrete-hosted uranium deposits shows that their formation is closely related to the evolution of the drainage system. The groundwater table and the mixing zone near the playa lake represent two important elements of

the drainage system. They control chemical parameters (listed above) which determine precipitation of carnotite.

The groundwater table in the alluvial filling the drainage valley often undergoes seasonal fluctuation, and evaporation can play an important role in controlling precipitation of carnotite (Mann and Deutscher, 1978; Boyle, 1982). Evaporation of upwelling groundwaters in drainage channels can cause an increase in the concentration of dissolved potassium, vanadium and uranium (Butt et al., 1984). Precipitation of carnonite can also be linked to the changes in the pH and in the concentration of CO_2 in the ground water induced by evaporation.

Evaporation is also important in the playa deposits where it can control salinity of lake waters and precipitation of gypsum-bearing sediments. However mixing of more saline lake waters (relatively enriched in potassium, calcium) and the incoming groundwaters from the drainage channel can be equally important in the formation of carnotite. Such mixing can cause an increase in the concentration of potassium and calcium in the groundwater which may lead to the precipitation of carnotite. In a similar way, an increase in the concentration of calcium can destabilise uranyl-carbonate complexes and cause precipitation of carnotite (Mann and Deutscher, 1978).

According to Mann and Deutscher (1978) redox process could also have contributed to the formation of carnotite in some calcrete-hosted uranium deposits. In this model interaction of mildly reduced groundwaters with mafic rocks in the greenstones can cause dissolution of vanadium to form V^{+4} bearing complexes. Vanadium from these groundwaters mixes with overlying uranium-bearing fluids either through diffusion and/or by upwelling of the waters caused by a subsurface bar. Mixing causes oxidation of vanadium from V^{+4} to V^{+5} to form carnotite.

4.4 SPECIATION AND SOLUBILITY OF URANIUM AT TEMPERATURES BETWEEN 100 AND 200°C

The speciation and solubility of uranium at temperatures between 100° and 200°C is important for understanding of transport and deposition of uranium in low to moderate temperature basin-related fluid-flow systems. These include unconformity-related uranium deposits where the systems operate at temperatures between 150° and 250°C (Jefferson and Delaney, 2007) and uranium-rich zones in sediment-hosted stratiform copper deposits in which the average temperature of the system varies between 70° to 110°C (Hitzman et al., 2005).

The stability of aqueous species of uranium at 100°C and 200°C is shown in Figs. 4.10 and 4.11. The type of dominant complex will be determined by the activities of ligands such as F^{-}, Cl^{-}, CO_3^{+2}, PO_4^{-2} and SO_4^{-2}, which are controlled primarily by the solubility of minerals such as apatite, fluorite, carbonates and sulphates. In acidic fluids and reducing conditions, the chloro-complex of U^{+4} (UCl_2^{+2}) is dominant at 100°C (Fig. 4.11). At temperatures >100°C it is difficult to determine the stability of UCl_2^{+2} because of the uncertainties associated with its basic thermodynamic data. The uranyl phosphate complex is stable at pH values between 4 and 9 in both reducing and very oxidising conditions.

The solubility contours (Fig. 4.11) show that at 100°C a reduced fluid with 1m chloride ($\log fO_2$(g) values at the hematite-magnetite buffer and lower) can transport 10 ppb uranium only at pH < 2.5 (Fig. 4.11, see the red line). In more chlorine-rich fluids the contour will move to the areas of higher pH. For instance a fluid with a total salinity of 5m chloride and 10 ppb uranium will remain in solution as UCl_2^{+2} at a pH of 3.5. However at pH > 4 the fluid will have to be highly oxidised (many orders of magnitude higher than the fO_2 level buffered by the hematite-magnetite assemblage). As for temperatures of 25° and 50°C (see preceding sections) reduction is the main process causing deposition of uranium oxides at most geological conditions; pH control becoming important only in the restricted fields of very acidic (pH < 3.5) or alkaline (pH > 8) conditions.

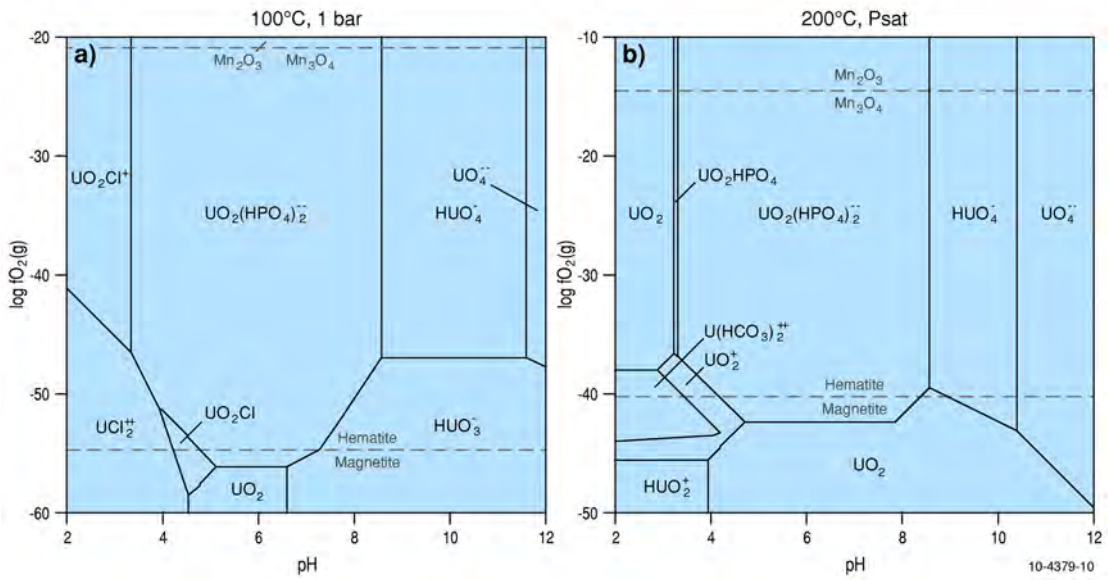

Figure 4.10: *LogfO_2-pH diagrams calculated at Σ[C] = 0.001m, Σ[S] = 0.001m, Σ[P] = 1.0x10^{-5}m, Σ[Cl] = 3.65m, Σ[F]= 5.3x10^{-5}m. The fluid is undersaturated with respect to uranium oxides. The diagrams show dominant aqueous species of uranium. Because of uncertainty in the thermodynamic data for UCl_2^{+2} at temperatures > 100°C it is not included in the diagram at 200°C. Dashed lines marked Mn_3O_4/Mn_2O_3 and Hematite/Magnetite show the position of fO_2 buffers.*

The calculations for the diagrams at 200°C do not the UCl_2^{+2} species because of the uncertainties associated with the basic thermodynamic data for this complex. A reliable dataset for this complex is essential to investigate the behaviour of uranium in reduced fluids. With no UCl_2^{+2} in the calculations, the speciation and solubility of uranium at 200°C is very similar to that at 100°C (compare Figs. 4.11 and 4.12).

Oxidation-reduction reactions are important for the formation of both unconformity-related uranium and uranium-rich, sediment-hosted copper deposits. The calculations at 100° and 200°C show that geologically realistic concentrations of uranium (>1 ppm) can only be transported in highly oxidised fluids (many orders of magnitude of logfO_2 values higher than the level buffered by the hematite-magnetite assemblage). The very low pH (<3) required to transport uranium in reduced fluids have not been reported for basin-derived, diagenetic fluids. Hence a fluid-flow regime that maintains fluids of very high oxidation states as they move to the site of deposition is essential to form uranium deposits associated with diagenetically-derived, basinal fluids. This problem will be discussed in some detail in Chapter 6.

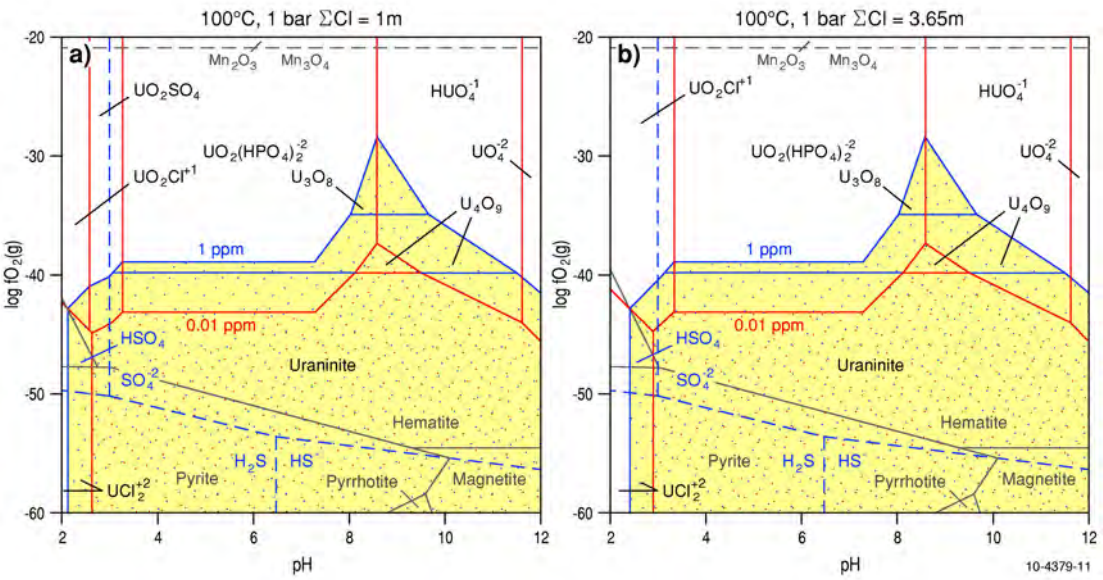

Figure 4.11: *log fO2-pH diagrams showing solubility of uraninite and other uranium oxides at 100°C. Diagrams are calculated at Σ[C] = 0.001m, Σ[S] = 0.001m, Σ[P] = $1.0x10^{-5}$m, Σ[F]= $5.3x10^{-5}$m (3.11a).The effect of salinity on the solubility can be judged by comparing Fig. 4.11a (Σ[Cl] = 1m) and Fig. 4.11b (Σ[Cl] = 3.65m). Stability fields of minerals in Fe-S-O system are shown in grey lines. Stability field of sulphur species in blue dashed lines .The stability field of uraninite at with 1 ppm dissolved uranium(blue stipples) moves to relatively more oxidising conditions. fO_2 buffers corresponding to the Mn_3O_4/Mn_2O_3 assemblage is shown by dashed line*

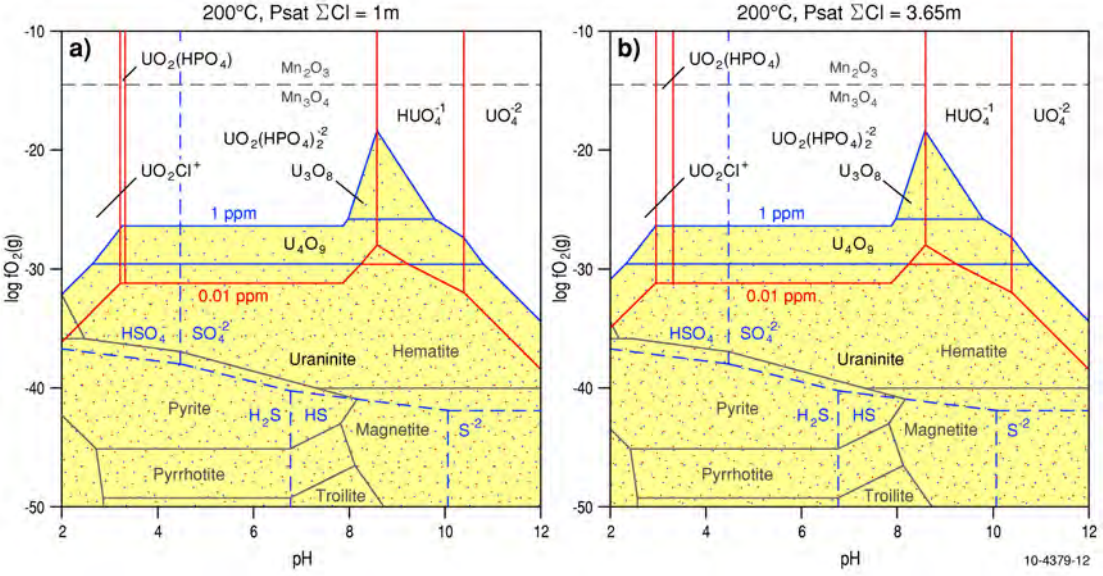

Figure 4.12: *log fO_2-pH diagrams calculated at Σ[C] = 0.001m, Σ[S] = 0.001m, Σ[P] = $1.0x10^{-5}$m, Σ[F]= $5.3x10^{-5}$m, 200°C. Stability fields of minerals in Fe-S-O system are shown in grey lines. Stability field of sulphur species in blue dashed lines. The effect of salinity on the solubility can be judged by comparing Fig. 4.12a (Σ[Cl] = 1m) and Fig. 4.12b (Σ[Cl] = 3.65m). The stability field of uraninite at with 1 ppm dissolved uranium(blue stipples) moves to relatively more oxidising conditions. fO_2 buffers corresponding to the Mn_3O_4/Mn_2O_3 assemblage is shown by dashed line. Chloro-complex of tetravalent uranium (UCl_2^{+2}) not included in the calculation.*

5. Speciation and solubility of uranium at temperatures ≥300°C

Characterising of uranium solubilities at temperatures ≥300°C is important for understanding hydrothermal uranium systems associated with low grade metamorphism, deep burial, deeper parts of some geothermal systems, and magmatic-hydrothermal systems. These conditions might be also important at uraniferous iron-oxide copper-gold systems of the Olympic Dam type at the early stages of evolution of these systems.

At sub-magmatic temperatures, solubilities of uranium were experimentally investigated by Peiffert et al. (1994), Peiffert et al. (1996), and Zharikov et al. (1987), at 770°C and 500-600°C, respectively. These studies reveal that extremely high uranium solubilities (up ~1000 ppm) are possible in aqueous chloride-fluoride brines in equilibrium with peralkaline melt and uranium oxides. Uranium speciation at these conditions is dominated by halide complexes, most notably fluoride. The oxidation state of these uranium complexes remained uncertain.

At present, the problems with calculating complete equilibrium speciation within these fluids preclude quantitative interpretation of these experiments. However, these studies have clearly demonstrated the potential for high uranium-bearing capacity of post-magmatic fluids. A remaining issue is whether there is a potential to retain this capacity at intermediate temperatures and whether there is an option to ensure smooth magmatic to "epithermal" transition for uranium hydrothermal systems at mid-crustal conditions. The latter implies at least partially rock-buffered conditions in terms of pH and fO_2.

5.1 PREVIOUS WORK

Komninou and Sverjensky (1996) modelled formation of unconformity-type uranium deposits that formed between 150° and 300°C by Na-Ca-Cl brines. For their calculations they have chosen 200°C as a representative temperature. The pH of fluids was calculated from the equilibrium between K-feldspar, white mica, quartz, and aqueous solution. They concluded that at syn-ore conditions ($\log fO_2$ from −33.7 to −41.5), uranium was transported mainly as uranyl and uranyl-chloride complexes ($UO_2Cl_2^0$ (aq); UO_2Cl^+; $UO_2(OH)^+$; UO_2^{+2}; $UO_2(OH)_2^0$ (aq)). Komninou and Sverjensky (1996) have not provided sources to thermodynamic data for uranium species but instead referred to unpublished databases by Shock (1989) and Sverjensky. Thus, at least thermodynamic properties of their uranium hydroxide complexes are generally consistent with those adopted in this study.

Haynes et al. (1995) completed geochemical modelling of an ore-forming scenario at Olympic Dam at temperatures up to 250°C using speciation model and thermodynamic data from the SOLTHERM by Reed (unpublished data, 1993). The choice of 250°C was limited by the available thermodynamic data for uranium. However, these authors have not provided any discussion on uranium speciation in Olymic Dam type fluids.

5.2 URANIUM SOLUBILITY FROM 25° TO 300°C

Based on the compiled dataset for uranium aqueous species (Table 3.1), we have calculated solubilities of uranium oxides (UO_2(cr), U_4O_9(cr), U_3O_8(cr)) and aqueous uranium speciation as a function of temperature and redox state for simple fluids in H–O–Cl–U and H–O–Cl–C–S–P–U systems (Figures 5.1 to 5.4). For given chlorinity values, fluid pH was controlled by equilibrium with quartz-K-feldspar-muscovite-albite and quartz-kaolinite-muscovite assemblages that would approximate unaltered and altered felsic rocks, respectively.

Figure 5.1 shows the total concentration of dissolved uranium in two-dimensional space. Particular plots (a to f) illustrate the changes in overall uranium solubility not only in response to change in temperature and redox conditions, but also due to the coupled effects of changing the fluid chlorinity, namely (1) formation of the uranous and uranyl chloro-complexes and (2) changing pH of the fluids via the rock buffering equilibria such as

$3KAlSi_3O_8 + 2H^+ = KAlSi_3O_{10}(OH)_2 + 6SiO_2 + 2K^+$.

Activity of the K^+ ion will be controlled by K^+/Na^+ exchange with other phases (e.g., albite, $KAlSi_3O_8$) (or by a specified K/Na ratio in the fluid) and overall charge balance mostly controlled by the Na–K–Cl subsystem of the fluid components. For a given mineral assemblage higher chlorinities (equivalent top higher activities of K^+) will fix lower pH values.

Figure 5.1 shows fundamental behaviour of uranium in low- to mid-temperature hydrothermal systems:

1. The overall effect of the redox change is *the first-order* control of the uranium solubility at all temperatures;
2. For a wide range of oxidation conditions (i.e., at fO_2 values > −50, where speciation is dominated by uranyl VI complexes), increasing temperature at a fixed oxidation state (in terms of fO_2) results in a decrease in uranium solubilities;
3. At less oxidising conditions (speciation dominated by U^{IV} and U^{V} complexes), the temperature dependence is more complicated, especially when we consider addition of other ligands to the H-O-U system (Figure 5.1 illustrates the effect of added chlorine);
4. Addition of chlorine to the system (i.e., transition from diluted fluids to brines) enhances uranium solubility but does not change the overall solubility pattern (for the exception of the higher temperature – reduced corner of the plots).

Figure 5.1 implies that surficial and sub-surficial hydrothermal systems (partly open to oxygen, or formed at strongly oxidised conditions) are much more favourable for uranium transport than essentially rock-buffered, medium temperature hydrothermal fluids.

Despite being instructive in terms of depicting the overall solubility patterns, the concentration-fO_2-temperature diagrams are cumbersome for tracing the redox evolution in mineral systems and for exhibiting the uranium speciation within the fluids. Thus these diagrams can be dissected further in terms of isothermal fO_2-slices (Figure 5.2) or fO_2 buffer-specific temperature slices (Figure 5.3). The particular examples discussed here are plotted for 1M total fluid chlorinities (~5.5 weight percent of NaCl equivalent).

Examination of Figure 5.2 reveals that at temperatures from 200° to 300°C reduced fluids (fluids with fO_2 values close to pyrite-pyrrhotite-magnetite and magnetite-hematite redox buffers) are dominated by UO_2^0 (aq) (U^{IV}) and UO_2^+ (U^V) complexes. Fluids formed at more oxidised conditions (e.g., towards Mn_3O_4-Mn_2O_3 buffer and higher fO_2 values) will be dominated by UO_2OH^+, HUO^{4-}, UO_3^0 (aq), and UO_2Cl^+ U^{VI} complexes. The latter is consistent with previous theoretical results reported by (Komninou and Sverjensky, 1996). Note that lower pH values imposed by the quartz–kaolinite – muscovite buffer result in higher uranium solubilities compared to the quartz–K-feldspar– muscovite–albite buffer. Thus, within the developing alteration zones both fluid reduction and neutralisation will result in uranium precipitation.

Figure 5.3 represents the total solubility of uranium for redox conditions buffered by Mn_2O_4-Mn_2O_3, magnetite-hematite, respectively.

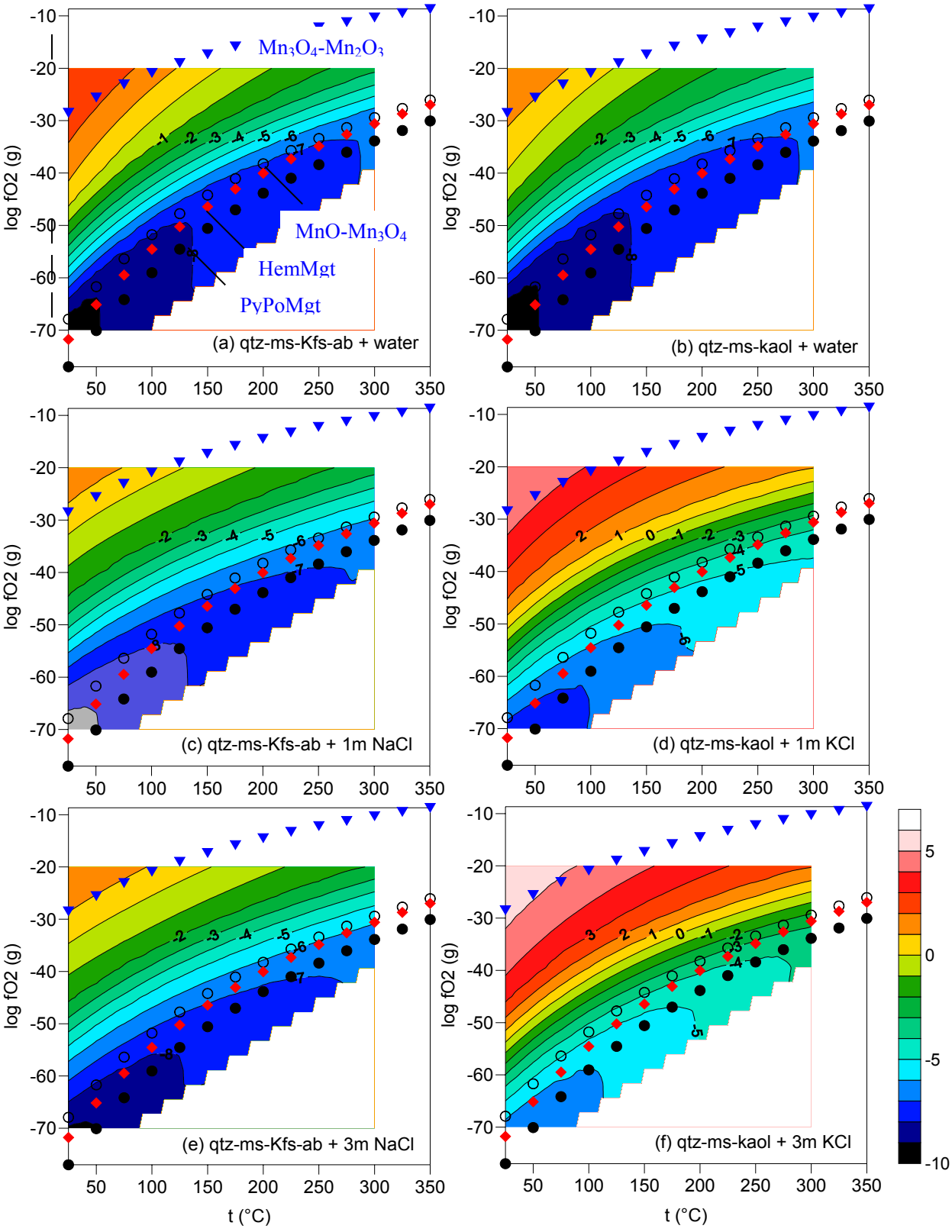

Figure 5.1: *Total solubilities of uranium oxides, UO_2 (cr) to U_3O_8 (cr), in an H-O-Cl-U system as a function of temperature and oxidation state calculated along mineral pH buffers for fluids of variable chlorinities. Uranium concentrations are presented as log U in ppm (e.g, 0 corresponds to 1 ppm of U). The points outline positions of mineral redox buffers.*

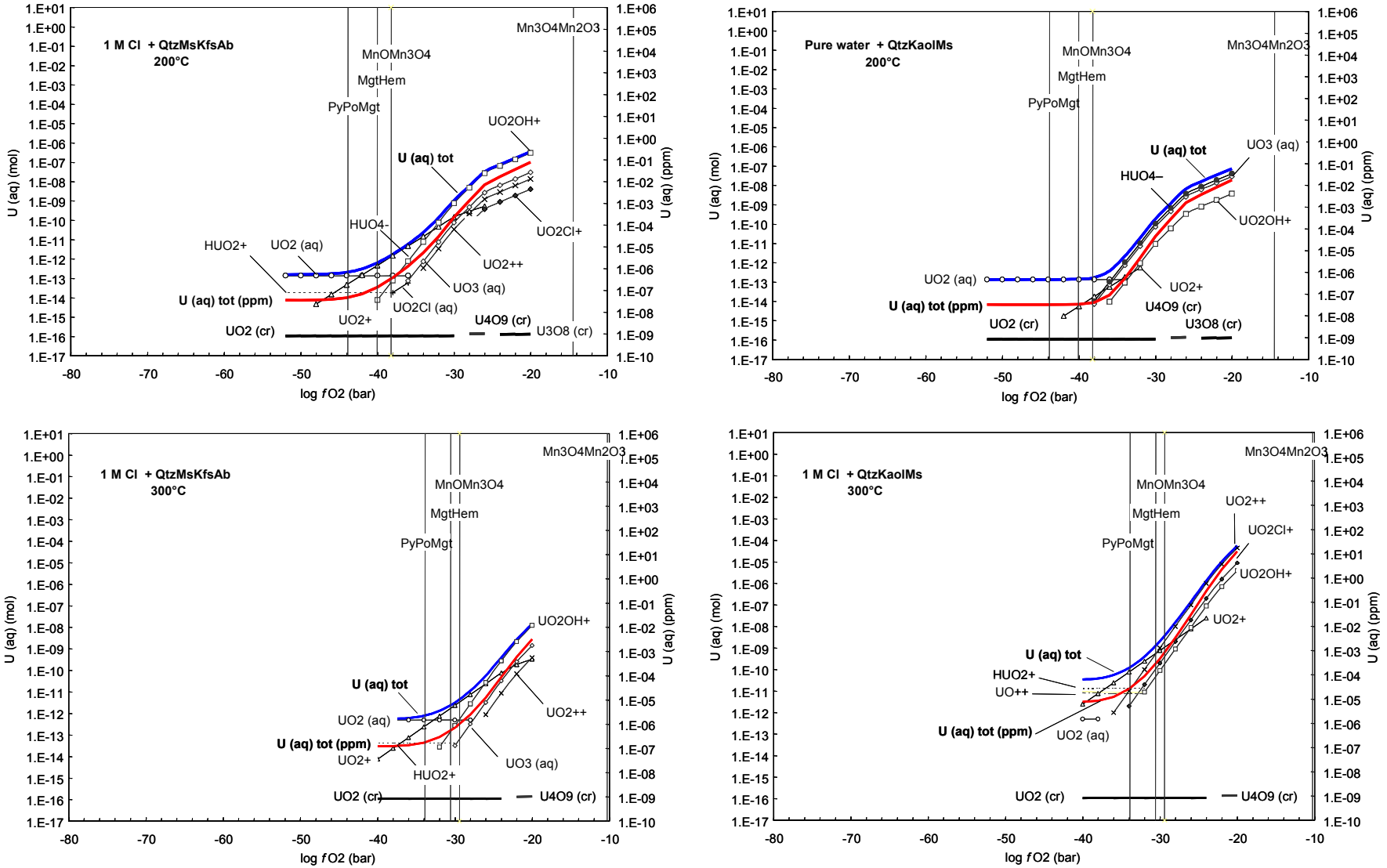

Figure 5.2: *Total uranium solubility and speciation in 1M total chloride solution at 200 and 300°C in equilibrium with quartz-muscovite-K-feldspar-albite and quartz-kaolinite-muscovite assemblages. Only uranium species contributing more than 1 mol% are shown.*

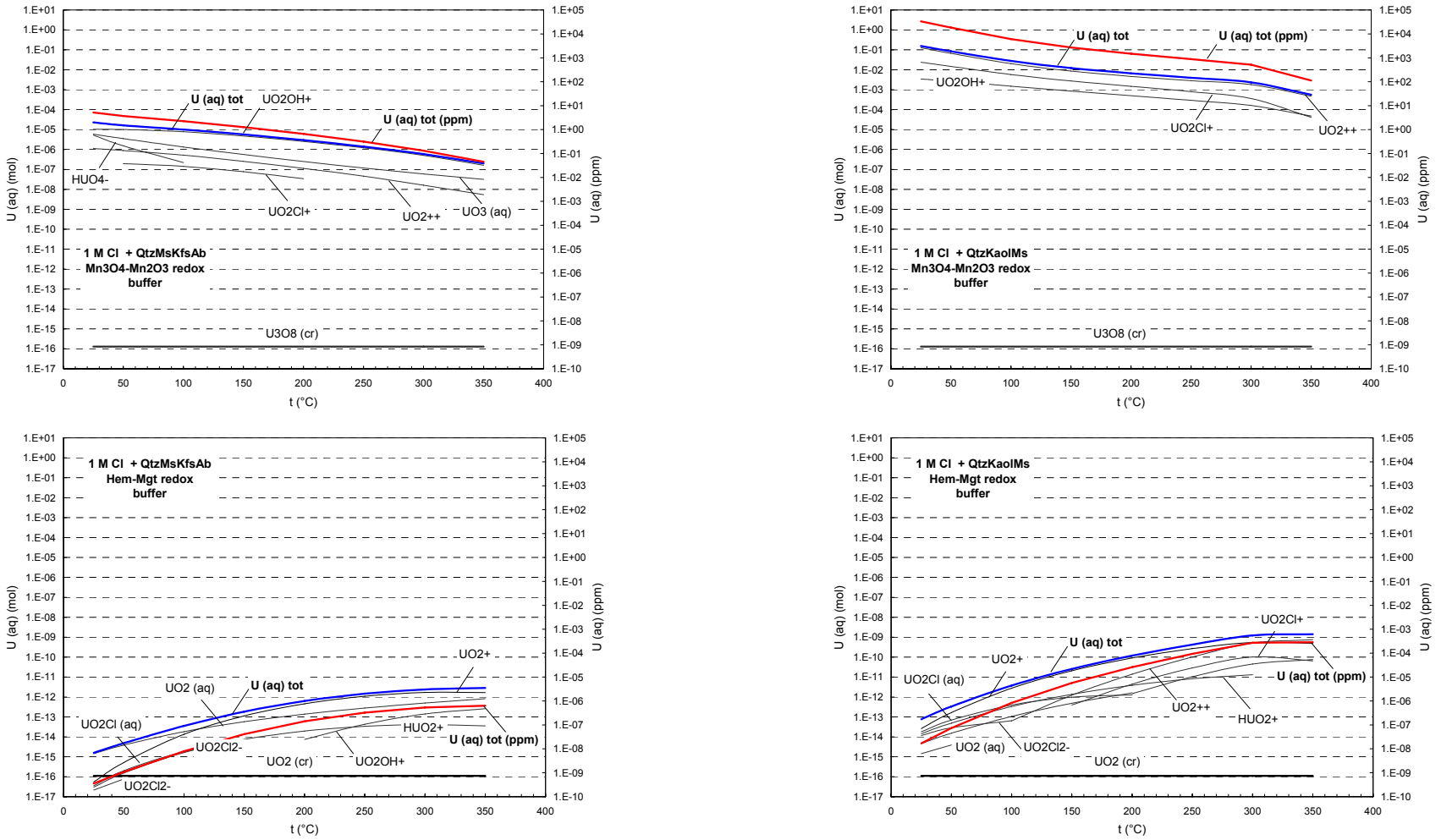

Figure 5.3: *Total uranium solubility and speciation in 1M total chloride solution with additional ligands in equilibrium with quartz-muscovite-K-feldspar-albite and quartz-kaolinite-muscovite assemblages along Mn_3O_4-Mn_2O_3 and hematite-magnetite redox buffers as a function of temperature.*

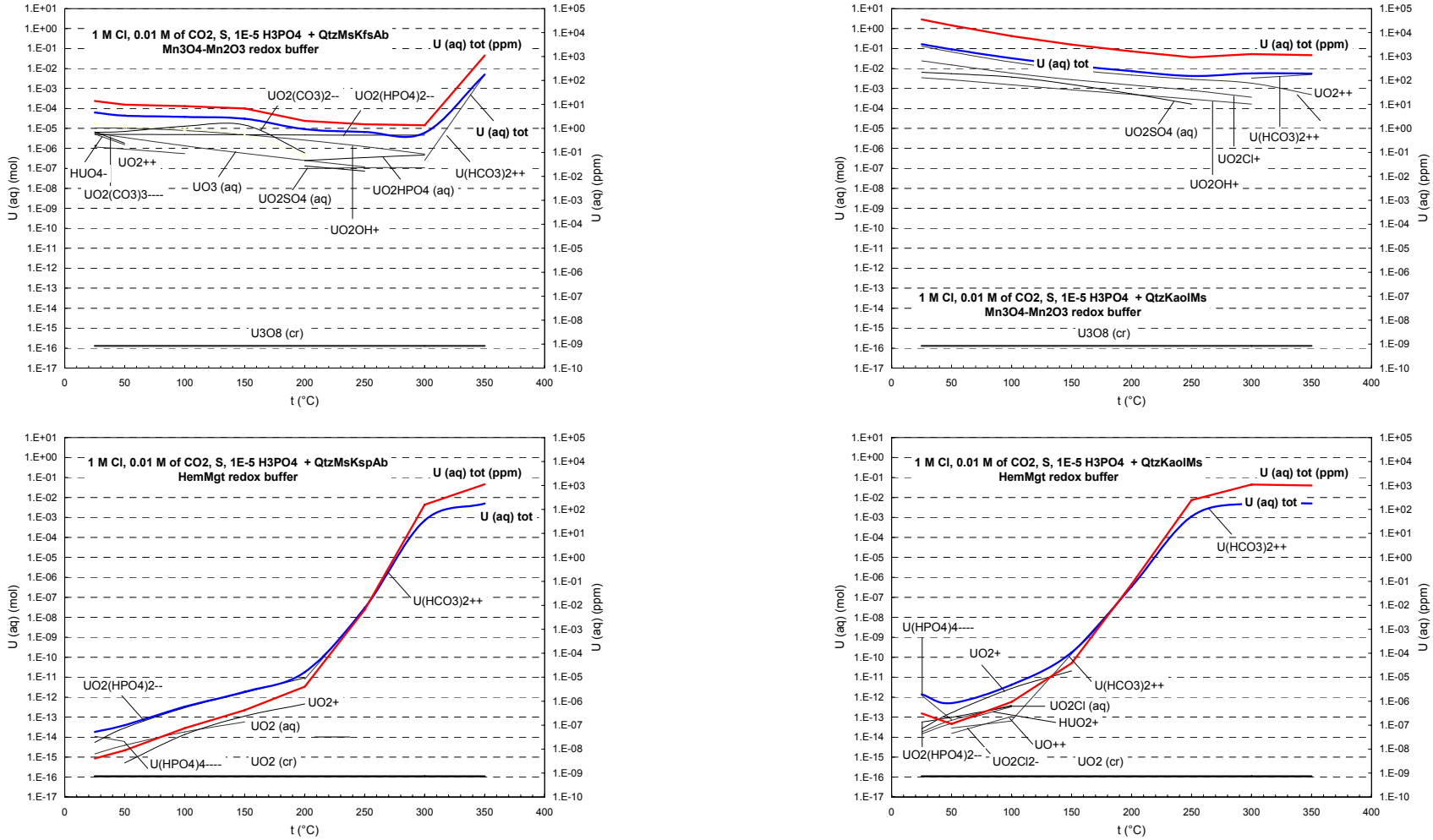

Figure 5.4:. *Total uranium solubility and speciation in 1M total chloride solution with additional ligands in equilibrium with quartz-muscovite-K-feldspar-albite and quartz-kaolinite-muscovite assemblages along Mn_3O_4-Mn_2O_3 and hematite-magnetite redox buffers as a function of temperature.*

Figure 5.4 examines the effect of other ligands – CO_3^{-2}, HCO_3^{-}, SO_4^{-2}, and PO_4^{-3} – on uranium solubility and speciation. The latter significantly elevate uranium solubilities. At Mn_2O_4-Mn_2O_3, buffer the speciation is mostly dominated by uranyl complexes, though the most stable of them can extend to lower redox values of the hematite-magnetite buffer ($UO_2(HPO_4)_2^{-2}$; Figure 5.4 (b)).

5.2.1 Uranium speciation and uncertainties in thermodynamic data

At temperatures around 300°C calculation of uranium speciation becomes somewhat problematic due to uncertainties in the thermodynamic data. In constructing the plots of the Figures 5.1 to 5.4, we have excluded the UCl_2^{+2} complex from consideration at temperatures above 50°C, as it completely dominates solubility diagrams and predicts unrealistically high uranium concentrations. Another potential problem is associated with bicarbonate complexes of U^{IV}, namely $UHCO_3^{+3}$ and $U(HCO_3)^{+2}$. Depending on oxidation state and pH, they dominate speciation and predict extremely high concentrations of uranium at temperatures higher than 150°C.

It should be noted that problems can be identified not only for the U^{IV} chloride and bicarbonate complexes. Even thermodynamic properties of UO_2^0 (aq), are, in fact, problematic. Shock et al. (1997) recommended thermodynamic properties of UO_2^0 (aq) based on solubility experiments by Parks and Pohl (1988). However, his combination of experimental results and theoretical predictions is highly inconsistent with low-temperature data recommended by NEA (Guillaumont et al., 2003) (see Chapter 2 and Figure 5.5).

If one adopts the thermodynamic properties of UO_2^0 (aq) recommended by Shock et al. (1997), uranium solubilities as U^{IV} at 300°C will be approximately 2.7 orders of magnitude higher compared to the values calculated based on the NEA data; in any case, the temperature dependence of the UO_2(cr) = UO_2^0 (aq) reaction is virtually non-existent and will not help to elevate further uranium concentrations at higher temperatures.

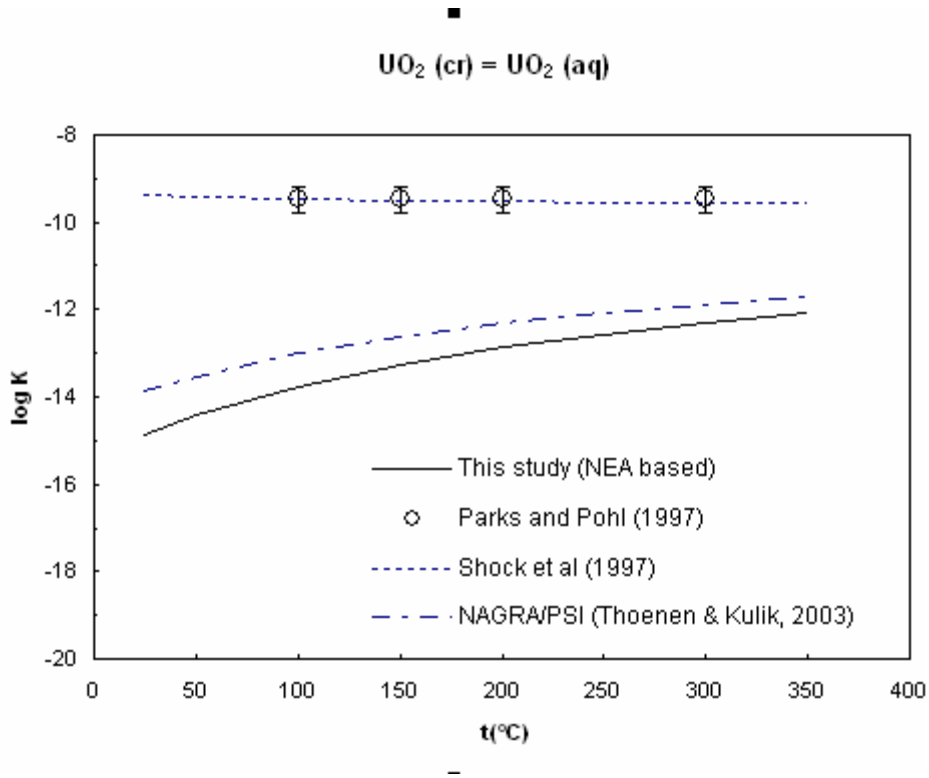

***Figure 5.5**: Comparison of UO_2^0 (aq) stability based on different sources of thermodynamic data.*

5.3 pH-fO_2 DIAGRAMS AT 300°C

Figure 5.6 further examines the effect of other ligands (CO_3^{-2}, HCO_3^-, SO_4^{-2}, and PO_4^{-3}) on the uranium solubility and speciation (compare to Figure 5.4). It displays calculated speciation for fluids of 1m and 3.65m chloride (equivalent to ~5.5 and 20 wt% NaCl). For the specified fluid composition, uranium solubility at 300°C (Fig. 5.6) is dominated by phosphate complexes at oxidised conditions and pH ranging from ~8 to 4. However at pH <4 the stability of the problematic U^{+4}-bicarbonate complex results in solubilities of >1ppm U at both reduced and oxidised conditions. In the absence of UCl_2^{+2} complex, increasing chlorinity from 1m to 3.65m has little effect on uranium solubility or speciation, though $UOCl_2^+$ dominates at highly oxidised and acid conditions.

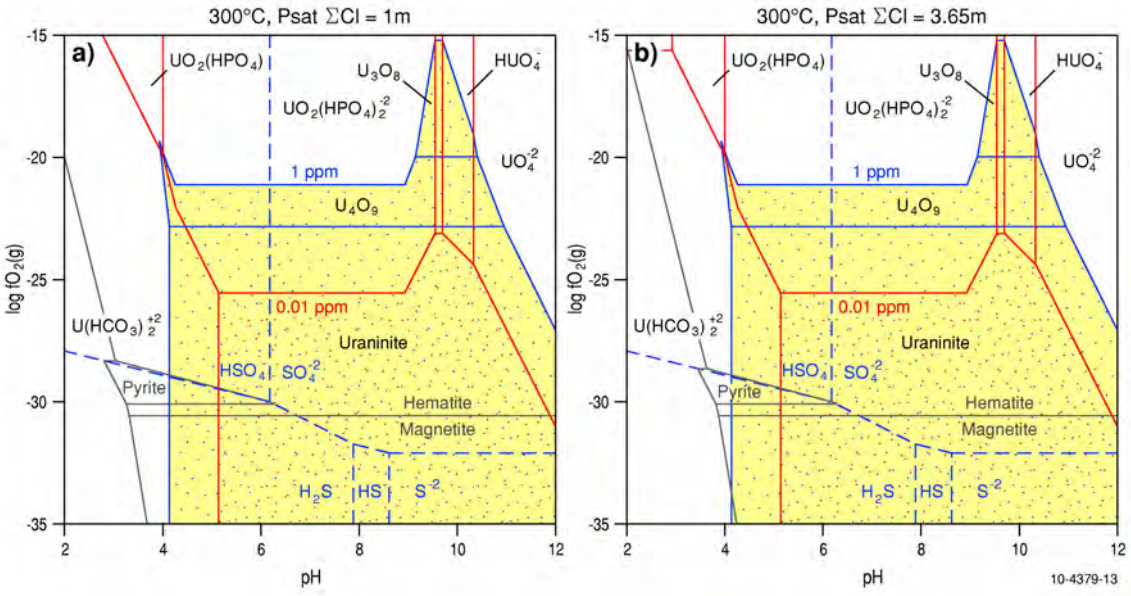

Figure 5.6: *Log fO_2-pH diagram at 300°C. Diagram calculated at Σ[Cl] = 1m (A) and 3.6m (B), respectively; Σ[C] = 0.001m, Σ[S] = 0.001m, Σ[P] = 1x10^{-5}m, Σ[F] = 1x10^{-4}m.*

6. Chemical modelling of selected uranium systems

6.1 URANIUM SYSTEMS ASSOCIATED WITH BASINAL FLUIDS

Calculations presented in the previous chapters show that at low to moderate temperatures (≤ 200°C) geologically important concentrations of uranium (~1 ppm) can be transported only in highly oxidised fluids unless the fluids are extremely acidic. Under more reduced conditions (with log fO_2 values less than those of the hematite/magnetite buffer), the fluid needs to be very acidic (pH <2) to transport a similar concentration (~1 ppm) of uranium. Sandstone- and calcrete-hosted uranium deposits are thus formed by a steady flow of shallow oxygenated ground waters through highly permeable aquifers. High permeability and active fluid recharge creates a fluid-flow regime in which the oxidation-reduction front between oxidised and reduced rocks progressively migrates through the aquifer. In such a fluid-flow regime the oxidation state of the uranium-bearing fluid may be maintained at a very high level, close to saturation with atmospheric oxygen.

Practical applications of generic calculations of uranium solubilities are limited by somewhat adhoc assumptions on the concentrations of ligands that control uranium complexing in natural waters and hydrothermal solutions. For further meaningful discussions, these calculations must be customised for particular mineral systems, including real rock and fluid compositions, and their evolution in space and time.

This chapter presents results of numerical modelling of the geochemical evolution of initially oxidised fluids recharging an intracontinental rift basins filled with sediments and subjected to red-bed style alteration. More precisely, the modelling is aimed at examining the meteoric water influx component of the fluid-flow model proposed for sediment-hosted stratiform copper deposits (Brown, 2003; 2005; 2006; 2009). According to this model, sands in an intracontinental rift basin undergo burial and diagenesis under conditions where the basin is continuously recharged by highly oxidised meteoric waters. The high salinity of fluids is derived from the dissolution of evaporites commonly associated with rift sediments. According to Brown (2006) and Walker (1989), the resulting oxidation of the consolidating sandstones, accompanied by their reddening, can leach copper into the fluid. It can be argued that similar alteration and dissolution of felsic minerals such as feldspars and micas and other accessory minerals such as epidote and monazite can also release uranium (Brown, 2006). Thus, our modelling was aimed at achieving the following tasks:

- Test the potential of a topographic recharge model (Brown, 2005) for generating fluids capable of transporting geologically important concentrations of uranium along with base metals;
- Explain the spatial and temporal zoning of uranium and base metal deposits commonly observed in many uranium districts;
- Assess the uranium potential of regions known for large sediment-hosted stratiform copper deposits.

.

6.1.1 Chemical modelling of topographically recharging fluid flow system

Numerical modelling of the geochemical evolution of fluids due to their infiltration in the sedimentary basin was completed in two independent steps.

Firstly, we examined the solubilities of base-metal and uranium minerals in simple closed-box fluid-rock systems open to oxygen. The chosen method is the same as the approach used for calculation of the solubility diagrams in Chapter 5, but with more realistic and complex compositions for the equilibrated rock and fluid. These simple models approximate the behaviour of metals in response to changing redox conditions and allow first-order prediction of metal ratios achievable in fluids with variable redox state.

Secondly, we have examined the spatial and temporal evolution of an oxidised fluid infiltrating a sedimentary basin using an equilibrium-dynamic model of "step-flow-through" reactors (Shvarov, 1999; Shvarov and Bastrakov, 1999).

Mass transfer calculations were performed with the HCh package for geochemical modelling developed at Moscow State University (Shvarov, 1999; Shvarov and Bastrakov, 1999). HCh was chosen because of its simplicity and flexibility for setting up various geochemical models (Shvarov, 1999; Shvarov and Bastrakov, 1999) and because of the very good numerical convergence for calculating equilibria in complex chemical systems. Also, it can calculate the compositions of coexisting fluids and mineral assemblages for temperatures up to 1,000ºC and pressures up to 500 Mpa. With HCh it is possible to simulate a broad range of geochemical processes such as liquid-gas-rock interaction (including infiltration metasomatism), fluid mixing, gas partitioning and boiling. The chemical equilibrium at each calculation step is computed using the Gibbs free energy minimisation approach. The up-to-date specifications of the package can be found at the Geoscience Australia website:

http://www.ga.gov.au/minerals/research/methodology/geofluids/HCh.jsp

In order to incorporate most of the minerals that occur in deposits associated with basinal fluids, the 22-component system Al-Ba-C-Ca-Cl-Cu-F-Fe-H-K-Mg-Mn-Na-O-P-Pb-S-Si-Ti-U-V-Zn was modelled.

Chemical modelling of fluid-rock interaction has been done for two separate fluids of ~ 5 wt% and ~ 20 wt% total salinity (Table 6.1). The first fluid represents a normal low-salinity basinal fluid (Hanor, 1994). The second fluid was chosen to understand the effect of higher salinity on the system. For both types of calculations we used the same rock composition. It represents a sandstone containing mafic and felsic silicates (Hanor, 1994 and Table 6.2). In these rock-fluid systems, at low fluid-rock ratios the pH is buffered by quartz-K-feldspar- muscovite-albite/paragonite assemblages

Table 6.1: Composition of fluids used in the calculation (in moles/Kg)

Component	Fluid 1(Concentration, moles/kg)	Fluid 2 (Concentration moles/kg)
NaCl	0.9	3.6
KCl	0.004	0.016
$CaCl_2$	0.073	0.29
$MgCl_2$	0.01	0.04
$FeCl_2$	0.001	0.004
H_3PO_4	0.00001	0.0004
H_2S	0.001	0.001
Total salinity	~ 5 wt%	~ 20 wt%

Table 6.2: Composition of sandstone with mafic minerals (in wt%)

Mineral	Concentration (wt%)
Quartz	70.09
Microcline	0.79
Albite	1.97
Anorthite	1.04
Hedenbergite	0.29
Ferro-anthophyllite	0.49
Muscovite	11.37
Annite	0.29
Epidote	3.06
Chamosite	2.41
Illite	1.96
Kaolinite	0.58
Calcite	1.97
Dolomite	0.02
Siderite	0.01
Ilmenite	0.03
Magnetite	0.91
Pyrite	0 (3.54)*
Galena	0.012 (~ 100 ppm Pb)
Sphalerite	0.015 (~ 100 ppm Zn)
Chalcopyrite	0.030 (~ 100 ppm Cu)
Uraninite	0.005 (~ 45 ppm U)

* wt% of pyrite used for calculations involving pyrite-rich sandstone

6.1.1.1 Solubility of uranium, copper, zinc and lead

The first set of calculations estimate the solubility of uranium, copper, lead and zinc in a fluid (~ 5wt% total salinity) in equilibrium with the unaltered sandstone (Table 6.2) at a fluid to rock ratio of 1:1. The calculations show that, like uranium, the solubility of copper, zinc and lead also depend on the oxidation state of the fluid (Figs. 6.1A and 6.1B). At both 25°C and 100°C the solubility increases rapidly with an increase in fO_2. At fO_2 levels corresponding to Mn_3O_4/Mn_2O_3 buffer the fluid can dissolve between 10 and 100 ppm uranium and more than 1000 ppm copper, zinc and lead. The solubility of all metals drops rapidly as fO_2 approaches the level of hematite-magnetite buffer, falling well below 1 ppb.

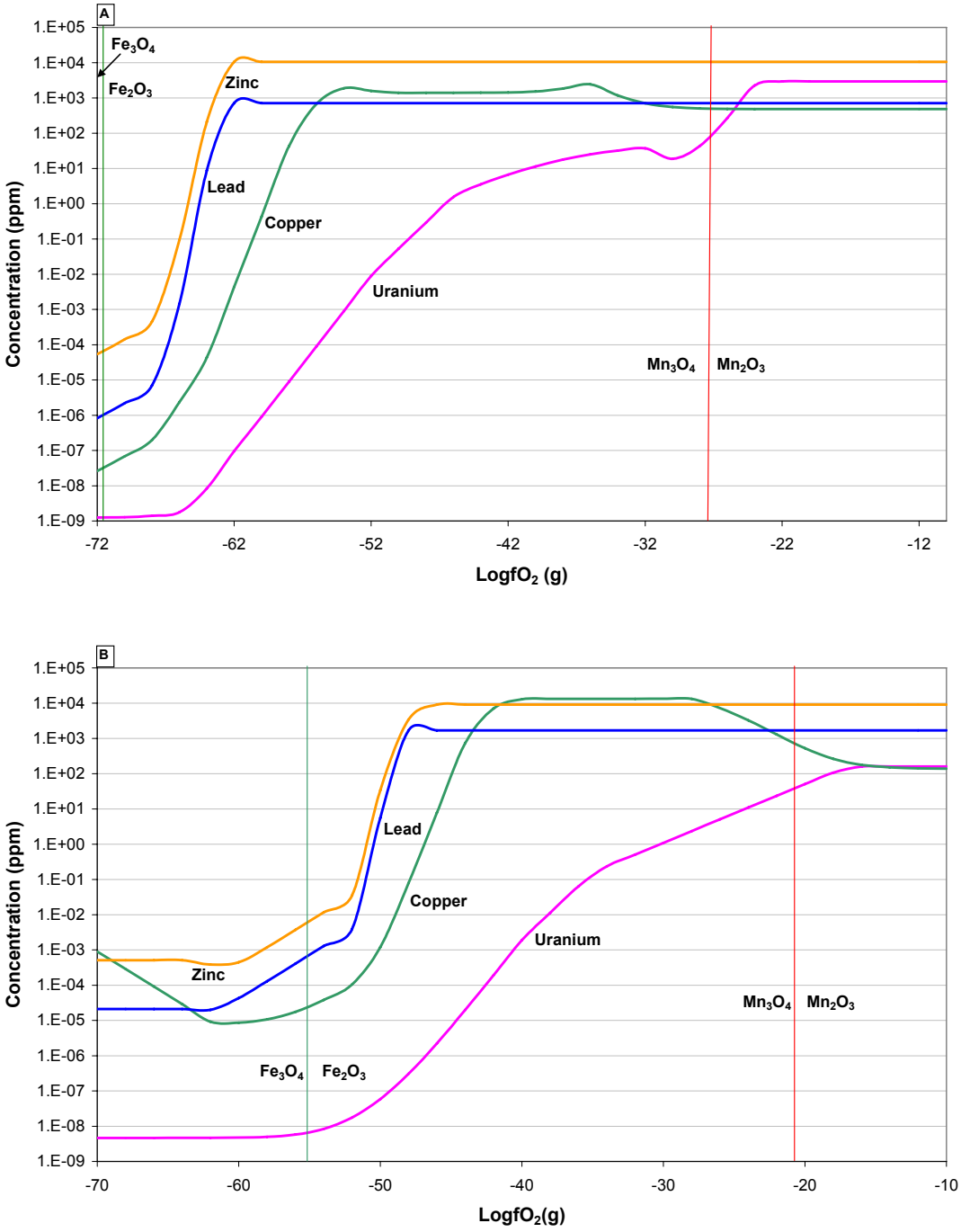

***Figure 6.1**: Diagrams showing solubility of uranium, copper, lead and zinc in a 5 wt% NaCl fluid in equilibrium with quartz-K-feldspar-muscovite-albite/paragonite assemblage as a function of oxidation state. (A) 25°C; (B) 100°C. Vertical straight lines labelled Fe_3O_4/Fe_2O_3 and Mn_3O_4/Mn_2O_3 show fO_2 levels corresponding to these buffers at 25°C and 100°C.*

The diagrams also help to predict the behaviour of uranium, copper, zinc and lead in various types of fluid-rock reactions. For instance, if an oxidising fluid reacts with a rock it will leach zinc first followed by lead, copper and uranium. Similarly if an oxidised fluid containing uranium, copper,

zinc and lead reacts with a reduced rock uranium will be precipitated first, followed by copper, lead and zinc.

The sequential dissolution and precipitation of uranium, copper, lead and zinc as a function of the oxidation state can, in many cases, explain the metal and mineral zoning observed in many districts with unconformity-related uranium (e.g. Rum Jungle Uranium Field) and sediment-hosted stratiform copper (e.g. Central African Copper Belt).

6.1.1.2 Chemical modelling of fluid-rock reactions in a recharging fluid flow system

The spatial and temporal evolution of an oxidised fluid infiltrating a sedimentary basin was modelled using the "step-flow-through-reactor" technique in terms of HCh terminology (e.g., Shvarov and Bastrakov, 1999). The adopted methodology is similar to "flush" models reviewed by Bethke (2007). In the "step-flow-through-reactor" model, successive batches of a fluid react with batches of rock along a postulated fluid-flow line ("stream pipe"), evolving in composition as they pass through the system and displace the preceding fluid batches from the subsequent reactors.

This modelling technique allows tracking of the temporal evolution of the system at a particular point in space, with time being proportional to the number of fluid batches that entered the system (or "waves", using HCh terminology) and the spatial evolution of the system along the fluid path for a particular time slice. Detailed discussion of the application of the "step-flow-through-reactor" technique to modelling of infiltration metasomatism is provided by Shvarov (2000).

A hypothetical hydrothermal system is assumed to recharge at highlands at the surface in equilibrium with atmospheric oxygen and carbon dioxide at 25°C (Fig. 6.2). To represent progressive heating of the fluid-rock system along the fluid infiltration path, the temperatures of the subsequent reactors (stages) are increased stepwise (Fig. 6.2).

The initial composition of the fluids and sandstone are shown in Tables 6.1 and 6.2. At the first fluid-rock equilibration step at 25°C, the system is open to the atmospheric oxygen and carbon dioxide (i.e., fO_2 and fCO_2 are fixed). The fluid to rock ratio at this step is 1:1. After the initial equilibration, the fluid reacts with a fresh batch of sandstone at a higher temperature (increasing by 25°C at each step) until the temperature reaches 200°C. At each temperature step, 1 kg of fluid reacts with 0.1 kg of rock (i.e. the "instantaneous" fluid to rock ratio is 10:1). At these steps, the redox conditions within the fluid-rock reactors are controlled by chemical reactions in the fluid-rock system.

At each temperature the same batch of rock interacts with a fresh batch of oxidising fluid, causing the rock to oxidise (Fe^{+2}-bearing silicates are replaced by magnetite and hematite) and change to a red (oxidised) sandstone (Fig. 6.3). The first reaction between the fluid and the rock causes the oxidation state of the fluid to drop (point 1 on Fig. 6.3) but as more and more Fe^{+2}-bearing silicates are oxidised the capacity of the rock to reduce the fluid diminishes and after it has been completely oxidised, the fluid is able to pass through it keeping intact its initial very high oxidation state (see the abrupt shift in the blue line at the boundary between partly red bed sandstone and red bed sandstone on Fig. 6.3).

Figures 6.4A and 6.4B show changes in the concentration of total uranium, copper, lead and zinc in the fluid as successive batches of the oxidised fluid react with the unaltered sandstone at 75°C and

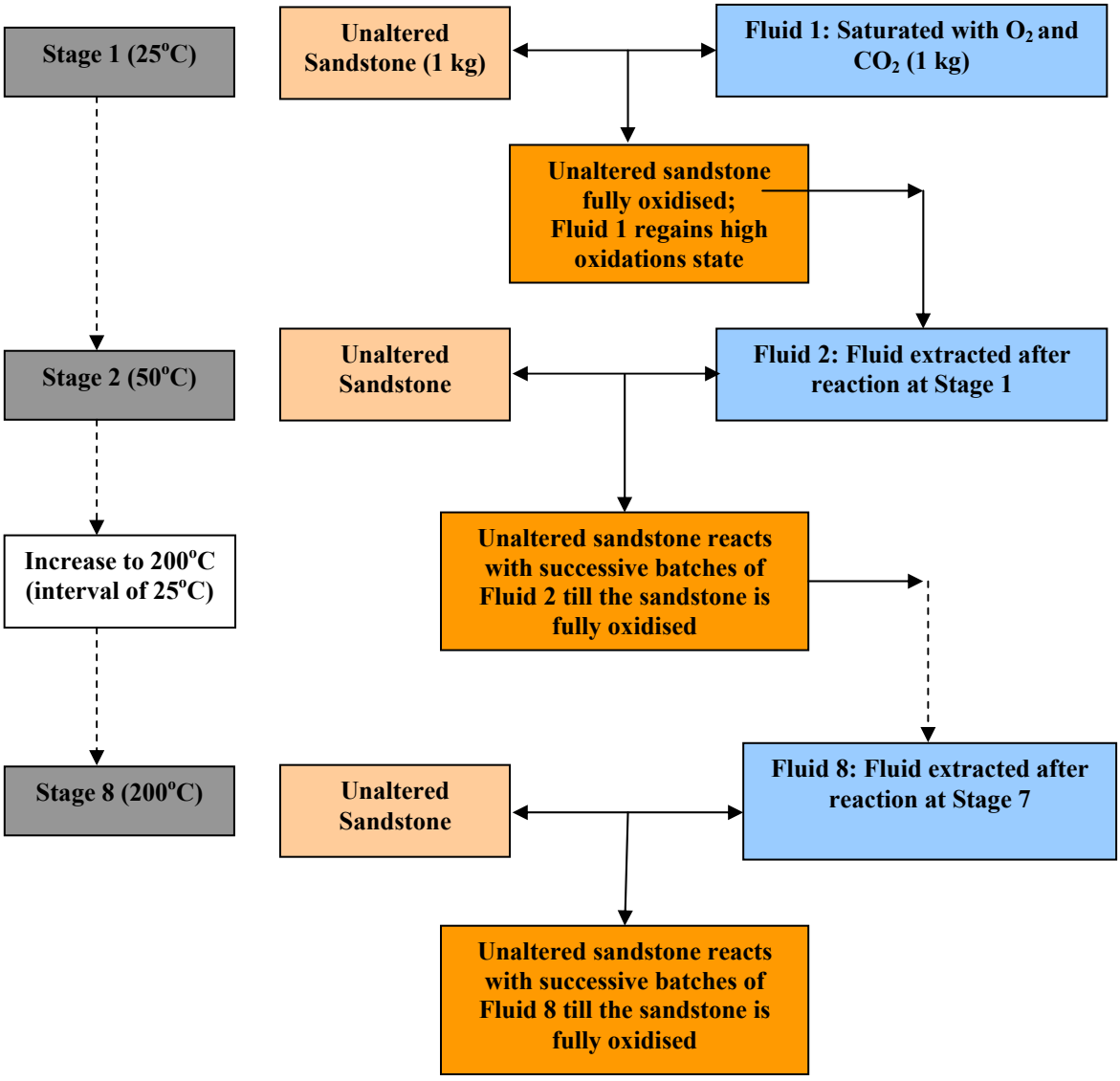

Figure. 6.2*: Flow-chart showing stages in the modelling of fluid-rock reactions discussed in this study. At each temperature interval the unaltered sandstone is reacted with fully oxidised fluid from the previous step until the sandstone is fully oxidised. See text and Figures 6.3 and 6.4 for details.*

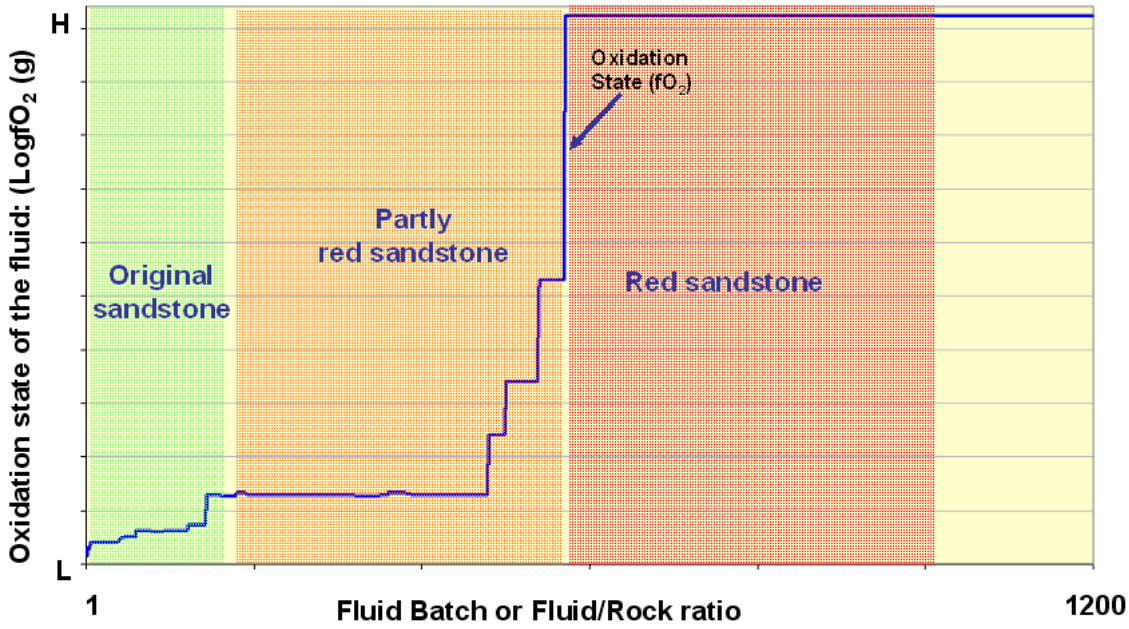

***Figure 6.3**: Schematic diagram showing change in the oxidation state of the fluid and rock at a fixed temperature. Letters 'L' and 'H' on the y-axis denote low and high states of oxidation.*

100°C respectively. The concentration of zinc in the fluid reaches a maximum of 350 ppm after ~40 batches (fluid:rock ratio of 400:1) of the fluid have reacted with the rock (Fig. 6.4A). At this point all zinc in the rock (as sphalerite) is dissolved. Lead reaches the maximum of ~240 ppm at the fluid to rock ratio of ~1800, followed by copper (~80 ppm) at the fluid to rock ratio of ~1900. Uranium which requires the highest oxidation level to dissolve reaches a maximum of ~275 ppm at a fluid to rock ratio of ~3800. At around a fluid to rock ratio of 4000 the sandstone is completely oxidised and the fluid which reacts with it thereafter retains its initial high oxidation state.

The pattern of sequential leaching of zinc, lead, copper and uranium is repeated at 100°C (Fig. 6.4B). The only significant difference is that at 100°C the complete dissolution of zinc, lead , copper and uranium occurs at higher fluid to rock ratios than at 75°C , i.e., at 100°C the rock requires interaction with more fluid to be fully oxidised (i.e. a fluid to rock ratio of ~6000 at 100°C compared to ~4000 at 75°C).

The progressive fluid-rock reaction also changes the mineral composition of the rock. Figures 6.5A and 6.5B show changes in the concentration of uranium oxides (including uraninite) and copper sulphides (chalcopyrite and bornite). At 75°C as the same portion of the rock reacts with successive batches of oxidised fluids carrying uranium and copper, the concentration of copper sulphides in the rock gradually increases reaching a maximum of ~0.4 wt% (Fig. 6.5B). After reaching a fluid to rock ratio of ~2000 the sulphides begin to dissolve as oxidation state rises and at a fluid to rock ratio of ~2500 the sulphides undergo complete dissolution. The fluids remain saturated with respect to tenorite (CuO), the concentration of which reaches a maximum (~0.1 wt%) at a fluid to rock ratio of ~4500 after which it too dissolves completely. Oxides of uranium precipitate as soon as the fluid reacts with the rock and reach a maximum of ~4 wt% at a fluid to rock ratio of ~3800, after which they begin dissolving. When the rock is completely oxidised and the inflowing fluid begins to retain its initial oxidation state (at a fluid to rock ratio of ~4000) the uranium oxides are completely leached out of the sandstone.

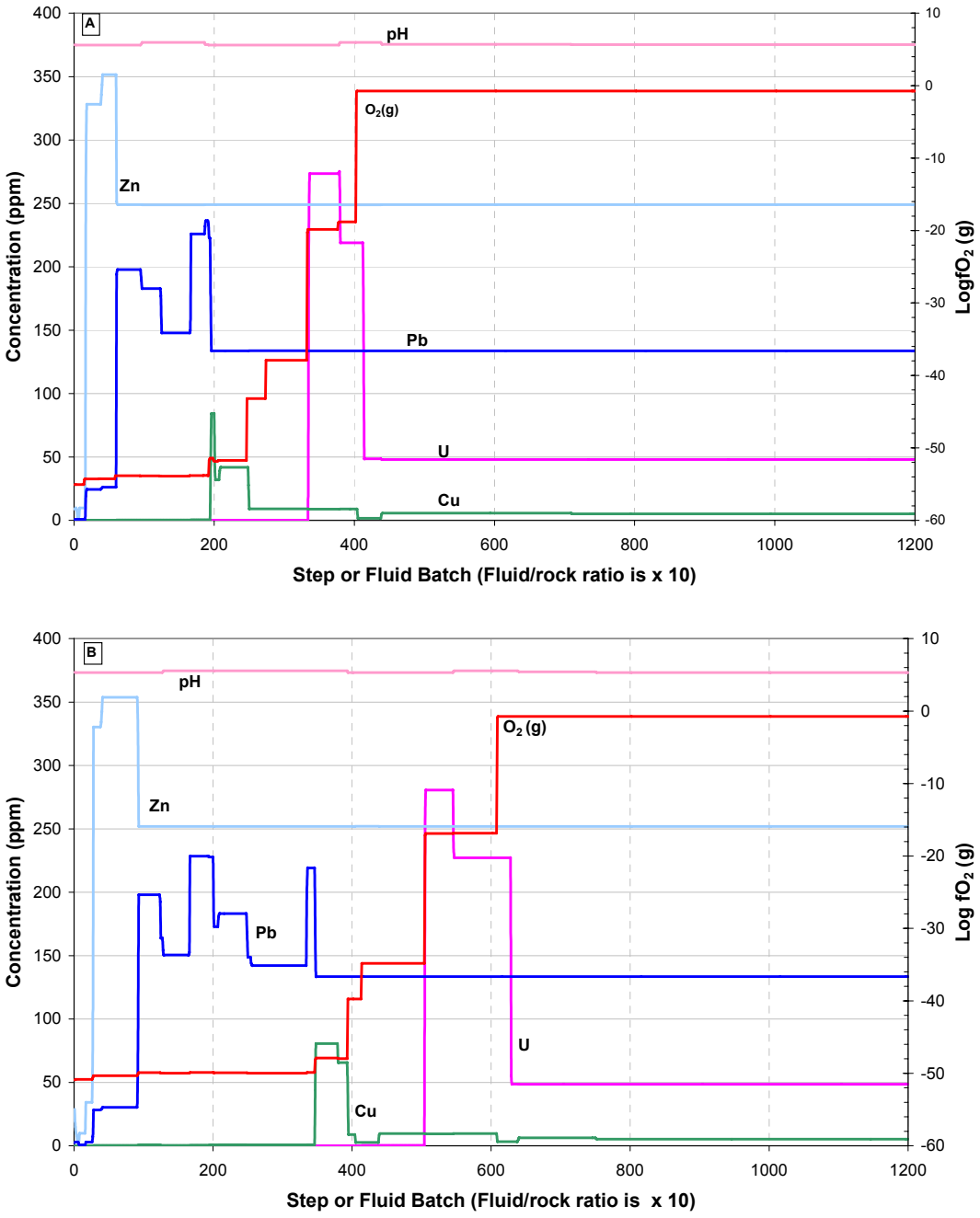

Figure 6.4: *Change in the concentration of uranium, copper, lead and zinc in a fluid with a salinity of 20 wt% NaCl as successive batches of the fluid react with sandstone containing mafic minerals at 75°C (A) and 100°C (B). See Tables 6.1 and 6.2 for the initial composition of fluid and rock. The x-axis gives the number of the fluid batch reacting with the rock. . The fluid to rock ratio is ten times higher than the step number because at each step 1 kg of fluid reacts with the same 0.1 kg of the rock.*

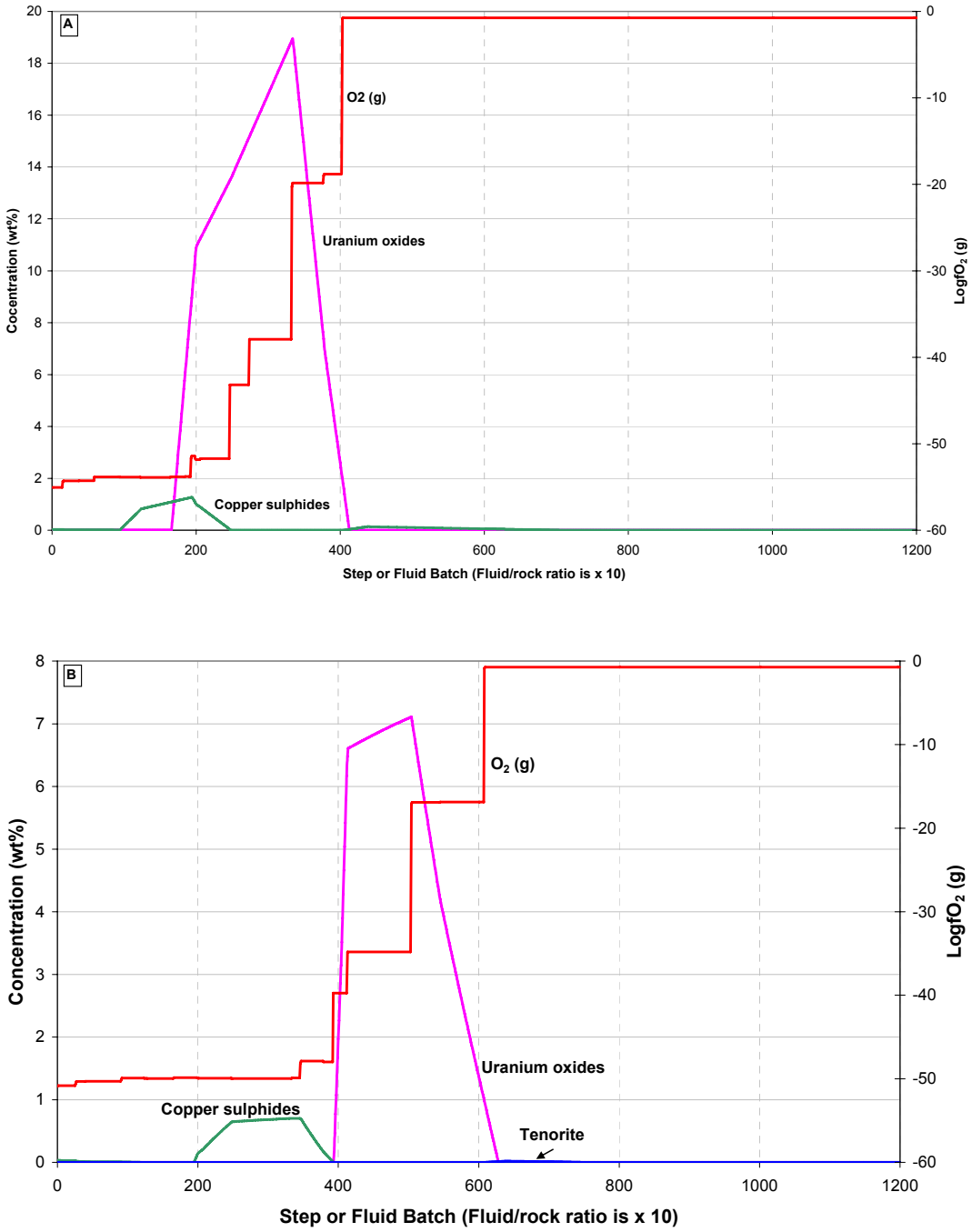

Figure 6.5: *Change in the concentration of uranium oxides and copper sulphides (chalcopyrite and bornite) formed in the sandstone as it reacts with successive batches of a fluid with a salinity of 20 wt% NaCl. (A) : 75°C ; (B) 100°C. See Tables 6.1 and 6.2 for the initial composition of fluid and rock. The x-axis gives the number of the fluid batch reacting with the rock. The fluid rock ratio is ten times higher as at each step 1 kg of fluid reacts with the same 0.1 kg of the rock.*

The above pattern is repeated at 100°C (Fig. 6.5B) with two significant differences:

- Precipitation and complete dissolution of copper and uranium minerals occurs at higher fluid to rock ratios;
- The maximum concentration of copper and uranium minerals precipitated in the reaction is higher; ~0.8 wt% for copper and ~7 wt% for uranium.

The effect of salinity of the initial fluid on the fluid-rock reaction is shown in Figures 6.6A and 6.6B. These figures also show the effect of the increased concentration of pyrite in the unaltered sandstone. In Fig. 6.6A, the salinity of the fluid is 4 times less than in Fig. 6.6B but the unaltered sandstone contains pyrite (3.54 wt%, Table 6.2), whereas in Fig. 6.6B the fluid is more saline (20 wt% NaCl) but the unaltered sandstone does not contain pyrite. The changes in salinity and in the concentration of pyrite in the unaltered sandstone do not alter the overall pattern of oxidation-reduction reactions; the sequence in which the elements reach their maximum concentration (zinc, lead, copper and uranium) does not change. However the fluid to rock ratio at which this occurs changes slightly, with a fluid of higher salinity requiring higher fluid to rock ratios. The most significant difference, however, is the maximum concentrations reached by these elements in the two cases. A reaction of a 20 wt% NaCl fluid with a sandstone without pyrite produces a fluid with a containing ~80 ppm copper and ~280 ppm uranium, whereas a fluid with lower salinity reacting with a sandstone rich in pyrite causes the concentration to rise to ~500 ppm copper and ~1200 ppm uranium. Thus the presence of pyrite in the unaltered sandstone has a more significant effect on the meta solubilities than does a change in the initial salinity of the fluid.

The influence of increased concentration of pyrite in the unaltered sandstone is also reflected in the pH of the fluid. The presence of pyrite lowers the pH of the fluid by one and a half units (from ~5.8 to ~4.2). This is because dissolution of pyrite produces a fluid richer in SO_4^{-2}, the presence of which makes uranyl sulphate complexes more stable. In a fluid with high salinity but no pyrite in the unaltered sandstone, the hydroxy complexes of uranium are predominant. The increased concentration of copper in a fluid reacting with pyrite-rich sandstone is also the result of the lower pH of the fluid. Under such conditions tenorite (CuO) is not stable which causes an increase in the concentration of dissolved copper.

Figure 6.7 shows the results of fluid-rock interaction at 200°C. Although most sediment-hosted stratiform copper deposits are formed at temperatures close to 100°C (Hitzman et al., 2005), the calculations at 200°C provide some information to test if a topographically recharging fluid-flow can explain transport of uranium in unconformity-related uranium systems, where diagenetic fluids often reach temperatures close to 200°C. These calculations show that in general at 200°C the fluid-rock reactions follow the same pattern as at lower temperatures, reaching similar maximum concentrations of metals. However the fluid to rock ratios required at 200°C are much higher than at 100°C. For example, complete oxidation of the sandstone at 200°C occurs at a fluid to rock ratio of ~12,000 whereas at 100°C the required ratio is ~6000.

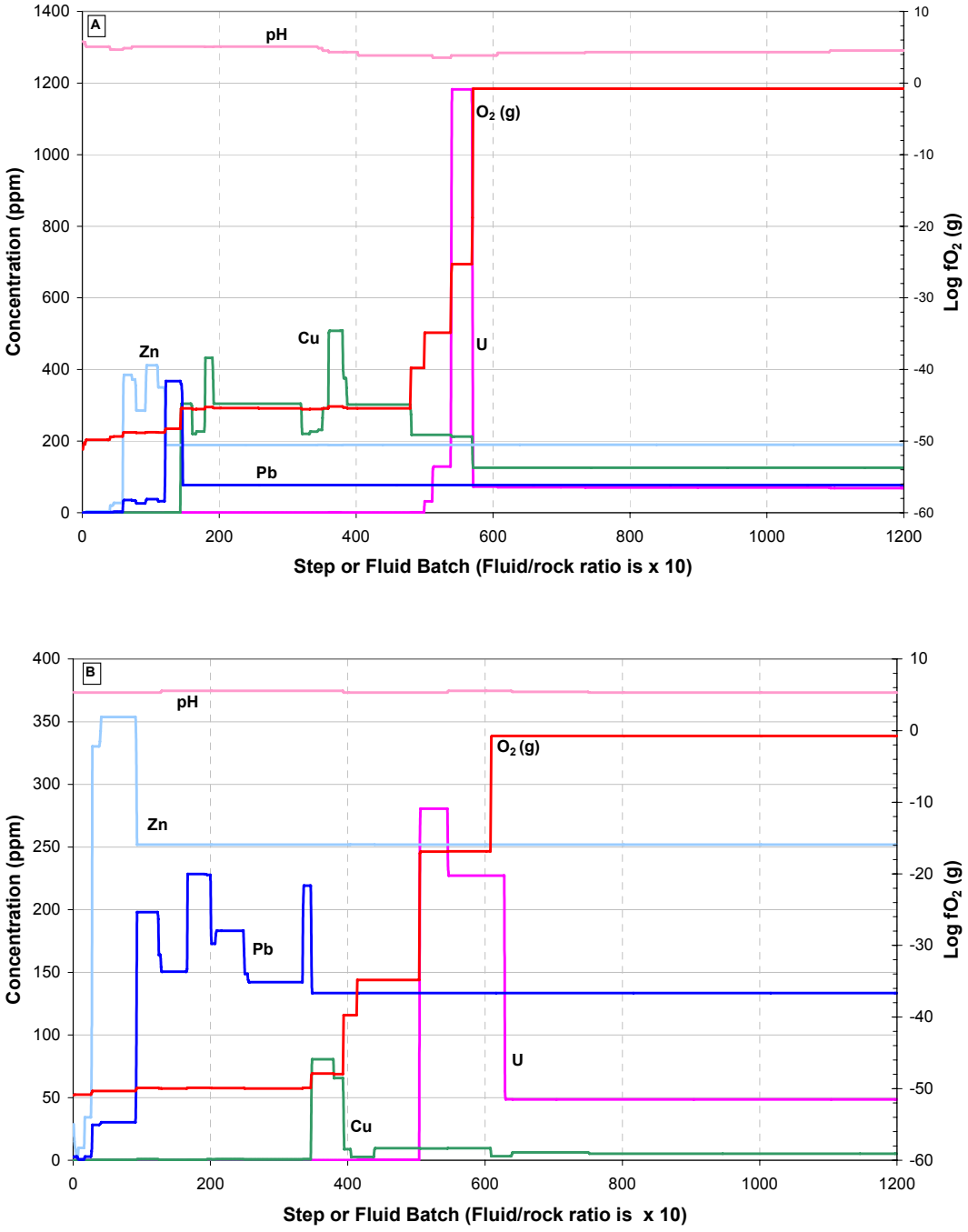

Figure 6.6: *Effect of pyrite in the sandstone on the concentration of metals in a fluid as successive fluid batches react with the same sandstone at 100°C. (A) 5 wt% NaCl fluid; unaltered sandstone with 3.5 wt% pyrite; (B) 20 wt% NaCl fluid; no pyrite in unaltered sandstone. The presence of pyrite outweighs the effect of increased salinity; although the fluid is 4 times less saline (Fig, 6.6A), the increased amount of pyrite lowers the pH of the fluid and makes the sulphate complexes of uranyl more dominant which increases the concentration of uranium in the fluid (~ 1200 ppm vs ~280 ppm). See Tables 6.1 and 6.2 for the initial composition of fluid and rock. To read pH values, use the additional right-hand y-axis above the logfO_2 (g) axes.*

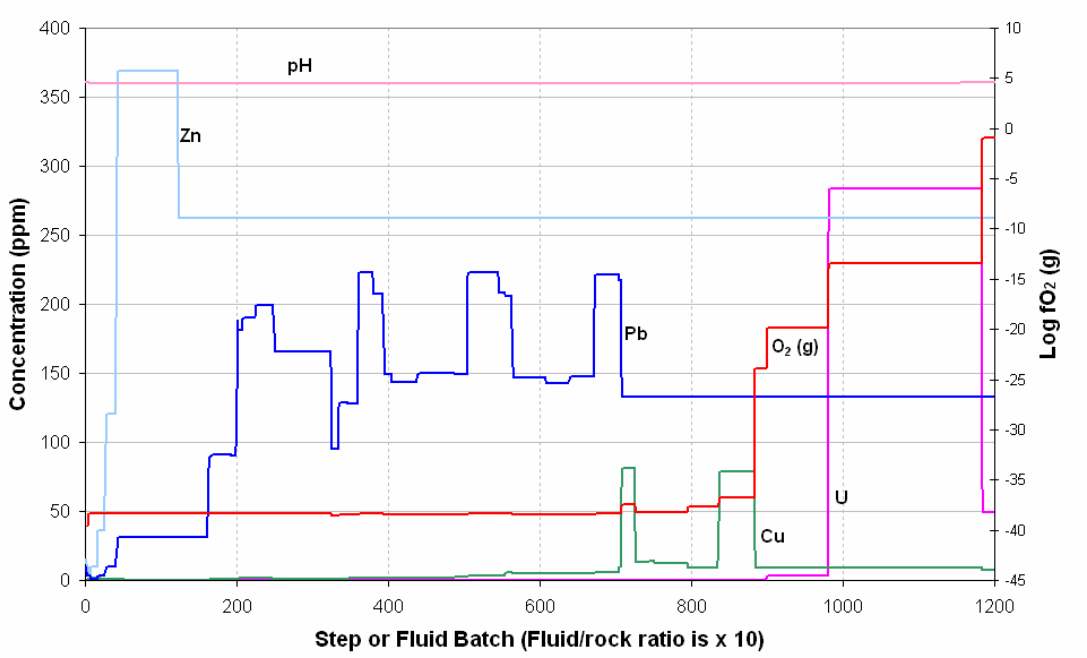

Figure 6.7: *Change in the concentration of uranium, copper, lead and zinc in a fluid with a salinity of 20 wt% NaCl as successive batches of the fluid react with sandstone containing mafic minerals at 200°C. See Tables 6.1 and 6.2 for the initial composition of fluid and rock. The x-axis gives the number of the fluid batch/step reacting with the rock. The fluid rock ratio is ten times higher as at each step 1 kg of fluid reacts with the same 0.1 kg of the rock. To read pH values, use the additional right-hand y-axis above the logfO_2 (g) axes*

6.1.2 Discussion and summary

Chemical modelling of topographically recharging fluid-flow in a basin reveals that geologically important concentrations of uranium, copper, lead and zinc can be successfully transported to the site of metal deposition. The main modelling results can be summarised as follows.

The behaviour of uranium, copper, zinc and lead in these fluids is dominantly controlled by the oxidation state of the fluid and the rock. In this system of fluid-rock interaction, zinc is the first ore forming element extracted from the sandstone source followed by lead, copper and uranium.

An unaltered sandstone initially containing 100 ppm each of copper, lead, and zinc and 45 ppm uranium, on reacting with successive batches of oxidised fluid can generate a fluid with ~350 ppm zinc, ~220 ppm lead, ~80 ppm copper and ~280 ppm uranium at various fluid to rock ratios at 25ºC. In these calculations we have assumed the same sandstone to be the source of all four ore forming elements. Geologically this is not very likely. Hence the presence of an appropriate source rock is essential for a fertile system for that deposit (uranium or copper) to function. In some cases the same basins may have different but spatially close (e.g. interlayered beds of felsic or mafic rocks) source rocks. In such situations a favourable fluid-flow regime is essential to extract different elements from different source rocks. Although spatial zoning between uranium and base metals (particularly copper, see below a discussion on the Westmoreland field) has been observed in many mineralised districts, it is relatively rare to find large uranium deposits present in a dominantly base metal district and or large base metal deposits in uranium districts. To some extent this may be related to the presence or absence of a suitable metal source.

Ore forming elements reach their maximum concentration in the fluid at different fluid to rock ratios. Thus if the fluid flow is stopped (caused, for example, either by tectonic activity and/or by a drop in the permeability of the sandstone aquifer) after reaching a fluid to rock ratio of ~3800 (Fig. 6.4b) the fluid will be rich in zinc (~250 ppm), lead (~140 ppm) and copper (~80 ppm, its maximum concentration), with very little uranium. This fluid, when released from the basin, if allowed to react with a reductant (e.g., carbonaceous shale) will form a base metal ore zone with little or no uranium. On the other hand if the fluid flow is maintained and reaches the fluid to rock ratio of ~4500, the fluid will be rich in uranium (~280 ppm), zinc (~250 ppm), lead (~140 ppm) with very little copper (< 10 ppm). Reduction of this fluid will result in the formation of a uranium-rich ore zone with lead and zinc but very little copper. Thus, the fluid flow regime in the basin (where and when it stops and restarts) will determine the mineral composition of the ore zone (uranium-rich against uranium poor). Some of the factors which can control the fluid flow regime in the basin include: variation in the permeability (primary and secondary) in the aquifer; and changes in the hydraulic head at the basin margin caused by periodic tectonic activity.

Very high fluid to rock ratios are required to achieve complete oxidation of the sandstone after which the fluid can flow through it unreduced. The ratios are ~4200 at 75^{o}C, ~6000 at 100^{o}C, and ~12000 at 200^{o}C. There are no model-independent or directly measured estimates of fluid to rock ratios in basins. Swenson et al. (2004) estimated a cumulative fluid to rock ratios of ~3200 over time (25 Ma)) for basins hosting red bed copper deposits in North Michigan. Theoretically, for artesian basins with a flow rate of 1m/year a cumulative fluid to rock ratio of 500,000 can be achieved over one million years. It is not clear if such fluid flow rates are achieved in topographically recharging basins. However the high fluid to rock ratios provide a critical constraint for a fertile mineral system to operate in such basins, which means that aquifers with extremely high permeability (primary and secondary) will be favourable for uranium mineralisation.

Zones enriched in base metals and uranium are formed in the aquifer as topographically recharging fluid moves in it, causing oxidation (Fig. 6.6A and 6.6B). At 75^{o}C, a uranium-rich zone containing up to 4 wt% uranium oxides may be formed. At 100^{o}C the zone can contain up to 7 wt% uranium oxides. Copper-rich zones contain less than 1 wt% Cu at the two temperatures.

However both uranium- and copper-rich zones are destroyed by further reaction with subsequent batches of oxidised fluid (i.e. at fluid to rock ratios of ~4000 at 75^{o}C and ~6000 at 100^{o}C). The preservation of these zones depends on the fluid flow regime in the basin and requires cessation of fluid flow after reaching a particular value. In basins with red bed copper deposits it is therefore possible to expect uranium-rich zones in the aquifer (Fig. 6.8). Such uranium-rich zones have been described in a number of sediment hosted copper deposits in the Central African Copper Belt (Unrug, 1988).

In basins with topographically recharging meteoric water, the fluids can transport up to ~280 ppm uranium at temperatures (~200^{o}C) relevant for basinal fluids involved in unconformity-related uranium systems. Thus a topographically recharging model provides a favourable scenario for unconformity-related systems. The source rock in these calculations contained 45 ppm uranium, which means that the fluid-flow system caused ~5.5 times enrichment (i.e. increased from 45 ppm to 250 ppm in the fluid). If fluviatile sandstone on an average contains between 3 to 5 ppm uranium, the fluid-flow system outlined above can potentially generate fluids bearing up to 25 ppm uranium.
The presence of pyrite in the unaltered sandstone has a far more significant effect on the solubility of ore forming elements than the salinity of the initial fluid. Oxidation of pyrite-rich sandstone generates more acidic fluids dominated by SO_4^{-2} which forms stable complexes with uranium and

the maximum concentration of the uranium increases to ~1200 ppm (Fig. 6.6A). In more acidic fluids tenorite is not stable which increases the solubility of copper in the fluids (Fig. 6.6B).
The presence of evaporitic beds in the basin is a critical element of fertile systems. They are essential to generate fluids with salinities (5 to 20 wt% NaCl) assumed in these calculations.

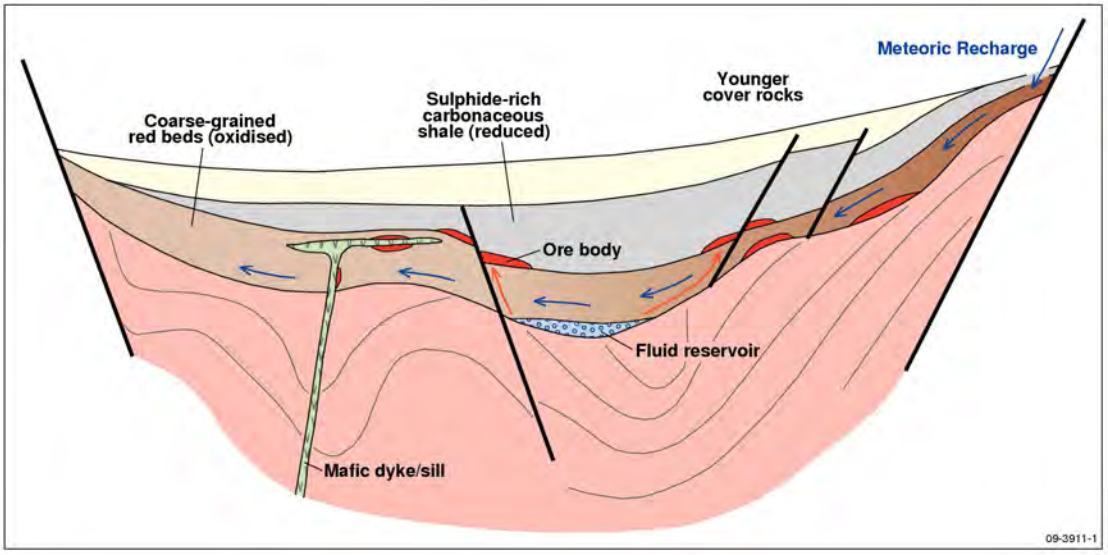

***Fig. 6.8**: Schematic diagram showing the possible location of uranium-rich zones (red zones labelled orebody) in a red bed sandstone aquifer in the presence of topographically recharging meteoric waters.*

6.2 WESTMORELAND URANIUM-COPPER SYSTEM

The above modelling of topographically recharging fluid-flow in a generalised sedimentary basin suggests that geologically significant quantities of uranium, copper, lead and zinc can be transported in oxidised basinal brines under conditions similar to those occurring in unconformity-related systems. However, in order to verify this, it is necessary to constrain the modelling with parameters from a real geological system. Therefore, we have chosen to model the Westmoreland unconformity-related system as this region contains a number of uranium and copper deposits.

The Westmoreland uranium-copper system is located near the south-eastern margin of the Paleoproterozoic-Mesoproterozoic McArthur Basin. There are at least 50 uranium and copper prospects of various size and grade in the Westmoreland region (Ahmad and Wygralak, 1990), but the three largest uranium deposits are Redtree, Huarabagoo and Junnagunna (Fig. 6.9). These three deposits have a collective inferred and indicated resource of 23.6 kt U_3O_8 (Laramide Press Release 23/04/2009). The copper prospects are small and subeconomic and occur as veins in the host rocks. Tin deposits also occur in the region but are thought to be related to magmatic fluids and are not considered further in this study.

6.2.1 Geology of the Westmoreland System

The oldest rocks in the Westmoreland region are Paleoproterozoic quartz-feldspar-mica schists and gneisses of the Murphy Metamorphics (not shown in Fig. 6.9), which are only exposed in the Northern Territory. These metamorphics are essentially a sequence of shale, siltstone, greywacke

and volcanics deposited in geosynclinal conditions and metamorphosed to greenshcist facies, now consisting of quartz-albite-muscovite±biotite schist and gneiss. U-Pb data from detrital zircons suggests a maximum depositional age of 1853 ± 4 Ma for the Murphy Metamorphics (Wygralak and Mernagh, 2009).

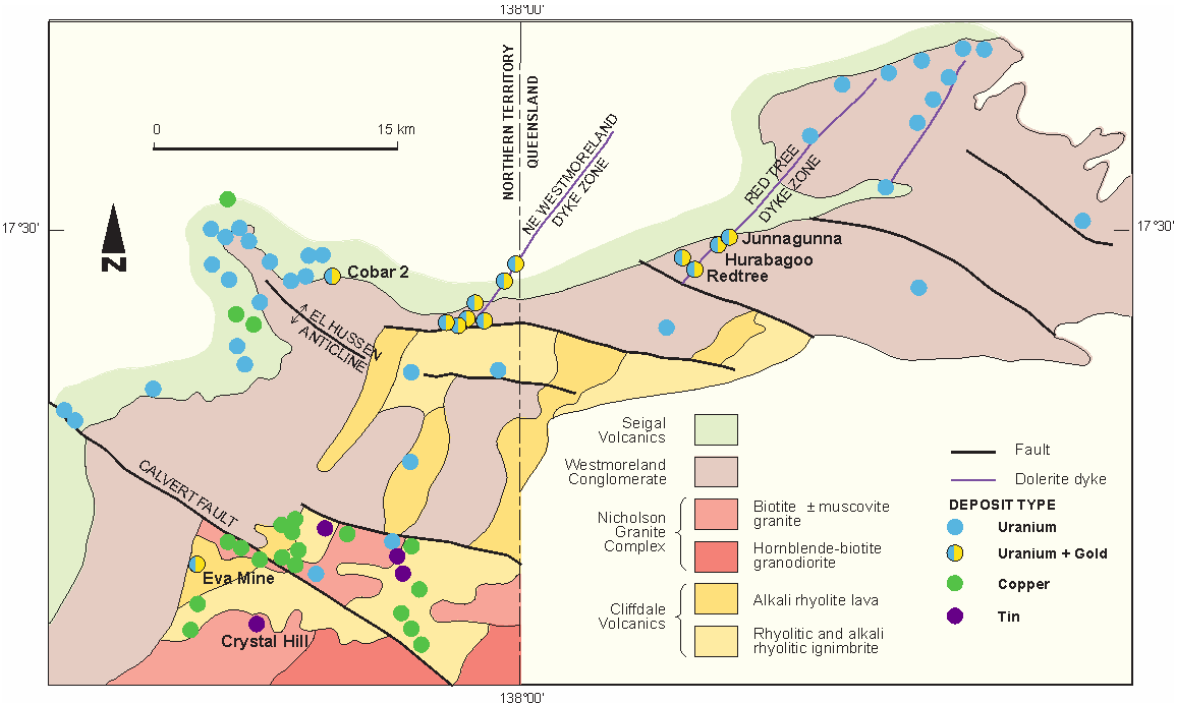

Figure 6.9: *Geological setting of mineral deposits and mineral occurrences in the Westmoreland uranium field (modified from Lally and Bajwah, 2006).*

Paleoproterozoic felsic lavas and ignimbrites (Cliffdale Volcanics) unconformably overlie the metamorphic rocks. The lower sequence of the Cliffdale Volcanics is dominated by coarse, poorly sorted ignimbrites of dacitic and rhyolitic composition. The light coloured ignimbrites are rich in quartz phenocrysts while in the dark varieties, feldspar is abundant and quartz is insignificant or absent. Minor constituents include biotite, actinolite, sphene and magnetite. The upper sequence consists essentially of flow-banded alkali rhyolite and minor tuff (Ahmad and Wygralak, 1989).

The Nicholson Granite Complex can be divided into two broad groupings based on its chemical and mineralogical composition. Group A includes granodiorite, granite and adamellite; the dominant rock type is porphyritic biotite±hornblende-bearing adamellite containing mafic xenoliths. The groundmass includes quartz, plagioclase, perthite, hornblende and biotite with accessory titanite, apatite, zircon and monazite. Group B includes granite, adamellite and alkali granite; the dominant rock type is even grained biotite-muscovite granite with rare hornblende. Zircon, apatite, and fluorite are common accessory minerals but titanite is rare (Ahmad and Wygralak, 1989). The upper units of the Cliffdale Volcanics and the Nicholson Granite have been dated at ~1840 Ma (M. Ahmad, Northern Territory Geological Survey, personal communication). Multiphase intrusions of the Nicholson Granite Complex (granites and adamellites) intrude the metamorphics and Cliffdale Volcanics.

The basal unit of the overlying McArthur Basin, the Westmoreland Conglomerate, is a fluvial deposit, more than 1200 m thick, and comprises arkose, conglomerate and quartz arenites. The Westmoreland Conglomerate has been subdivided into four stratigraphic units (Ahmad and Wygralak, 1990). Most of the uranium mineralisation is within the upper unit (Ptw4 unit), which is a porous, coarse-grained sandstone, conglomeratic in part, and 80 - 90 m thick. U-Pb dating of detrital zircon from the Westmoreland Conglomerate has returned maximum depositional ages of 1865 ± 7 Ma for the lower section, and 1843 ± 4 Ma for the upper section of the Westmoreland Conglomerate respectively (Wygralak and Mernagh, 2009). Basaltic lavas of the Seigal Volcanics conformably overlie the Westmoreland Conglomerate, and these are followed by dolomite, sandstone and mafic and felsic volcanic rocks of the upper part of the Tawallah Group.

Aphyric, medium-grained, dolerite dykes and minor sills intrude along north-east trending fault and fracture zones which intersect the Westmoreland Conglomerate. The most significant of these are the Redtree and the Northeast Westmoreland dyke zones (Fig. 6.9). The Redtree dyke zone is over 15 km long and has been intruded by a complex series of dykes, with individual dykes generally less than 20 m wide. The Westmoreland uranium deposits (Redtree, Junnagunna and Huarabagoo) lie along the Redtree dyke zone.

Faults in the Westmoreland uranium field developed at low strains, apparently in response to WNW-ESE directed compression. They transect and postdate Isan D_2 and D_3 fold systems but in part reactivate older basement faults. Subsequent contractional reactivation of earlier "extensional fault systems" is thought to have occurred at least three times during and after basin development (Scott et al., 2000).

6.2.1.1 Uranium and Copper Mineralisation

The Redtree uranium deposit occurs at the south-western end of the Redtree dyke zone (Fig. 6.9). It comprises both horizontal and vertical mineralisation with grades ranging from 0.15 to over 2 % U_3O_8 in four lenses. The horizontal mineralisation is up to 15 m thick and is entirely hosted by sandstone and is associated with chlorite and minor hematite alteration. The mineralisation thickens and steepens near the dyke where it is 30 – 40 m thick.

The Junnagunna uranium deposit occurs at a fault intersection west of the Redtree dyke zone and south of the north-west trending Cliffdale fault (Fig. 6.9). Uranium mineralised zones in the Junnagunna deposit are predominantly flat-lying and concentrated within the upper unit of the Westmoreland Conglomerate, just below the Seigal Volcanics. Minor discordant mineralisation occurs within the Westmoreland Conglomerate adjacent to the Redtree dyke. The stratiform mineralisation is 0.5 to 10 m thick and grades from ~0.3 to 1 % U_3O_8. Limited mineralised zones also occur on the northern side of the Cliffdale fault and the eastern side of the Redtree dyke zone.

The Huarabagoo uranium deposit is located approximately 3 km north-east of the Redtree deposit (Fig. 6.9) and is a zone of vertical mineralisation in a structurally complex area of the Redtree dyke zone. In this zone there were multiple injections of smaller dykes (steeply dipping and horizontal) associated with the two main vertical dykes. Most of the mineralisation is within the Westmoreland Conglomerate adjacent to the dykes and the remainder is in the dykes. No grades are available for Huarabagoo but it appears to be geologically similar to the Redtree deposit (Laramide Press Release 23/04/2009).

Pitchblende is the dominant primary uranium mineral. It occurs as the massive variety or as colloform masses. Hematite is almost invariably associated with pitchblende and together they replace the clay or quartz matrix in the Westmoreland Conglomerate. In volcanic units, pitchblende

occurs as replacement along the edges of veins which are often filled with quartz. Small grains of gold up to 10 μm diameter have been observed in a few samples. Rare grains of pyrite, marcasite, chalcopyrite bornite, gersdorffite (NiAs) and safflorite ($CoAs_2$) have also been observed (Ahmad and Wygralak, 1989).

Quartz overgrowths are prevalent on the quartz clasts of the Westmoreland Conglomerate. Alkali feldspars, lithic clasts, Fe and Mg silicates and detrital quartz in the conglomerate were replaced by diagenetic illite, chlorite, dickite and rare pyrite (Polito et al., 2005). In the Seigal Volcanics, chlorite and illite replaced Fe and Mg silicates and plagioclase respectively. Quartz veins transect lithified sandstones and peak diagenetic minerals in the Westmoreland Conglomerate indicating that they were the last phase to form (Polito et al., 2005).

Most of the copper prospects occur in either the Cliffdale Volcanics or the Seigal Volcanics. The copper mineralisation is controlled by ill-defined, steeply dipping fractures or shear zones and consists of secondary minerals such as malachite, azurite, chalcocite and chrysocolla. Chalcopyrite is the only important sulphide in the primary zone along with minor pyrite.

Two types of vein-style copper mineralisation occur in the Westmoreland region. In the first type, vein quartz is lacking and clays, chlorite or micaceous minerals are associated with the mineralisation. In the second type, vein quartz is the major gangue mineral. The copper mineralisation occurs in the Nicholson Granite Complex, the Cliffdale Volcanics and the Seigal Volcanics.

6.2.2 Constraints on Mineralisation

The origin of the fluids and metals in the Westmoreland region is still open to interpretation. One possibility is that the basement is the source of the uranium and copper and the overlying basin is the source of the fluids. In this scenario, uranium is derived from the breakdown of monazite and/or other uranium-bearing minerals along fault zones as basinal brines interact with the basement. The copper may originate from a magmatic source or may be leached from the volcanic rocks.

Another possibility is that the basin is the source of both the metals and the fluids. The uranium in this model is sourced from the breakdown of uranium-bearing phases such as uraninite, monazite, zircon, phosphates and tourmaline, by basinal fluids in deep paleoaquifiers in the basin. Once again the copper in this model may originate from a magmatic source or may be leached from the volcanic rocks. Zones of faulting and brecciation, particularly in the basement, are important for focusing the fluids and enhancing their interaction with reduced rock assemblages.

As mentioned in previous chapters, uranium ions in aqueous solution can form a large range of complexes due to the four possible oxidation states as well as hydrolytic reactions that lead to the formation of polymeric ions. The uranium precipitates when the oxidised basinal brine carrying the metals interacts with a reduced basement lithology, or volcanic units with chloritic alteration, or mixes with basement derived, reduced fluids. Copper may be co-transported with uranium in the oxidised basinal brines. The copper would be transported mostly as chloride complexes.

Five different styles of uranium mineralisation have been documented in this area (Ahmad and Wygralak, 1990):

Type 1 uranium mineralisation in the Westmoreland district consists of stratabound mineralisation in the uppermost sandstone unit (Ptw4) of the Westmoreland Conglomerate, subparellel to the contact

with the overlying basic volcanics of the Seigal Volcanics. This style contains the bulk of the known resources. The Seigal Volcanics normally overlie the Westmoreland Conglomerate, but in places reverse faulting has resulted in the Cliffdale Volcanics overlying the conglomerate. Where this occurs a similar style of mineralisation is observed at the contact between the Cliffdale Volcanics and the Westmoreland Conglomerate. In the vicinity of the Long Pocket prospect (~ 5 km east of Junnagunna) a similar style of mineralisation occurs within the Ptw4 sandstone along the upper and lower contacts of a sub-horizontal dolerite sill.

Type 2 uranium mineralisation consists of discordant, steeply dipping zones of mineralisation adjacent to the contact with tholeiitic dykes. Stratabound mineralisation may grade into steeply dipping zones of mineralisation adjacent to the dykes.

Type 3 mineralisation is associated with fractures in the altered Seigal Volcanics. The contact of the Seigal Volcanics with the Westmoreland Conglomerate is 100 – 200 m below the surface at the sites of mineralisation.

Type 4 mineralisation is situated in the Cliffdale Volcanics, not far from their contact with the unconformably overlying Westmoreland Conglomerate. It is possible that the Westmoreland Conglomerate once covered these occurrences and has been subsequently eroded away.

Type 5 uranium occurrences are associated with faults and fractures within the basement and are entirely hosted by the Murphy Metamorphics.

Polito et al., (2005) found that two generations of diagenetic quartz exist in the Westmoreland Conglomerate, but neither was coeval with the precipitation of uranium. Illite crystillinity measurements, electron microprobe compositions, and stable isotope values revealed that I^1 illite, C^1 chlorite, and D^1 dickite formed from 200º±50ºC basinal fluids with a $\delta^{18}O_{fluid}$ value of 4±3 per mil and a δD_{fluid} value of -31±10 per mil (Polito et al., 2005). Disturbed $^{40}Ar/^{39}Ar$ ages from I^2 illite and $^{207}Pb/^{206}Pb$ ages from uraninite grains in H^2 hematite suggest that the uraninite was precipitated together with I^2 illite and H^2 hematite between 1606 ± 80 and 1655 ± 83 Ma (Polito et al., 2005). Polito et al. (2005) suggests that the evolved basinal brine that formed the diagenetic minerals in the Westmoreland Conglomerate was the same as that which transported uranium to the site of uraninite deposition. Ahmad and Wygralak (1989) have demonstrated that the Westmoreland Conglomerate contains large quantities of altered lithic fragments derived from the Murphy tectonic ridge. This ridge is dominated by felsic rocks that have whole-rock uranium concentrations around 30 ppm and host zircons with uranium concentrations between 200 and 1000 ppm (Page et al., 2000).

6.2.3 Geochemical Modelling

As the fluid reservoirs and the metal sources are not currently well constrained, the geochemical modelling was confined to the study of the transport and depositional processes. Our unpublished fluid inclusion studies of uranium and copper occurrences in the Westmoreland region indicate that the metals were transported in $CaCl_2$-bearing fluids (i.e. basinal brines) at temperatures up to 220°C. In accordance with the fluid inclusion results an input fluid with 7.0 wt.% NaCl, 0.03 wt.% $CaCl_2$, 0.0012 wt.% KCl was used as the input fluid. A small amount of NaF (0.0004 wt.%) was also added to the fluid as uranium may be transported as fluoride complexes. Note that the input fluid does not contain any uranium or copper species and these can only enter the fluid via fluid:rock interaction. The rock compositions used in the modelling are given in Table 6.3.

Table 6.3 Rock compositions (moles/kg) used in the HCh modelling

Mineral	Westmoreland Conglomerate[a,b]	Seigal Volcanics[a,c]	Nicholson Granite[a,d]
Quartz	10.29	0	6.22
K-Feldspar	0.19	0	1.33
Albite	0.07	0.812	0.24
Anorthite	0.03	0.83	0.16
Forsterite	0	0.31	0
Ferrosilite	0	0.613	0
Diopside	0	0.529	0
Hedenbergite	0	0.761	0
Pargasite	0	0	0.022
Ferropargasite	0	2.0	0.022
Muscovite	0.47	0	0.048
Annite	0	0	0.075
Chamosite	0.06	0	0
Kaolinite	0.03	0	0
Hematite	0	0.000	0
Magnetite	0.3	0.220	0.134
Apatite	0	0	0.012
Fluorite	0	0	0.080
Pyrite	0.041	0	00.084
Chalcopyrite	26 ppm	138 ppm	38 ppm
Uraninite	6.0 ppm	2.0 ppm	6.2 ppm

[a] Mineral concentrations are expressed as moles/kg except for chalcopyrite and uraninite which are expressed as parts per million.
[b] Westmoreland Conglomerate composition is from Hills (1973).
[c] Seigal Volcanics composition is from Rawlings (2001).
[d] Nicholson Granite composition is from Gardner (1978).

In the first part of this report it was shown that the topographic recharge model for generating fluids is able to transport geologically realistic concentrations of uranium and other base metals. The following modelling was carried out to determine if a similar model can explain uranium transport and deposition in unconformity-related uranium systems using the Westmoreland geology to constrain the system. A "flow-through" reactor model (see Fig. 6.2) was used to simulate the fluid:rock interaction. The numerical modelling was carried out in two main parts; the first involving the reaction of Cu-rich and U-rich fluids from aquifers in the Westmoreland conglomerate with the overlying Seigal Volcanics and the second involving reaction of Cu-rich and U-rich fluids equilibrated with both the Westmoreland Conglomerate and the underlying Nicholson Granite with the overlying Seigal Volcanics (see Table 6.4). The second model simulated fluid flow in deeper (and hotter) parts of the basin to test the transport of uranium and copper at higher temperatures.

Table 6.4 Summary of Numerical Modelling of uranium and copper mineralisation in the Westmoreland Region.

Model 1 – Oxidised fluid flow in the Westmoreland Conglomerate and Seigal Volcanics

Part 1 – Equilibration of an O_2 saturated fluid with the Westmoreland Conglomerate

Step 1 Equilibration of the fluid with the Westmoreland Conglomerate at 25ºC

Step 2 Progressive reaction of batches of the equilibrated fluid with the Westmoreland Conglomerate at temperatures from 50 – 125ºC

Part 2 – Equilibration of Cu-rich fluids with the overlying Seigal Volcanics

Step 1 Extraction of a Cu-rich fluid at step 560 of Part 1

Step 2 Progressive reaction of batches of the Cu-rich fluid with the Seigal Volcanics at temperatures from 125 – 50ºC.

Part 3 – Closed-system cooling of Cu-rich fluids in equilibrium with the overlying Seigal Volcanics

Step 1 Extraction of a 1 kg batch Cu-rich fluid at step 560 of Part 1

Step 2 Equilibration of this batch of Cu-rich fluid with the Seigal Volcanics at temperatures from 125 – 50ºC.

Part 4 – Equilibration of U-rich fluids with the overlying Seigal Volcanics

Step 1 Extraction of a U-rich fluid at step 639 of Part 1

Step 2 Progressive reaction of batches of the U-rich fluid with the Seigal Volcanics at temperatures from 125 – 50ºC.

Model 2 – Deep oxidised fluid flow in the Westmoreland Conglomerate and Seigal Volcanics

Part 1 – Equilibration of an O_2 saturated fluid with the Nicholson Granite

Step 1 Equilibration of the fluid with the Westmoreland Conglomerate at 25ºC and then equilibration of this fluid with the Nicholson Granite at 25ºC

Step 2 Progressive reaction of batches of the equilibrated fluid with the Westmoreland Conglomerate at temperatures from 50 – 200ºC

Part 2 – Equilibration of Cu-rich fluids from the Nicholson Granite with the overlying Seigal Volcanics

Step 1 Extraction of a Cu-rich fluid at step 80 of Part 1

Step 2 Progressive reaction of batches of the Cu-rich fluid with the Seigal Volcanics at temperatures from 200 – 50ºC.

Part 3 – Closed-system cooling of Cu-rich fluids from the Nicholson Granite with the overlying Seigal Volcanics

Step 1 Extraction of a 1 kg batch Cu-rich fluid at step 80 of Part 1

Step 2 Equilibration of this batch of Cu-rich fluid with the Seigal Volcanics at temperatures from 200 – 50ºC.

Part 4 – Equilibration of U-rich fluids from the Nicholson Granite with the overlying Seigal Volcanics

Step 1 Extraction of a U-rich fluid at step 88 of Part 1

Step 2 Progressive reaction of batches of the U-rich fluid with the Seigal Volcanics at temperatures from 125 – 50ºC.

Part 5 – Closed-system cooling of U-rich fluids from the Nicholson Granite with the overlying Seigal Volcanics

Step 1 Extraction of a 1 kg batch U-rich fluid at step 88 of Part 1

Step 2 Progressive reaction of batches of the U-rich fluid with the Seigal Volcanics at temperatures from 200 – 50ºC.

6.2.3.1 Model 1 – Part 1: Equilibration of an O_2 saturated fluid with the Westmoreland Conglomerate

The first model simulates the flow of a topographic recharging fluid through the Westmoreland Conglomerate and the fluid later ascends through faults and fractures to interact with the overlying Seigal Volcanics. In this numerical model of the progressive fluid:rock interaction an O_2 saturated fluid at 25°C is initially reacted with the Westmoreland Conglomerate at a fluid:rock ratio of 10:1 (see Figure 6.10). Note as shown in Table 6.3, the iron oxide in the conglomerate is assumed to initially be magnetite which is later oxidised to hematite by fluid:rock interaction. The equilibrated fluid is then reacted with the Westmoreland Conglomerate at temperatures rising to 125°C at increasing fluid:rock ratios. The effect of this process on the concentration of uranium and copper in solution is shown in Figure 6.11a.

For example, at 50°C as more and more fluid reacts with the conglomerate the fluid becomes increasingly oxidised until at step 107, equivalent to a fluid:rock ratio of 1070:1, there is a sudden increase in the oxidation state of the fluid which causes a dramatic increase in Cu solubility which reaches a maximum concentration of 26.4 ppm. The fluid maintains its high Cu concentration until uraninite and chalcopyrite cease precipitation (Fig. 6.11b). Note that tenorite precipitates in place of chalcopyrite at higher fluid:rock ratios at 50°C. It is also interesting to note that immediately after the Cu concentration in solution decreases again the uranium concentration suddenly increases to a value of 38.5 ppm (Fig. 6.11a). This corresponds to a dramatic increase in the fO_2 of the fluid and the cessation of all uranium mineral precipitation due to the increased uranium solubility in the more oxidised fluid (Fig. 6.11b). The same process occurs at higher temperatures but as the temperature increases a higher fluid:rock ratio is required; i.e. the sudden increase in copper solubility occurs at steps 234, 373 and 519 for temperatures of 75º, 100º and 125°C respectively (Fig. 6.11a). It is also worth noting that while the maximum copper solubility only decreases slightly with increasing temperature there is a steady decrease in the maximum uranium solubility with increasing temperature up to 125 °C. This is due to the sensitivity of UO_2^+ to pH and fO_2 over the temperature

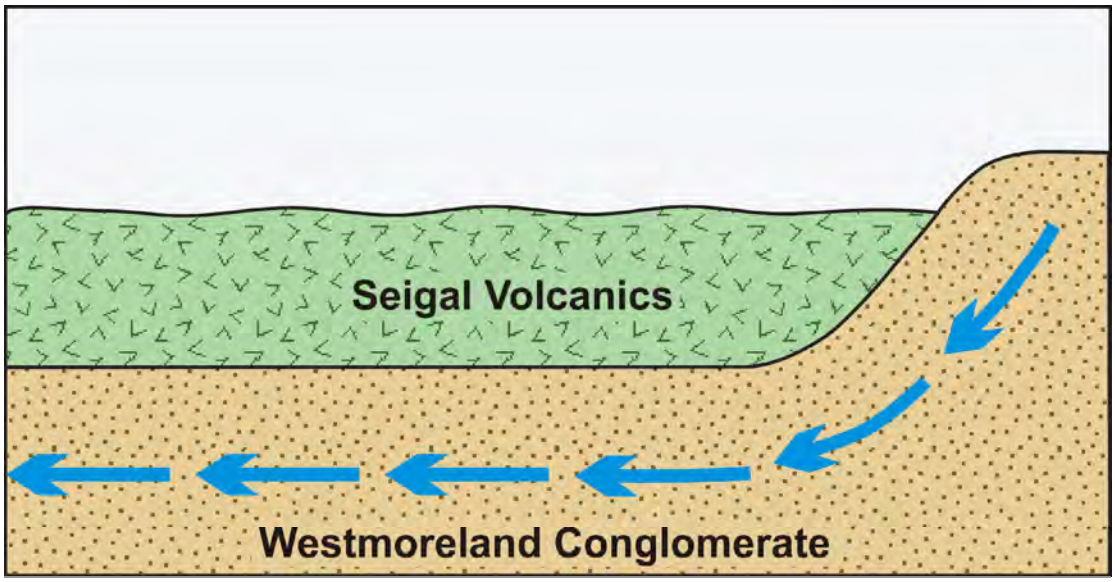

Figure 6.10: *A sketch of Model 1- Part 1, involving equilibration of an O_2 saturated fluid with the Westmoreland Conglomerate. Each blue arrow represents a new 1kg batch of fluid interacting with the Westmoreland Conglomerate. See text for details.*

range of this study when compared with $CuCl_2^-$ which is the dominant copper species over this temperature range.

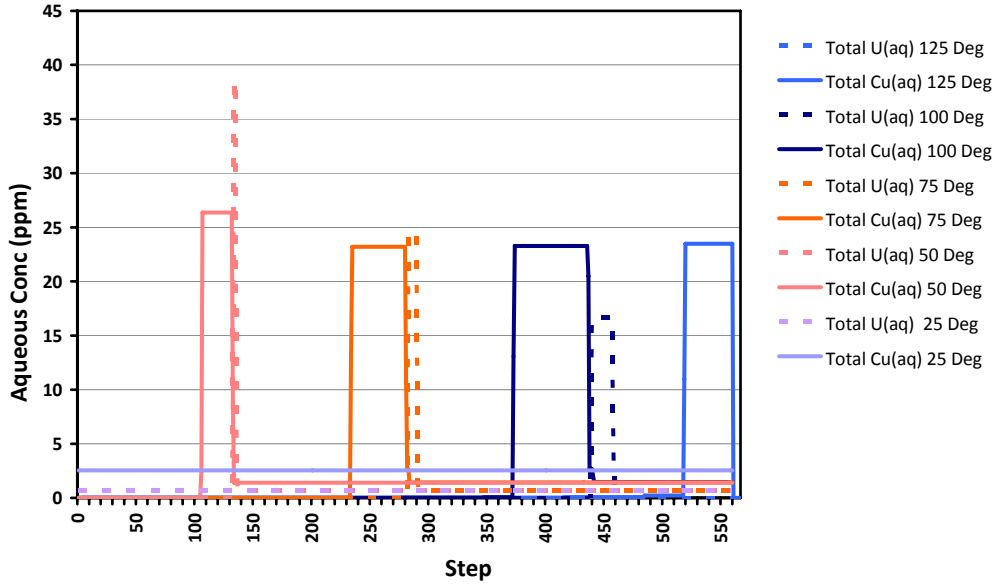

Figure 6.11 (a): *Predicted total uranium concentration and total copper concentration in an aqueous fluid in equilibrium with the Westmoreland Conglomerate at 25, 50, 75, 100 and 125°C respectively. See text for details.*

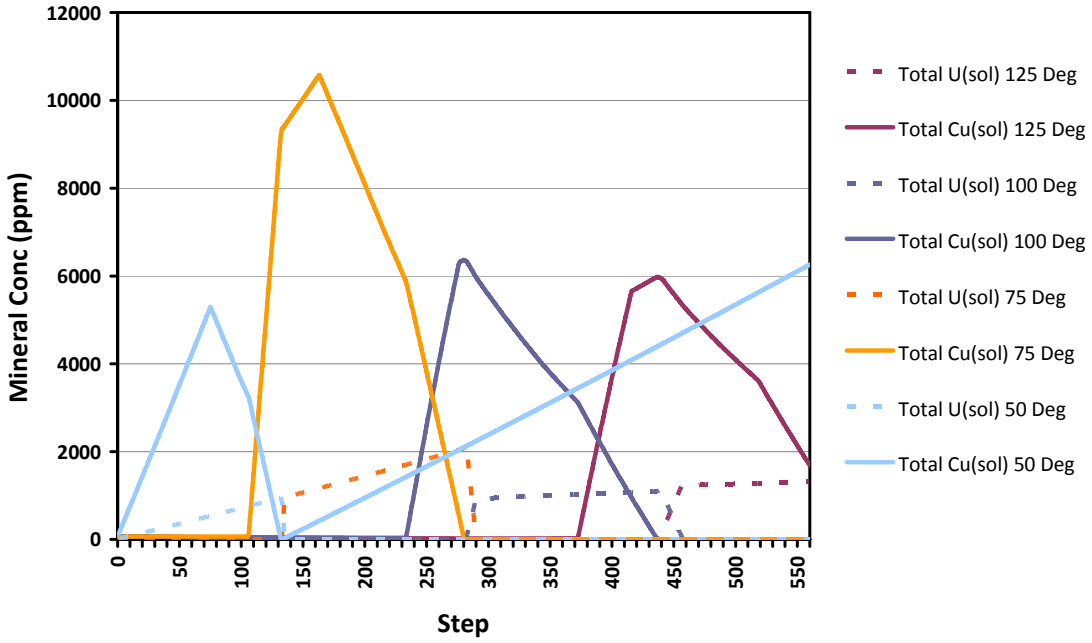

Figure 6.11 (b): *Predicted total uranium concentration and total copper concentration of minerals(denoted as solids(sol) in the legend) precipitated from an aqueous fluid in equilibrium with the Westmoreland Conglomerate at 25°, 50°, 75°, 100° and 125°C, respectively. See text for details.*

A similar pattern can be seen in Figure 6.11b which shows the total concentration of uranium and copper minerals precipitated from this model. At 50°C there is initially coprecipitation of both uraninite and chalcopyrite. The concentration of the chalcopyrite is about an order of magnitude greater than that of uraninite. The total concentration of chalcopyrite precipitated reaches a maximum of 5290 ppm at step 75, i.e. a fluid:rock ratio of 750:1. At higher fluid:rock ratios pyrite ceases to precipitate and both chalcopyrite and bornite precipitate but in decreasing amounts. However, uraninite continues to precipitate in increasing concentrations until the fluid becomes highly oxidised as mentioned above. At 50°C tenorite continues to precipitate at higher fluid:rock ratios but tenorite does not precipitate at higher temperatures. At all other temperatures the precipitation of uranium- and copper-bearing minerals ceases around the same fluid:rock ratio that causes the sudden drop in uranium solubility in the fluid (Fig. 6.11). Note that the highest concentrations of uranium- and copper-bearing minerals are predicted to precipitate from the 75°C fluid.

This simulation shows that both uranium and copper minerals are precipitated via reduction reactions due to the presence of magnetite and minor pyrite in the conglomerate. As the existing rocks have all been highly oxidised the iron oxide was assumed to be originally mostly magnetite. Therefore, the current model may overestimate the amount of magnetite that initially existed in the Westmoreland Conglomerate but is used to determine the maximum amounts of uranium and copper that may precipitate from this reaction. The model shows that stratabound deposits of uranium and copper may form in the Westmoreland Conglomerate in regions of high ferrous iron (or other reductants) in a mechanism similar to that for roll-front uranium deposits. These deposits would only be preserved if there was little or no passage of oxidised fluids after the deposit had formed.

6.2.3.2 Model 1 – Part 2: Equilibration of Cu-rich fluids with the overlying Seigal Volcanics

The second part of the model was designed to simulate interaction of the fluid, which had reacted with and completely oxidised the Westmoreland Conglomerate, with the overlying Seigal Volcanics (see Figure 6.12). This was done to investigate if the mafic Seigal Volcanics could precipitate the dissolved uranium from the fluid and to understand the effect of this lithology on copper solubility. This model assumes that diagenetic fluids at 125°C in the Westmoreland conglomerate leak into faults and structures in the Seigal Volcanics as a result of tectonic activity.

To obtain a copper-rich fluid, the fluid in equilibrium with the Westmoreland Conglomerate at 125°C in step 560 in the previous model was extracted and used as the input fluid for the second part of the numerical model. This step was chosen as it is the one where the fluid:rock ratio results in a fluid with an oxidation state equivalent to the intial fluid at 25°C. This fluid had a copper concentration of 23 ppm but the uranium concentration was only 4×10^{-7} ppm at 125°C (see Fig. 6.11a). The fluid was then reacted with fresh Seigal Volcanics at temperatures of 125, 100, 75, and 50°C to mimic the effect of different temperature fluids flowing through faults in the Seigal Volcanics.

The total copper and uranium concentrations in the fluid in equilibrium with the Seigal Volcanics are shown in Figure 6.13a. As may be expected, the uranium concentration is very low at all temperatures. Total copper concentrations are also very low with a maximum concentration of only 8.8×10^{-5} ppm at 125°C which decreases by almost an order of magnitude with each 25 °C drop in temperature (Fig. 6.13a). This implies that nearly all the uranium and copper is precipitated from the ore fluid as soon as it reacts with the Seigal Volcanics and that these volcanics provide an efficient environment for copper and uranium deposition.

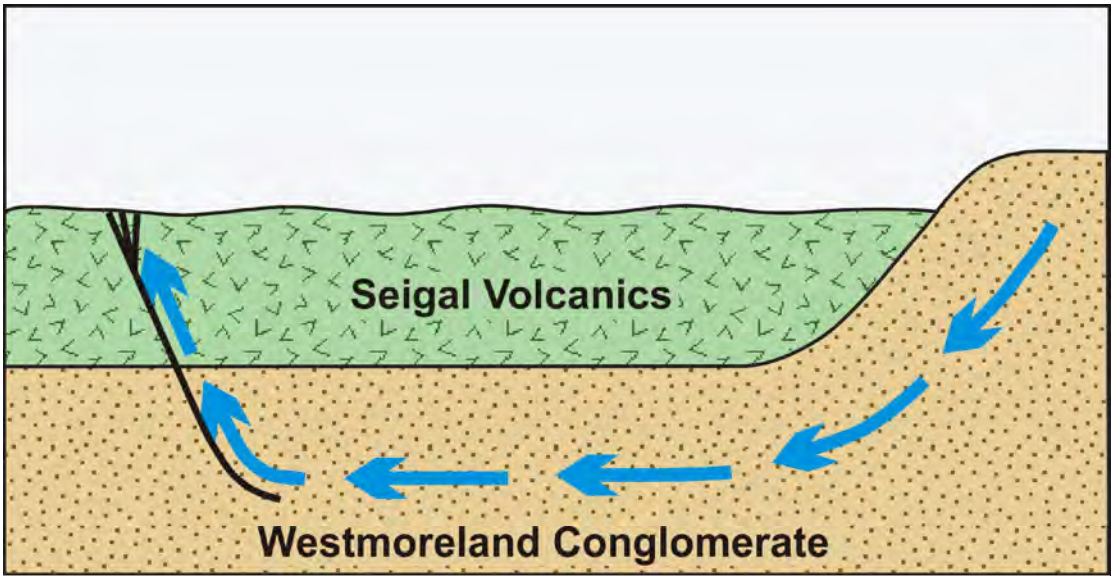

Figure 6.12 *A sketch of Model 1-Part 2, simulating equilibration of an O_2-saturated fluid from the Westmoreland Conglomerate with the mafic Seigal Volcanics. Each blue arrow represents a new 1kg batch of fluid. See text for details.*

The total concentration of copper and uranium minerals precipitated from solution is shown in figure 6.13b. Initially 700 ppm of copper (as chalcopyrite) is precipitated from the ore fluid at 125°C and the amount increases as the fluid:rock ratio increases. At lower temperatures the amount of copper precipitated with each batch of fluid remains almost constant at around 400 ppm. However, due to the low initial uranium concentration, only 2 ppm of uranium (as uraninite) is precipitated from each batch of fluid at all temperatures.

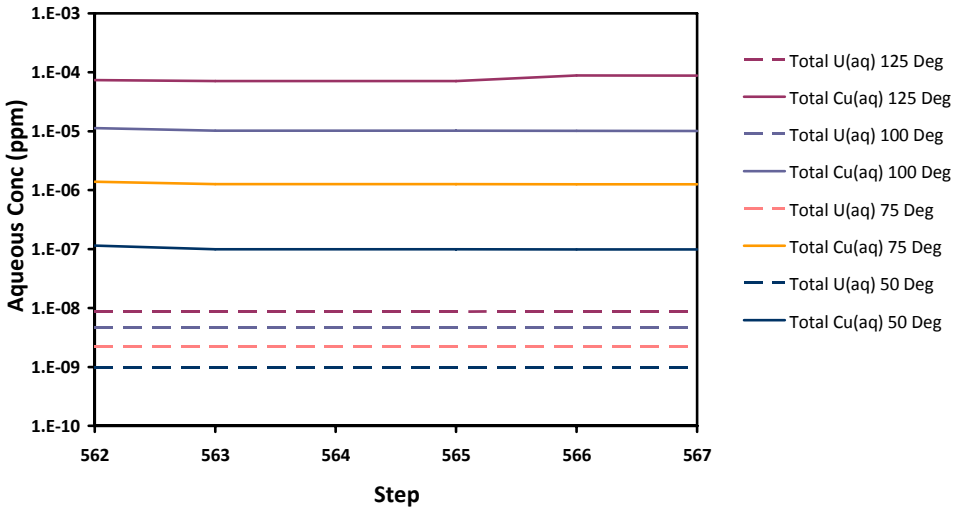

Figure 6.13(a): *Predicted total uranium concentration and total copper concentration in a Cu-rich fluid in equilibrium with the Seigal Volcanics at 50°, 75°, 100° and 125°C respectively. See text for details.*

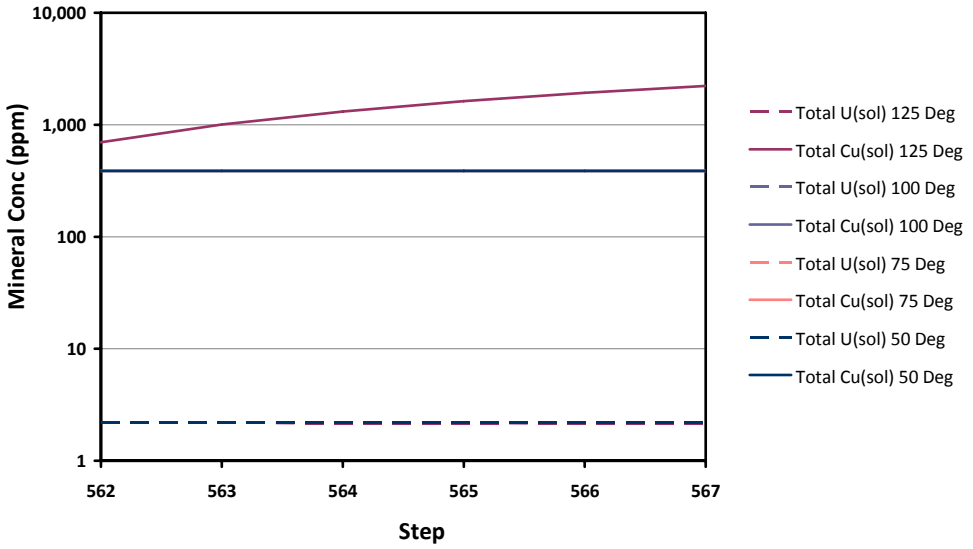

Figure 6.13(b) *Predicted total uranium concentration and total copper concentration of minerals(denoted as solids(sol) in the legend) precipitated from a Cu-rich fluid in equilibrium with the Seigal Volcanics at 50°, 75°, 100° and 125°C respectively. Note that the curves for 75° and 100° C are identical to those at 50° C and are not shown on the graph. See text for details.*

6.2.3.3 Model 1 – Part 3: Closed-system cooling of Cu-rich fluids in equilibrium with the overlying Seigal Volcanics

In this scenario a 1 kg batch of fluid which had reacted with and completely oxidised the Westmoreland Conglomerate at 125°C was extracted at step 560 from the numerical model in Part 1. As stated above this fluid contains 23 ppm copper but only 4 x 10^{-7} ppm uranium (see Figure 6.11a). This batch of fluid was then equilibrated with the Seigal Volcanics at temperatures of 125º, 100º, 75º and 50°C respectively. This cooling scenario differs from Part 2 as there is no input of additional batches of fluid as time progresses. The results are shown in Figure 6.14.

The concentration of copper and uranium species in solution is shown in Figure 6.14a. It can be seen that the initial solution at 125°C contains 23 ppm copper but on reacting with the Seigal Volcanics the concentration immediately drops to 7 x 10^{-5} ppm and remains at these low values at lower temperatures. As the concentration of uranium in the initial solution at 125°C is only 4 x 10^{-7} ppm, the uranium concentration remains low at all temperatures used in the modelling.

The concentration of copper and uranium minerals precipitated from the oxidised solution from the Westmoreland Conglomerate is shown in Figure 6.14b. The modelling predicts that 697 ppm of copper (as chalcopyrite) is precipitated at 125°C when the fluid equilibrates with the Seigal Volcanics. This then decreases to 387 ppm copper for fluids equilibrated at lower temperatures. However, as in Part 2 above only 2 ppm of uranium is predicted to precipitate after equilibration with the Seigal Volcanics at all temperatures from 125º to 50°C. This scenario demonstrates that copper deposits in the Seigal Volcanics could have been formed from Cu-bearing, oxidised fluids originating from the Westmoreland Conglomerate if suitable fluid:rock ratios were attained in the conglomerate.

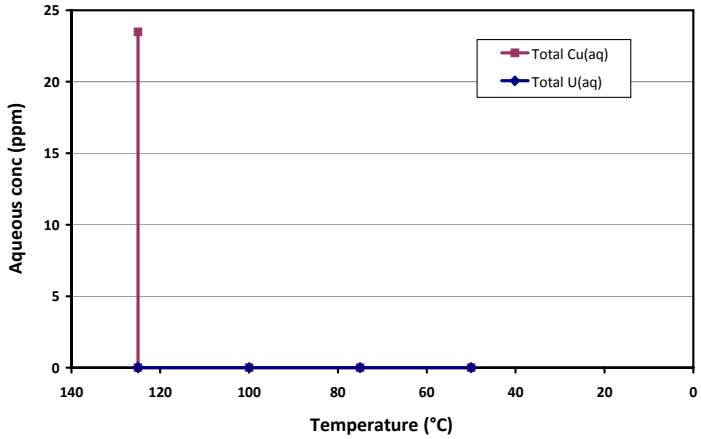

Figure 6.14(a): *Predicted total uranium concentration and total copper concentration of a Cu-rich fluid at 125°C which is allowed to cool and equilibrate with the Seigal Volcanics at 50°, 75°, 100° and 125°C respectively. See text for details*

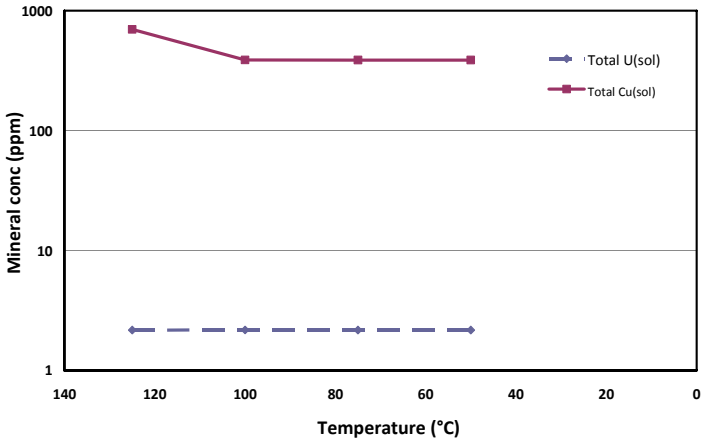

Figure 6.14(b): *Predicted total uranium concentration and total copper concentration of minerals (denoted as solids(sol) in the legend) precipitated from a Cu-rich fluid at 125°C which is allowed to cool and equilibrate with the Seigal Volcanics at 50, 75, 100 and 125°C respectively. See text for details*

6.2.3.4 Model 1 – Part 4: Equilibration of U-rich fluids with the overlying Seigal Volcanics

To obtain a uranium-enriched fluid, the fluid in equilibrium with the Westmoreland Conglomerate at 125°C in step 639 in Part 1 of the model (Fig. 6.11) was extracted and used as the input fluid for this section of the numerical model. This fluid had a uranium concentration of 11.6 ppm but the copper concentration was only 1.5 ppm (see Fig. 6.11a). The fluid was then reacted with fresh Seigal Volcanics at temperatures of 125, 100, 75, and 50°C to mimic the effect of different temperature fluids flowing through faults in the Seigal Volcanics as in Part 2 above.

The total copper and uranium concentrations in the U-rich fluid in equilibrium with the Seigal Volcanics are shown in Figure 6.15a. It is not surprising that the results are almost identical to those shown in Figure 6.13a as the same equilibrium conditions apply to the system in each case. This

time, however, the modelling was extended up to 700 steps but steady state conditions were obtained by step 670 in all cases (Fig. 6.15a). So, as above, nearly all the uranium and copper is precipitated from the ore-bearing fluid as soon as it reacts with the Seigal Volcanics.

The total concentration of uranium and copper minerals precipitated from solution is shown in Figure 6.15b. The first batch of fluid to react at 125°C results in the precipitation of 423 ppm chalcopyrite and 118 ppm of uraninite. So initially, at low fluid:rock ratios in the Seigal Volcanics a copper-rich deposit is predicted to form at 125°C. However, as the fluid:rock ratio increases the deposit becomes more enriched in uranium and by the end of the simulation, at a fluid:rock ratio of 600:1, the deposit is predicted to be uranium-rich and consist of 6750 ppm uraninite and 2440 ppm chalcopyrite. However, this uranium enrichment does not occur at lower temperatures where each batch of fluid precipitates a constant 378 ppm chalcopyrite and 2 ppm uranium (Fig. 6.15b). Therefore the modelling predicts that fluids at temperatures of 125°C will form uranium-copper deposits in the Seigal Volcanics whereas lower temperature fluids will form copper-rich deposits. By analogy, similar processes may be expected to occur when ore fluids from the Westmoreland Conglomerate interact with mafic dykes within the conglomerate.

The copper deposits in the Seigal Volcanics typically have low uranium contents which suggests that they have formed at temperatures below 125°C. Uranium-rich deposits will only form if the copper concentration in the ore fluid is very low. Therefore, fluids at different depths in the basement, i.e. at different temperatures, may have different U/Cu ratios resulting in different styles of mineralisation in different parts of the mineral system.

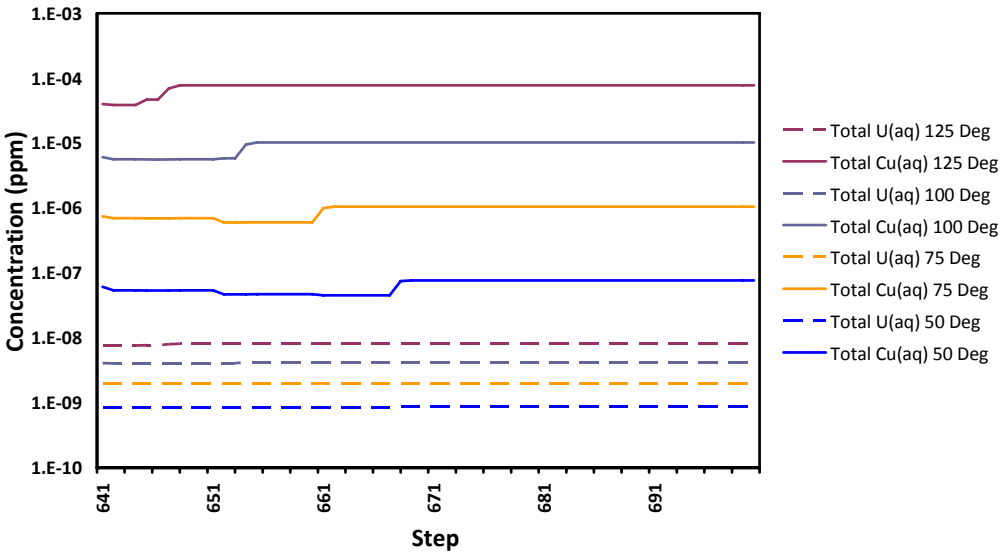

Figure 6.15(a) *Predicted total uranium concentration and total copper concentration in a U-rich fluid in equilibrium with the Seigal Volcanics at 50°, 75°, 100° and 125°C respectively. See text for details.*

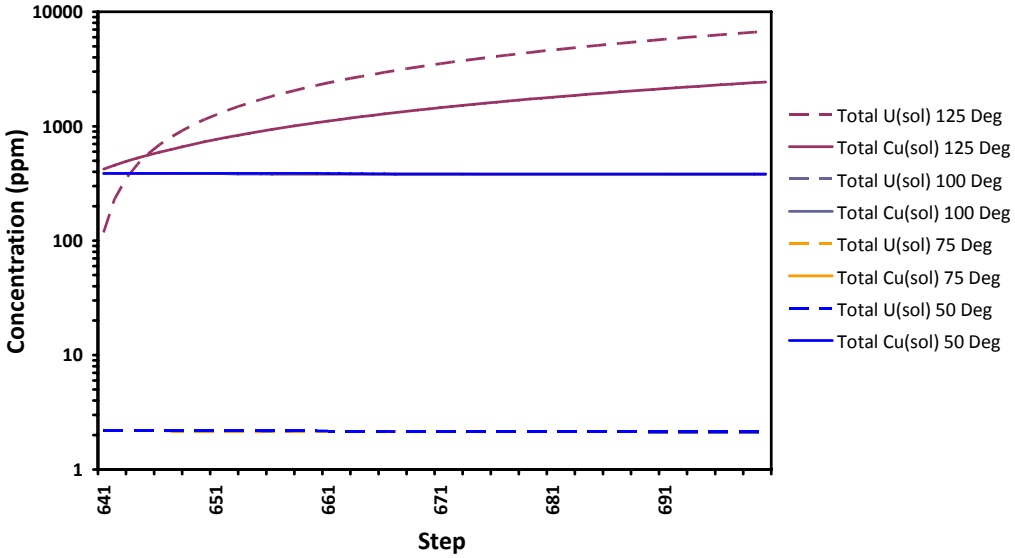

Figure 6.15(b): *Predicted total uranium concentration and total copper concentration of minerals (denoted as solids(sol) in the legend) precipitated from a U-rich fluid in equilibrium with the Seigal Volcanics at 50°, 75°, 100° and 125°C respectively. Note that the curves for 75° and 100° C are identical to those at 50° C and are not shown on the graph. See text for details.*

6.2.3.5 Model 2 – Part 1: Equilibration of an O_2 saturated fluid with the Nicholson Granite

The second model is similar to Model 1 and simulates the flow of a topographic recharging fluid through the Westmoreland Conglomerate until it is completely oxidised. Then the O_2 saturated fluid at 25°C from the Westmoreland Conglomerate is equilibrated with the Nicholson Granite at a fluid:rock ratio of 1:1. The composition of the Nicholson Granite is given in Table 6.3. The temperature of the system was then incrementally increased to 200°C at increasing fluid:rock ratios. Higher temperatures were used in this model to reflect the assumption that the groundwater would need to penetrate deeper into the basin in order to interact with the Nicholson Granite (see Figure 6.16). The effect of this process on the concentration of uranium and copper in solution is shown in Figure 6.17a.

As in Model 1, once the host rocks are completely oxidised by the O_2-saturated fluid, the concentration of copper followed closely by the concentration or uranium dramatically increases in the fluid. As shown in Figure 6.17(a), the number of steps required to achieve this increases with increasing temperature. As in Model 1 the maximum concentration of uranium in solution decreases with increasing temperature. However, the maximum copper concentration only increases slightly with increasing temperature. This is in accord with the earlier modelling results shown in Figure 6.4b which predict low copper solubility in these systems. The solubility of copper is controlled by chalcopyrite precipitation at low fO_2 but just as the oxidation state of the fluid starts to increase there is a small increase in copper solubility which is limited by the precipitation of chalcocite.

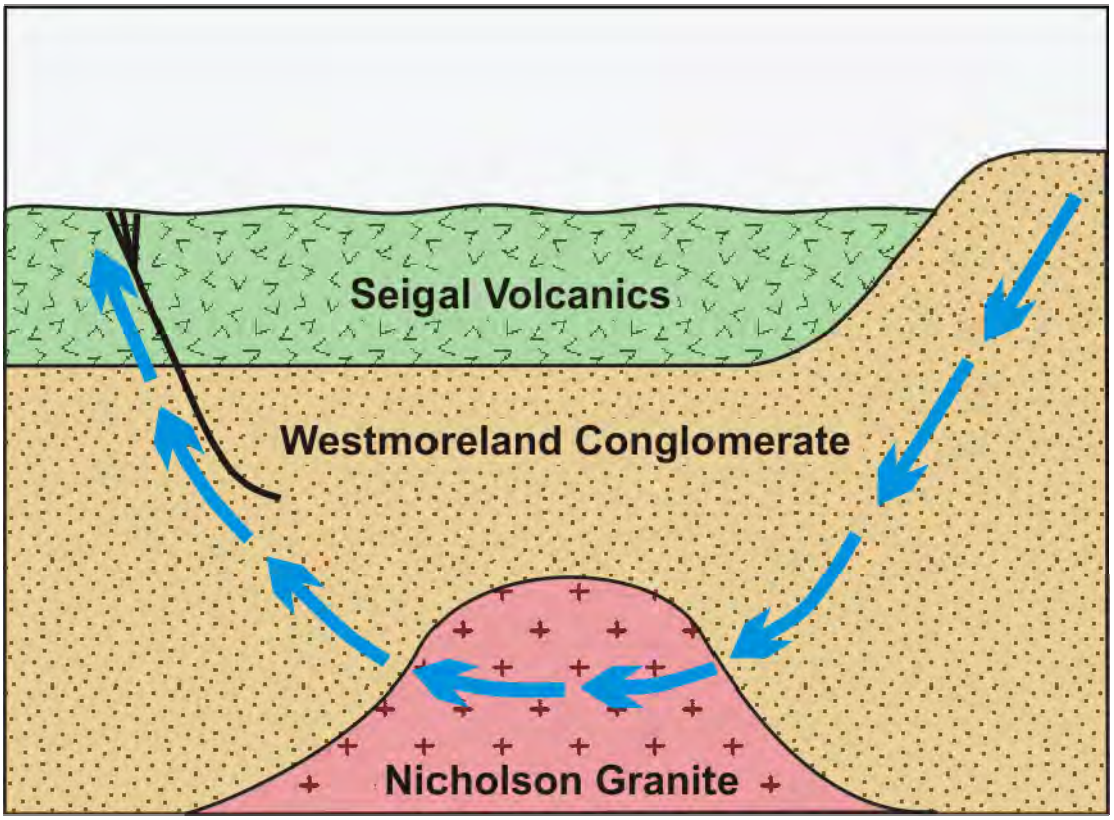

Figure 6.16: *A sketch of Model 2, simulating an O_2-saturated fluid from the Westmoreland Conglomerate (a) equilibrating with the Nicholson Granite at temperatures from 25° to 200°C, and (b) the equilibration of this fluid with the Seigal Volcanics. Each blue arrow represents a new 1kg batch of fluid. See text for details.*

The total concentration of uranium and copper minerals predicted to precipitate from this solution is shown in Figure 6.17b. As in Model 1 we observe a sudden onset of precipitation of both copper and uranium minerals with the initial onset of precipitation occurring progressively later as the temperature increases. However, in Model 2 the concentration of uranium minerals exceeds that for copper reaching values of approximately 1.5 wt.% at 150°C (Fig. 6.17b). In comparison the concentration of copper minerals only reaches 0.5 wt.% at 150°C before decreasing again at higher temperatures. This indicates that interaction of an oxidised fluid with a granite (i.e. Model 2) provides a more favourable environment for uranium ± copper mineralisation than simple fluid flow in a sandstone aquifer used in Model 1.

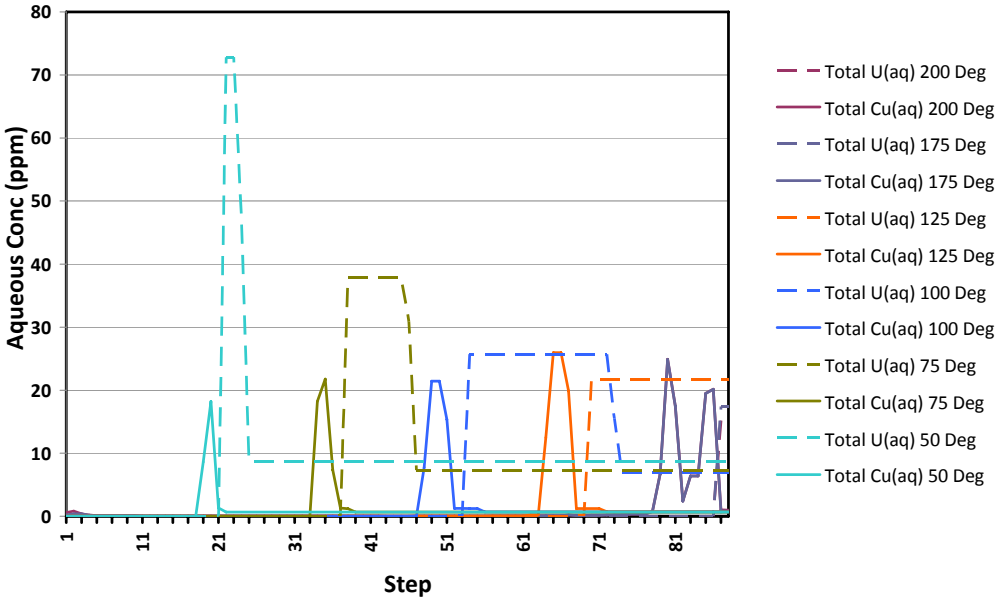

Figure 6.17 (a): *Predicted total uranium concentration and total copper concentration in an aqueous fluid in equilibrium with the Nicholson Granite at temperatures from 25° to 200°C. See text for details.*

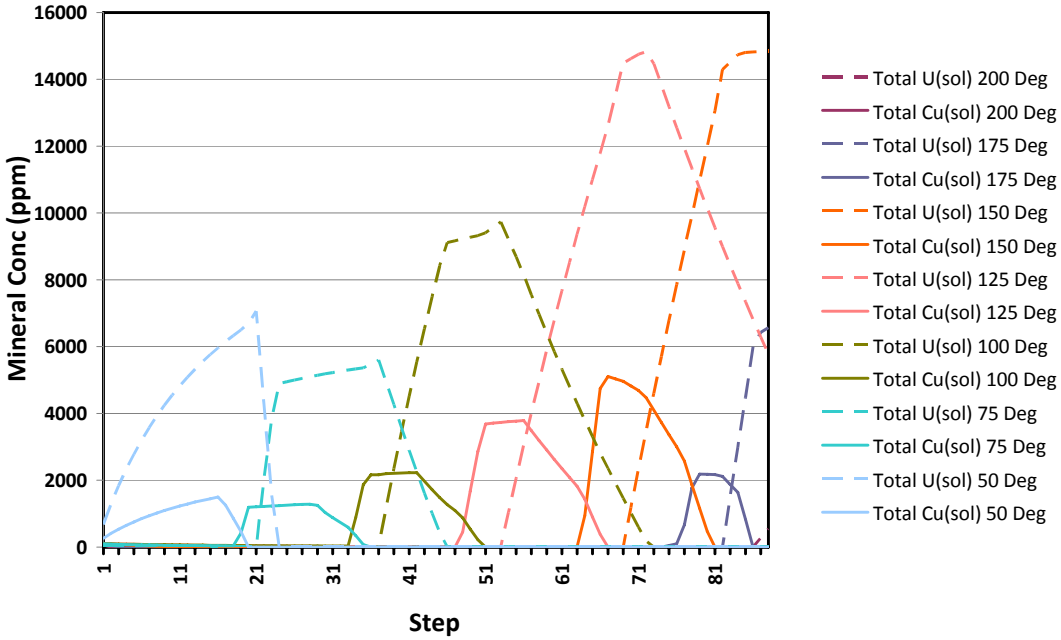

Figure 6.17 (b): *Predicted total uranium concentration and total copper concentration of minerals (denoted as solids(sol) in the legend) precipitated from an aqueous fluid in equilibrium with the Nicholson Granite at temperatures from 25° to 200°C. See text for details.*

6.2.3.6 Model 2 – Part 2: Equilibration of Cu-rich fluids from the Nicholson Granite with the overlying Seigal Volcanics

The second part of the model was designed to simulate interaction of the fluid, which had reacted with the Westmoreland Conglomerate and Nicholson Granite, with the overlying Seigal Volcanics (see Figure 6.16). To obtain a copper-rich fluid, the fluid in equilibrium with the Nicholson Granite at 200°C in step 80 in Model 2 – Part 1 was extracted and used as the input fluid for the second part of the numerical model. This fluid had a copper concentration of 24.9 ppm but the uranium concentration was only 3.76 x 10^{-6} ppm at 200°C. The fluid was then reacted with fresh Seigal Volcanics at temperatures of 200º, 175º.150º, 125º, 100º, 75º, and 50°C to mimic the effect of different temperature fluids flowing through faults in the Seigal Volcanics.

The total copper and uranium concentrations in the fluid from the Nicholson Granite in equilibrium with the Seigal Volcanics are shown in Figure 6.18a. With the exception of the fluid at 50°C there is a general increase in the total concentration of uranium and copper species in solution as more batches of fluid react with the Seigal Volcanics. As may be expected, the uranium concentration is very low at all temperatures but significant total copper concentrations up to 2 and 52 ppm are obtained from the fluids at 175º and 200°C, respectively.

The total concentration of copper and uranium minerals precipitated from the fluid from the Nicholson Granite in equilibrium with the Seigal Volcanic is shown in Figure 6.18b. As may be expected, very little uraninite is predicted to precipitate due to the low uranium concentration in the input fluid. However, at temperatures up to 100°C, around 380 ppm of copper minerals precipitate with each batch of fluid equilibrated with the Seigal Volcanics. At temperatures between 100º and 200°C the concentration of copper minerals gradually increases with each batch of fluid but at 200°C the copper concentration initially increases and then decreases with each batch of fluid (Fig. 6.18b). This indicates that, in this model, copper minerals may be resorbed and remobilised at temperatures above 200°C.

6.2.3.7 Model 2 – Part 3: Closed-system cooling of Cu-rich fluids from the Nicholson Granite with the overlying Seigal Volcanics

In this scenario, a 1 kg batch of the copper-rich fluid in equilibrium with the Nicholson Granite at 200°C in Model 2 – Part 1 was extracted at step 80 of the numerical model. As stated above this fluid contains 24.9 ppm copper but only 3.76 x 10^{-6} ppm at 200°C. This batch of fluid was then allowed to equilibrate with the Seigal Volcanics at decreasing temperatures of 200º, 175º, 150º, 125º, 100º, 75º and 50°C respectively. This simple cooling scenario differs from Part 2 as there is no input of additional batches of fluid as time progresses. The results are shown in Figure 6.19.

The concentration of copper and uranium species in solution is shown in Figure 6.19a. It can be seen that the initial solution at 200°C contains 24.9 ppm copper but on reacting with the Seigal Volcanics the concentration immediately drops to 0.01 ppm copper and remains at these low values at lower temperatures. As expected the fO_2 of the solution decreases steadily with temperature and the concentration of uranium species remains low at all temperatures used in the modelling.

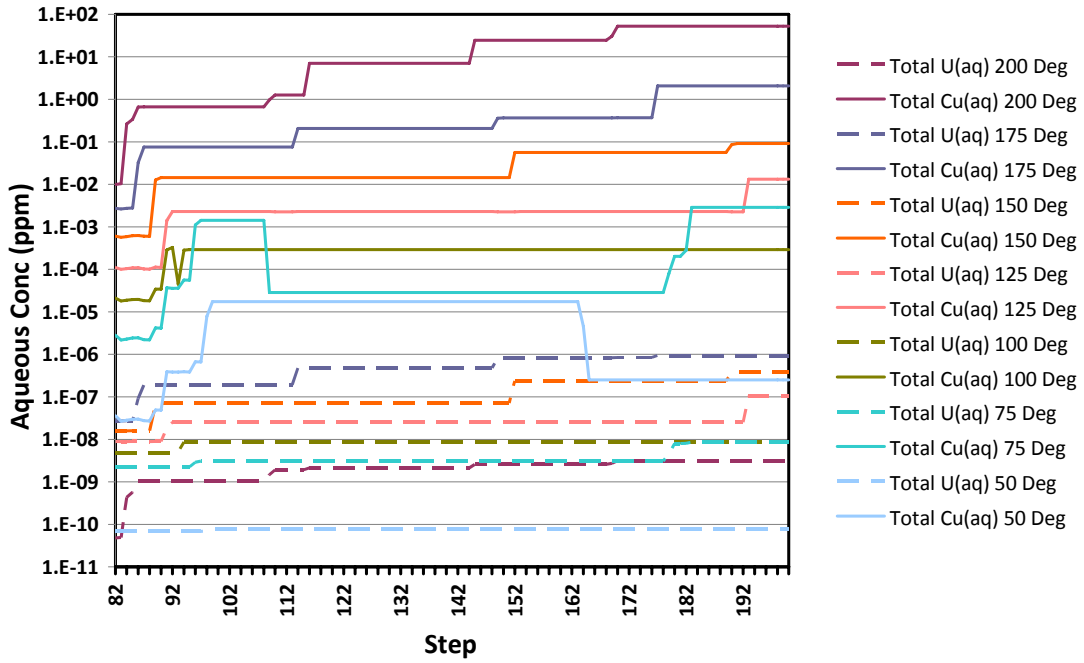

Figure 6.18(a): *Predicted total uranium concentration and total copper concentration in an ore fluid from the Nicholson Granite in equilibrium with the Seigal Volcanics at temperatures from 50° to 200°C respectively. See text for details.*

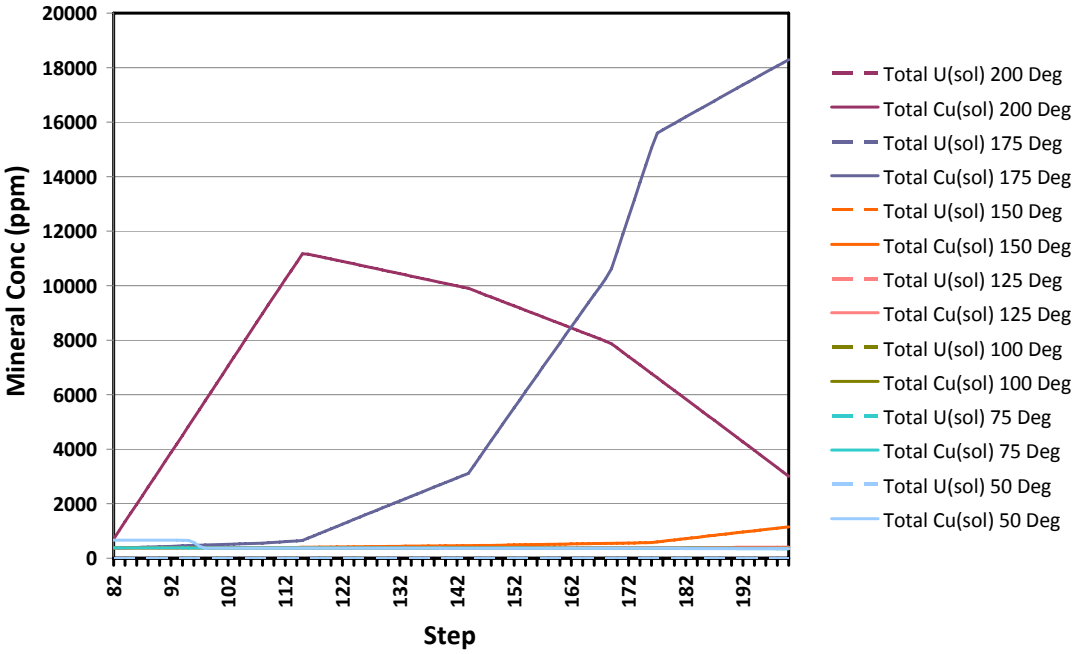

Figure 6.18(b): *Predicted total uranium concentration and total copper concentration of minerals(denoted as solids(sol) in the legend) precipitated from an ore fluid from the Nicholson Granite in equilibrium with the Seigal Volcanics at temperatures from 50° to 200°C respectively. Note that uranium concentrations remain close to zero at all temperatures. See text for details.*

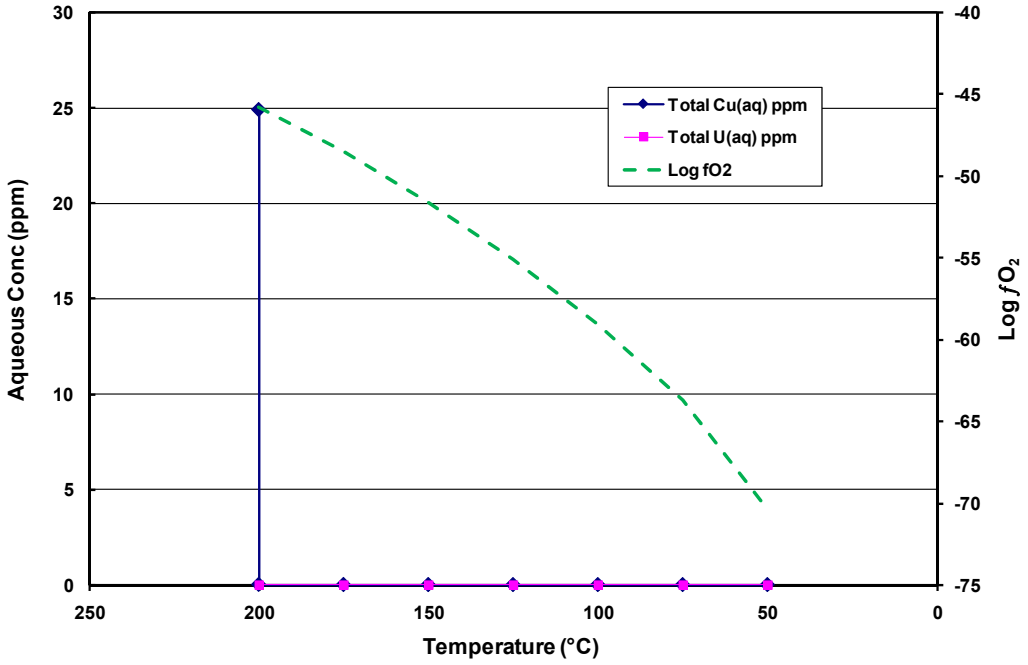

Figure 6.19(a): *Predicted total uranium concentration and total copper concentration in a Cu-rich fluid from the Nicholson Granite in equilibrium with the Seigal Volcanics at 200°C which is allowed to cool and equilibrate with the Seigal Volcanics at 200°, 175°, 150°, 100°, 75° and 50°C respectively. See text for details*

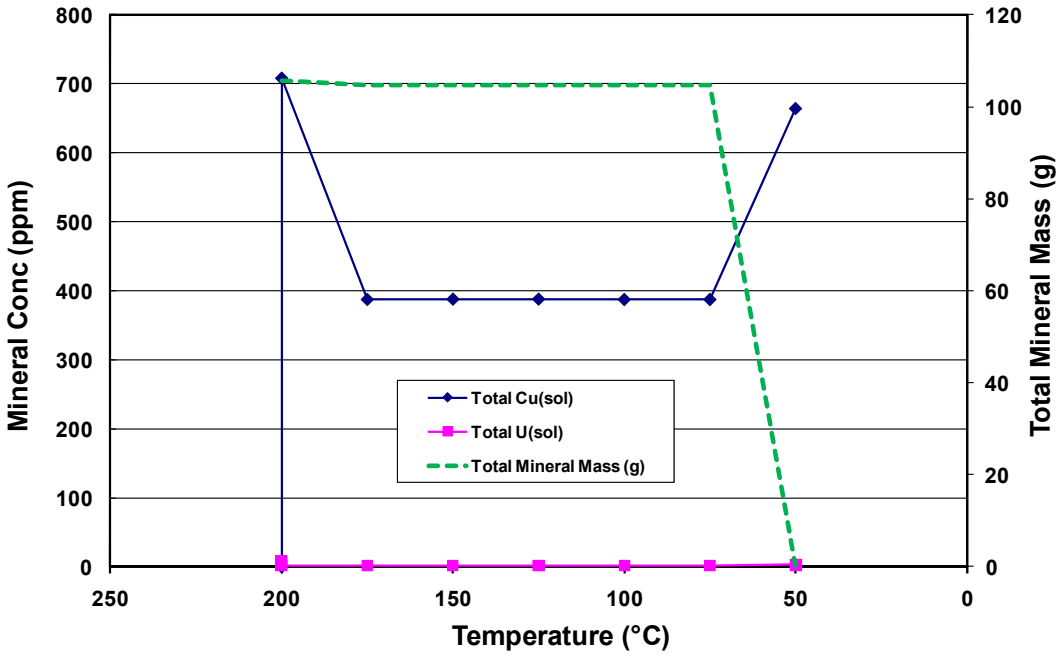

Figure 6.19(b): *Predicted total uranium concentration, total copper concentration and total mass of minerals (denoted as solids(sol) in the legend) precipitated from a Cu-rich fluid from the Nicholson Granite in equilibrium with the Seigal Volcanics at 200°C which is allowed to cool and equilibrate with the Seigal Volcanics at 200°, 175°, 150°, 100°, 75° and 50°C respectively. See text for details*

The concentration of copper and uranium minerals precipitated from the same solution is shown in Figure 6.19b. Equilibration of the fluid with the Seigal Volcanics at 200°C results in the immediate precipitation of 707 ppm of copper (as chalcopyrite), whereas at temperatures between 175° and 75°C only 387 ppm of copper (as chalcopyrite) is predicted to precipitate. For a fluid at 50°C, 663 ppm of chalcopyrite is predicted to precipitate, but the increase in copper concentration is due to the fact that the total amount of minerals precipitated at 50°C is less than 1% of the amount at higher temperatures. Therefore, if we ignore the result at 50°C, a constant amount of copper is precipitated by reaction of this fluid at temperatures below 175°C.

6.2.3.8 Model 2 – Part 4: Equilibration of U-rich fluids from the Nicholson Granite with the overlying Seigal Volcanics

To obtain a uranium-enriched fluid, the fluid in equilibrium with the Nicholson Granite at 200°C in step 88 in Model 2 - Part 1 was extracted and used as the input fluid for this part of the numerical model. This fluid had a uranium concentration of 15.2 ppm but the copper concentration was only 0.95 ppm. The fluid was then reacted with fresh Seigal Volcanics at temperatures of 200°, 175°, 150°, 125°, 100°, 75°, and 50°C to mimic the effect of cooler fluids flowing through faults in the Seigal Volcanics.

The total copper and uranium concentrations in the U-rich fluid are shown in Figure 6.20a. The Figure is very similar to Figure 6.18a except that at 200°C the total concentration of uranium species in solution exceeds that of copper at step 173. At this step there is also a dramatic increase in the fO_2 of the solution which indicates that the Seigal Volcanics have become completely oxidised by the infiltrating fluid at this temperature (See Figure 6.20a). At all other temperatures, the total uranium concentration is several orders of magnitude less than the total copper concentration (Fig. 6.20a).

The total concentration of uranium and copper minerals precipitated from the U-rich solution is shown in Figure 6.20b. At the lower temperatures around 380 ppm of copper minerals are precipitated from each batch of fluid. At 175°C the amount of copper minerals gradually increases up to around 2000 ppm per batch of fluid but the maximum amount decreases to around 600 ppm at 200°C. Each batch of fluid typically only precipitates around 2 ppm of uranium minerals (Fig. 6.20b). However, at 175ºC the amount of uranium starts to increase at step 173 and rises up to 3960 ppm of uranium at step 200. At 200°C the amount of uranium precipitated exceeds the amount of copper minerals for all but the first few steps (Fig. 6.20b) and rises to a maximum of 1.3 wt%.

A plot of the uranium/copper ratio concentration for the minerals precipitated in this scenario is shown in Figure 6.20(c). In this Figure it can be seen that the U/Cu ratio remains very low at temperatures below 175°C. However, at 175°C the U/Cu ratio exceeds 1.0 at step 186 which corresponds to a fluid:rock ratio of 970:1, while at 200°C the ratio exceeds 1.0 at a fluid:rock ratio of only 30:1 and copper ceases to precipitate at fluid:rock ratios above 730:1. Figure 6.20(d) indicates that uranium becomes the dominant mineral when the log fO_2 exceeds about -45 and copper mineralisation ceases completely when log fO_2 exceeds -40. These results demonstrate that relatively low-grade, copper-rich mineralisation in the Seigal Volcanics is favoured at low temperatures, and low fO_2 but relatively-high grade, uranium-only mineralisation is favoured at temperatures of 200°C or higher and high fO_2.

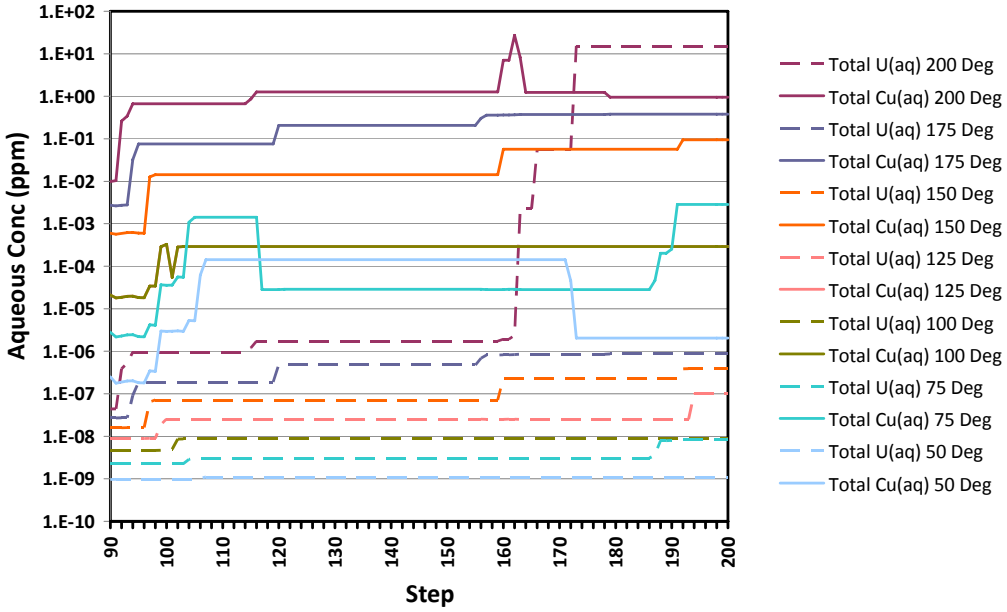

Figure 6.20(a): *Predicted total uranium concentration and total copper concentration in a U-rich fluid equilibrated with the Nicholson Granite during reaction with the Seigal Volcanics at 50°, 75°, 100°, 125°, 150°, 175° and 200°C respectively. See text for details.*

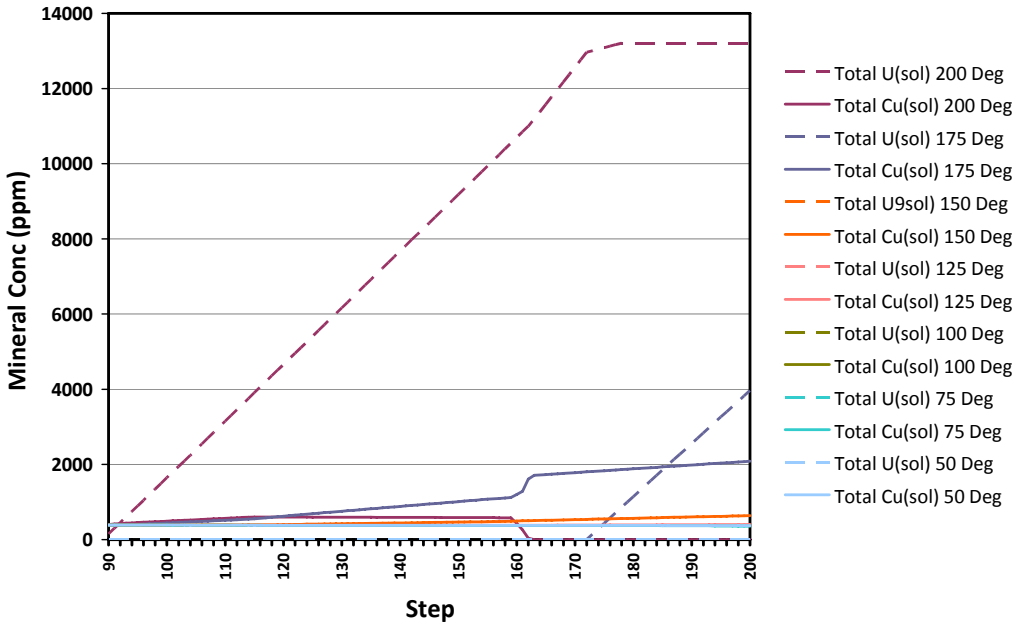

Figure 6.20(b): *Predicted total uranium concentration and total copper concentration of minerals (denoted as solids(sol) in the legend) precipitated from a U-rich fluid equilibrated with the Nicholson Granite during reaction with the Seigal Volcanics at 50°, 75°, 100°, 125°, 150°, 175° and 200°C respectively. See text for details.*

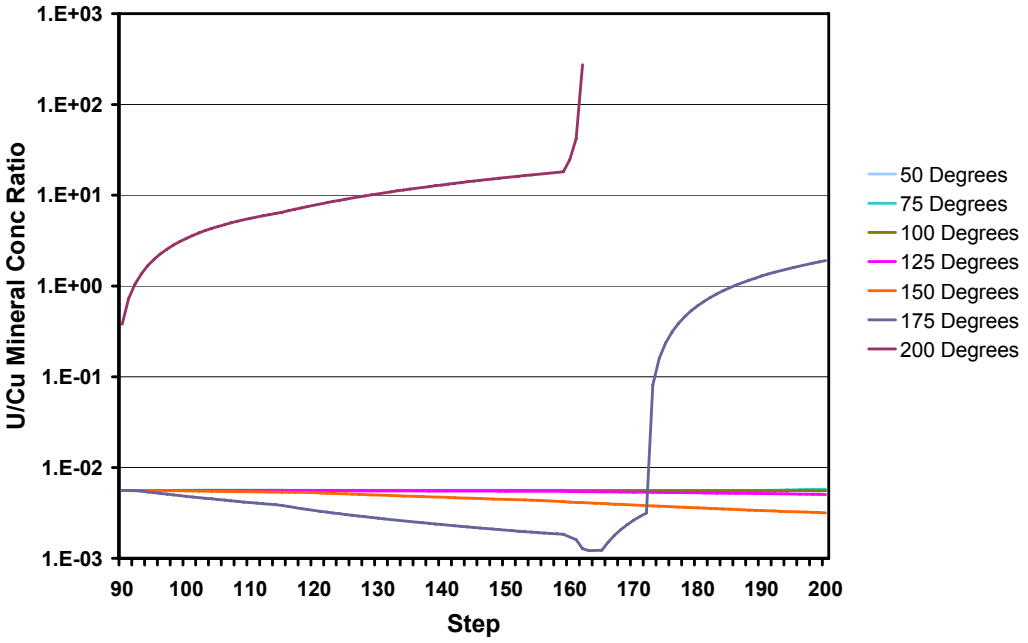

Figure 6.20(c): *Plot of the uranium/copper ratio concentration for minerals precipitated from a U-rich fluid equilibrated with the Nicholson Granite during reaction with the Seigal Volcanics at 50°, 75°, 100°, 125°, 150°, 175° and 200°C respectively. See text for details.*

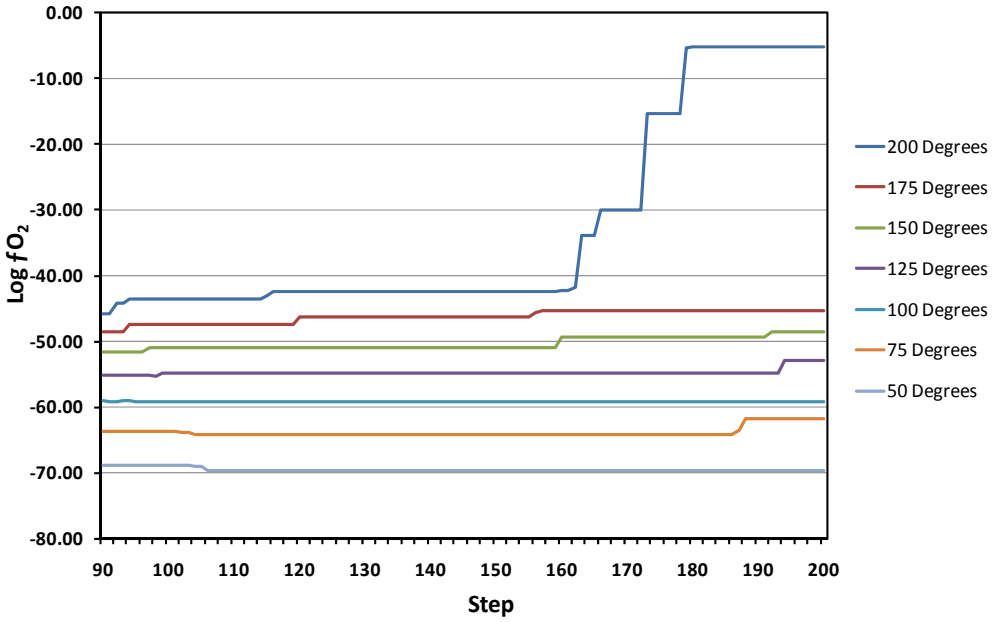

Figure 6.20(d): *Plot of Log fO_2 in a U-rich fluid equilibrated with the Nicholson Granite during reaction with the Seigal Volcanics at 50°, 75°, 100°, 125°, 150°, 175° and 200°C respectively. See text for details.*

6.2.3.9 Model 2 – Part 5: Closed-system cooling of U-rich fluids from the Nicholson Granite with the overlying Seigal Volcanics

In this scenario, a 1 kg batch of the uranium-rich fluid in equilibrium with the Nicholson Granite at 200°C in Model 2 – Part 1 was extracted at step 88 of the numerical model. This fluid contains 15.2 ppm of uranium species but only 0.95 ppm of copper species. This batch of fluid was then allowed to equilibrate with the Seigal Volcanics at decreasing temperatures of 200º, 175º, 150º, 125º, 100º, 75º and 50°C respectively. This simple cooling scenario differs from Part 4 as there is no input of additional batches of fluid as time progresses. The results are shown in Figure 6.21.

The concentration of copper and uranium species in solution is shown in Figure 6.21a. It can be seen that immediately upon reacting with the Seigal Volcanics at 200°C the concentration of uranium species decreases over nine orders of magnitude and continues to decrease to lower values at lower temperatures. In comparison the concentration of copper species in solution only decreases two orders of magnitude but continues to decrease another five orders of magnitude with decreasing temperature (Fig 6.21a). In this simple cooling scenario the log fO_2 of the solution decreases gradually with decreasing temperature as expected (Fig 6.21a).

The concentration of copper and uranium minerals precipitated from the same solution is shown in Figure 6.21b. This Figure shows that the original fluid from the Nicholson Granite would precipitate approximately 550 ppm of UO_3 (instead of uraninite) before it came in contact with the volcanic rock but would still precipitate approximately 150 ppm of uraninite when equilibrated with the Seigal Volcanics at 200°C. However, at lower temperatures, the fluid in equilibrium with the Seigal Volcanics would only precipitate approximately 2 ppm of uraninite. In contrast, a relatively constant amount (~387 ppm) of chalcopyrite is precipitated when the fluid is equilibrated with the Seigal Volcanics. This indicates that simple cooling of a U-rich fluid in contact with the Seigal Volcanics will only precipitate significant quantities of uranium at temperatures above 175°C. However, relatively significant quantities of copper minerals are precipitated at all temperatures in this model even from this U-rich fluid.

6.2.4 Summary

The geochemical modelling has shown that various topographically recharging fluid-flow models can explain the transport and deposition of uranium and copper in the Westmoreland mineral systems and the outcomes are summarised in Table 6.5. The first model involves the passage and equilibration of an oxidised fluid through the Westmoreland Conglomerate and then the leakage of this fluid up faults and shear zones into the overlying Seigal Volcanics. The simulation demonstrates that both uranium and copper minerals will precipitate by interaction of the fluid with the Westmoreland Conglomerate but it also shows that continuous fluid flow after uranium and copper precipitation will redissolve the minerals. Therefore, preservation of the uranium mineralisation in the Westmoreland Conglomerate will only occur if there is insignificant later fluid flow, for example, due to the aquifers being sealed by the precipitation of silica and other minerals.

The numerical modelling indicated that at 125°C and a fluid:rock ratio of 5600:1 the Westmoreland Conglomerate was completely oxidised, allowing the fluid to maintain its high oxidation state as it passes through this rock unit. The modelling showed that if this fluid was Cu-rich and was allowed to flow into the overlying Seigal Volcanics, then a significant amount of copper minerals would be precipitated as the fluid flowed through the volcanic rock. The modelling also predicts that U-rich fluids at temperatures of 125°C will form uranium-copper deposits in the Seigal Volcanics whereas

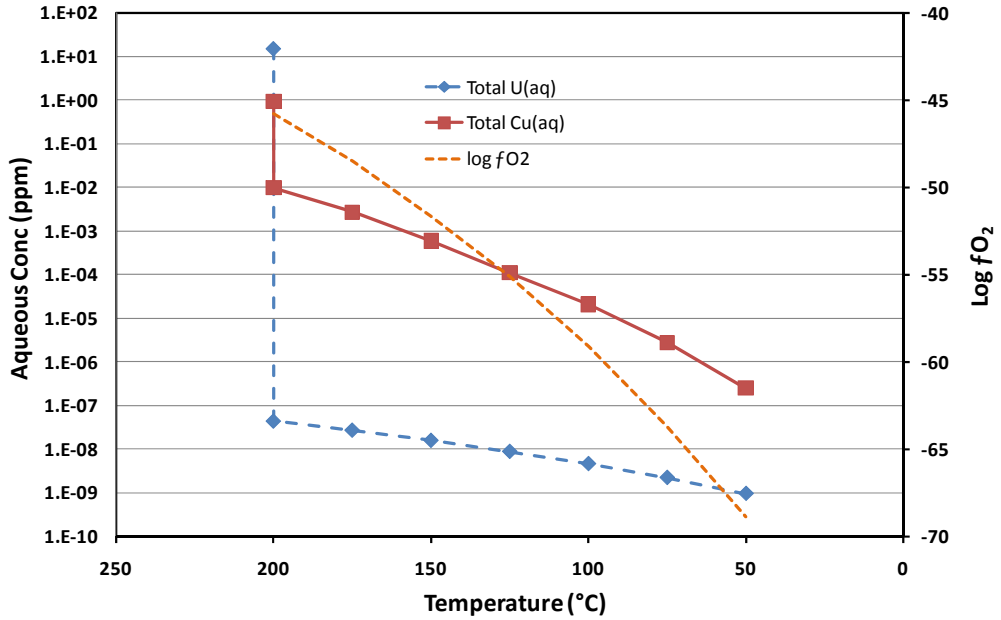

Figure 6.21(a): *Predicted total uranium concentration and total copper concentration in a U-rich fluid equilibrated with the Nicholson Granite Granite in equilibrium with the Seigal Volcanics at 200°C which is allowed to cool and equilibrate with the Seigal Volcanics at 200°, 175°, 150°, 100°, 75° and 50°C respectively. See text for details*

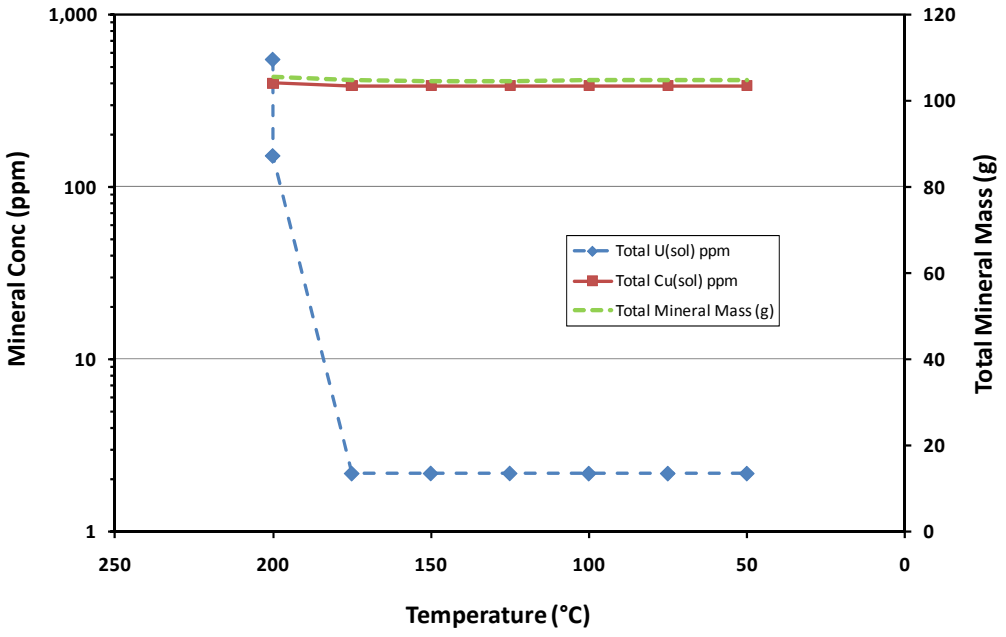

Figure 6.21(b): *Predicted total uranium concentration, total copper concentration and total mass of minerals (denoted as solids(sol) in the legend) precipitated from a fluid equilibrated with the Nicholson Granite Granite in equilibrium with the Seigal Volcanics at 200°C which is allowed to cool and equilibrate with the Seigal Volcanics at 200°, 175°, 150°, 100°, 75° and 50°C respectively. See text for details*

lower temperature fluids will form copper-rich deposits. In a second scenario, a batch of Cu-rich fluid was allowed to cool while in equilibrium with the Seigal Volcanics. This demonstrates that significant precipitation of copper minerals will occur upon initial equilibrium with the Seigal Volcanics at 125°C and the very little copper is precipitated on further cooling.

The second model was similar to the first but in this case the fluid penetrated deeper into the basin and also equilibrated with the underlying Nicholson Granite. Like the first model, significant quantities of uraninite and chalcopyrite are predicted to precipitate in the Westmoreland Conglomerate at specific fluid:rock ratios at the specified temperatures. However, the concentration of uraninite is predicted to be greater than the concentration of chalcopyrite.

The passage of Cu-rich fluids from the second model into the Seigal Volcanics results in increasing amounts of copper precipitation at all temperatures studied except 200°C. At 200°C the model predicts that the amount of copper precipitated will decrease again with increasing fluid:rock interaction as the Seigal Volcanics are progressively oxidised. The passage of U-rich fluids results in relatively low-grade, copper-rich mineralisation at low temperatures, and low fO_2 but relatively-high grade, uranium-only mineralisation at temperatures of 200°C or higher and high fO_2. In the second scenario, where a 200°C, Cu-rich fluid equilibrated with the Nicholson Granite cools in equilibrium with the Seigal Volcanics, the bulk of the copper precipitates at 200°C upon initial interaction with the Seigal Volcanics. However, for the same scenario with a U-rich fluid the bulk of the uranium precipitates at 200°C upon initial contact with the Seigal Volcanics but copper continues to precipitate down to 50°C.

Table 6.5 Summary of geochemical modelling outcomes.

Model 1 – Oxidised fluid flow in the Westmoreland Conglomerate and Seigal Volcanics

Part 1 – Equilibration of an O_2 saturated fluid with the Westmoreland Conglomerate

This model shows that stratabound deposits of uranium and copper may form in the Westmoreland Conglomerate in regions of high ferrous iron (or other reductants) in a mechanism similar to that for roll-front uranium deposits. These deposits would only be preserved if there was little or no passage of oxidised fluids after the deposit had formed.

Part 2 – Equilibration of Cu-rich fluids with the overlying Seigal Volcanics

At 125ºC 700 ppm of copper minerals are precipitated upon initial reaction with the Seigal Volcanics and the amount increases as the fluid:rock ratio increases. At lower temperatures the amount of copper precipitated remains constant at 400 ppm.

Part 3 – Closed-system cooling of Cu-rich fluids in equilibrium with the overlying Seigal Volcanics

This model also predicts that ~700 ppm of copper minereals will precipitate upon initial reaction with the Seigal Volcanics at 125ºC but the amount drops to 387 ppm at lower temperatures.

Part 4 – Equilibration of U-rich fluids with the overlying Seigal Volcanics

At 125ºC the model predicts that initially more copper minerals will precipitate than uranium minerals but the amount of uranium minerals deposited increases with increasing fluid:rock ratio until at a ratio of 600:1 there is 6750 ppm uraninite and 2440 ppm chalcopyrite. This uranium enrichment does not occur at lower temperatures where each batch of fluid precipitates a constant 378 ppm chalcopyrite and 2 ppm uranium minerals.

Model 2 – Deep oxidised fluid flow in the Westmoreland Conglomerate and Seigal Volcanics

Part 1 – Equilibration of an O_2 saturated fluid with the Nicholson Granite

This model predicts a sudden onset of precipitation of both copper and uranium minerals in the Westmoreland Conglomerate with the initial onset of precipitation occurring progressively later as the temperature increases. The concentration of uranium minerals exceeds that for copper minerals reaching values of approximately 1.5 wt.% at 150°C. In comparison the concentration of copper minerals only reaches 0.5 wt.% at 150°C before decreasing again at higher temperatures.

Part 2 – Equilibration of Cu-rich fluids from the Nicholson Granite with the overlying Seigal Volcanics

At temperatures up to 100°C, around 380 ppm of copper minerals precipitate with each batch of fluid equilibrated with the Seigal Volcanics. At temperatures between 100º and 200°C the concentration of copper minerals gradually increases with each batch of fluid but at 200°C the copper mineral concentration initially increases and then decreases with each batch of fluid. This indicates that, in this model, copper minerals may be resorbed and remobilised at temperatures above 200°C.

Part 3 – Closed-system cooling of Cu-rich fluids from the Nicholson Granite with the overlying Seigal Volcanics

Equilibration of the Cu-rich fluid with the Seigal Volcanics at 200°C results in the immediate precipitation of ~700 ppm copper minerals, whereas at temperatures between 175° and 75°C only 387 ppm of chalcopyrite is predicted to precipitate. A constant 387 ppm of copper minerals are precipitated by reaction of this Cu-rich fluid with the Seigal Volcanics at temperatures between 75 and 175°C.

Part 4 – Equilibration of U-rich fluids from the Nicholson Granite with the overlying Seigal Volcanics

This model predicts that mostly copper minerals will precipitate after reaction with the Seigal Volcanics at lower temperatures rising to around 2000 ppm copper minerals at 175ºC. Each batch of fluid typically only precipitates around 2 ppm of uranium minerals. However, at 175ºC the amount of uranium minerals increases to 3960 ppm and at 200°C the amount of uranium minerals rises to a maximum of 1.3 wt%.

Part 5 – Closed-system cooling of U-rich fluids from the Nicholson Granite with the overlying Seigal Volcanics

Cooling of the fluid from the Nicholson Granite will precipitate approximately 550 ppm of uranium minerals before it comes in contact with the overlying volcanics but would still precipitate approximately 150 ppm of uranium minerals when equilibrated with the Seigal Volcanics at 200°C. However, at lower temperatures, the fluid in equilibrium with the Seigal Volcanics will only precipitate approximately 2 ppm of uraninite. In contrast, a nearly constant ~387 ppm of copper minerals are precipitated when the fluid is equilibrated with the Seigal Volcanics. This indicates that simple cooling of a U-rich fluid in contact with the Seigal Volcanics will only precipitate significant quantities of uranium minerals at temperatures above 175°C. However, relatively significant quantities of copper minerals are precipitated at all temperatures in this model even from this U-rich fluid.

The above results indicate that oxidised fluids flowing through basinal aquifers will gradually oxidise the sediments as the fluid:rock ratio increases. They therefore induce an oxidation front, similar to a roll-front, where uranium and copper minerals are progressively deposited and remobilised. The modelling predicts that when these oxidised fluids interact with the overlying Seigal Volcanics, copper-rich mineralisation or copper mineralisation with minor uranium

mineralisation will occur. However, if these oxidised basinal fluids equilibrate with the Nicholson Granite before they react with the Seigal Volcanics, then relatively low-grade, copper-rich mineralisation is favoured at low temperatures, and low fO_2 but relatively-high grade, uranium-only mineralisation is favoured at temperatures of 200°C or higher and high fO_2. Therefore, at higher temperatures, the Nicholson Granite buffers the basinal fluids to a level that favours uranium transport over copper transport. This indicates that the formation of Cu-rich or U-rich mineralisation is dependent on the temperature and fO_2 of the basinal fluids. In other words, the depth of fluid flow, which is related to fluid temperature, and the fluid:rock ratio in the aquifer will determine the U/Cu ratio in the fluid if there is a suitable source for these metals. Therefore, both copper and uranium mineralisation may occur in the same mineral system but in different parts of the basin.

7. Conclusions: implications for exploration

7.1 CHEMICAL MODELLING OF SELECTED SYSTEMS ASSOCIATED WITH BASINAL FLUIDS

Chemical modelling of topographically recharging fluid-flow in a generalised sedimentary basin undergoing diagenesis reveals that geologically significant concentrations of uranium, copper, lead and zinc can be successfully transported to the site of deposition. The behaviour of these metals in solution is dominantly controlled by the oxidation state of the fluid and the host rocks. As the oxidised fluid flows through the reduced aquifer it will induce an oxidation front, similar to a roll-front, where zones of uranium and base metals are progressively deposited and remobilised. The preservation of these zones depends on the fluid flow regime in the basin and requires cessation of fluid flow after reaching a particular value. The modelling indicates that very high fluid:rock ratios are required in order to achieve complete oxidation of the sandstone aquifer after which the fluid can flow through it without precipitating any metals.

The presence of evaporitic beds in the basin is an important element of fertile systems. They are essential to generate fluids with the moderate to high salinities (5 and to 20 wt% NaCl) assumed in our calculations and for the transport of significant amounts of copper and other base metals. However, varying the composition of the sandstone has shown that the presence of pyrite in the unaltered sandstone has a far more significant effect on the solubility of ore-forming elements than the salinity of the initial fluid. This results from the oxidation of pyrite-rich sandstone which generates more acidic fluids dominated by SO_4^{-2} which then forms stable complexes with uranium.

More detailed models, which used the geology of the Westmoreland region in northern Australia to constrain the composition of the rocks and fluids, showed that these fluids are capable of transporting significant quantities of both uranium and copper species. Both these metals will precipitate by interaction of the fluid with the Westmoreland Conglomerate but, as shown by the generalised basinal model, further fluid flow after uranium and copper precipitation will remobilise the minerals once again. Therefore, preservation of the uranium mineralisation in the Westmoreland Conglomerate will only occur if there is a cessation of fluid flow after mineralisation.

Furthermore, fluids which penetrated deeper into the basin and also interacted with the Nicholson Granite were more likely to form copper-rich deposits when they initially interacted with the overlying Seigal Volcanics but uranium-rich deposits could form at temperatures of 150 °C or greater, particularly if fluid flow continued causing re-dissolution of the copper that precipitated earlier in the model. Therefore, this modelling has demonstrated that higher temperature basinal fluids (up to 200 °C) associated with unconformity-related systems may form high-grade uranium mineralisation.

In all modelled cases, the overlying, relatively reduced, volcanic unit was found to be an excellent trap rock that precipitated both uranium and copper from fluid:rock interaction or by cooling of fluids in equilibrium with the volcanic units. However, the formation of a uranium- or copper-rich deposit was strongly dependent on the composition of the basinal fluid at the time it was extracted from the aquifer in the Westmoreland Conglomerate.

The implications for exploration from this modelling are that the processes occurring in unconformity-related systems are similar to those that occur in lower-temperature sandstone-hosted

systems. Therefore, uranium, copper and other metals will be continually precipitated and remobilised within basinal aquifers until they become completely oxidised. At the conclusion of this process, however, it is the juxtaposition of oxidised and reduced rocks or fluids that controls precipitation of the metals from the ore fluids. This may occur at a reduction front near an unconformity, or when oxidised fluids encounter mafic igneous rocks or other reduced rocks within the basin, or when oxidised fluids mix with basement-derived, reduced fluids. The modelling also demonstrates that these deposits will only be preserved if there is limited interaction with oxidised fluids after the mineralisation event.

References

Ahmad, M. and Wygralak, A. S., 1989. Calvert Hills SE53-8 Explanatory Notes and Mineral Deposit Data Sheets. Darwin, Northern Territory Geological Survey. 55p.

Ahmad, M. and Wygralak, A. S., 1990. Murphy Inlier and Environs - Regional Geology and Mineralisation. *Geology of the Mineral Deposits of Australia and Papua New Guinea.* F. E. Hughes (ed). Melbourne, The Australasian Institute of Mining and Metallurgy. 819-826.

Barsukov, V. L. and Borisov, M. V., 2003. Models of uranium dissolution in natural waters of various Compositions. *Geochemistry International* **41**, 38-63.

Bennett, P. C. and Siegel, D. I., 1987. Increased solubility of quartz in water due to complexing by organic compounds. *Nature*, **326**, 684–686.

Bethke, C. M., 2007. Geochemical and Biogeochemical Reaction Modeling. Second Edition. Cambridge, Cambridge University Press, 564p.

Borisov, M. V. and Shvarov, Y. V., 1992. Thermodynamics of geochemical processes. Moscow, Moscow State University Publishing House, 254p.

Boyle, D., R, 1982. The Formation of Basal-Type Uranium Deposits in South Central British Columbia. *Economic Geology*, **77**, 1176 - 1209.

Brookins, D. G., 1975. Coffinite-uraninites tability relationsi n the Grants Mineral Belt. *Am. Assoc. Petroleum Geologists Bull.*, **59**, 905.

Brown, A. C., 2009. A process-based approach to estimating the copper derived from red beds in the sediment-hosted stratiform copper deposit model. *Economic Geology*, 104, 857-868.

Brown, A. C., 2006. Close linkage of copper (and uranium) transport to diagenetic reddening of "upstream" basin sediments for sediment-hosted stratiform copper (and roll-type uranium) mineralization. *Journal of Geochemical Exploration*, 89, 23-26.

Brown, A. C., 2005. Refinements for footwall red-bed diagenesis in the sediment-hosted stratiform copper deposits model. *Economic Geology*, **100**, (4), 765-771.

Brown, A. C., 2003. Redbeds: source of metals for sediment-hosted stratiform copper, sandstone copper, sandstone lead, and sandstone uranium-vanadium deposits. *Geochemistry of Sediments and Sedimentary Rocks: Evolutionary Considerations to Mineral Deposit-Forming Environments*. D. R. Lenz (ed). Geological Associateion of Canda, GeoText, 4. 121-133.

Butt, C. R. M., Mann, A. W. and Horwitz, R. C., 1984. Regional setting, distribution and genesis of surficial uranium deposits in calcretes and associates sediments in Western Australia. *Surficial Uranium Deposits, TECDOC-322*. (ed). Vienna. 121-127.

Capus, G., 1979. Matières organiques et minéralisations uranifères: exemples des bassins Permo-Carbonifères de l'Aumance (Allier) et de Lodève (Hérault). Institut National Polytechnique de Lorraine, PhD, p.

Cherkasova, E. V. and Ryzhenko, B. N., 2010. Physicochemical Computer Model of the Formation of the Granitoid Associated Uranium Mineralization. *Geochemistry International*, **48**, 238–259.

Cuney, M., 1978. Geologic environment, mineralogy and fluid inclusions of the Bois Noirs—Limouzat uranium vein, Forez, France. *Economic Geology*, **73**, 1576–610.

Dahlkamp, F. J., 1993. Uranium ore deposits. Heidelberg, Springer-Verlag, 460p.

De Voto, R. H., 1978. Uranium geology and exploration. Golden, Colorado School of Mines, 396p.

Gardner, C. M., 1978. Precambrian geology of the Westmoreland region, northern Australia : Part 3: Nicholson Granite Complex and Murphy Metamorphics . *Bureau of Mineral Resources, Geology and Geophysics, Record*, Bureau of Mineral Resources, Geology and Geophysics. 74 p.p.

Garrels, R. M. and Christ, C. L., 1965. Solutions, minerals, and equlibria. Boston, Jones and Bartlett Publishers, 450p.

Goldhaber, M. B., Hemingway, B. S., Mohagheghi, A., Reynolds, R. L. and Northrop, H. R., 1987. Origine of coffinite in sedimentary rocks by sequential adsorption reduction mechnism. *Bulletin de Mineralogie* **110**, (2-3), 131-144.

Gorman-Lewis, D., Burns, P. C. and Fein, J. B., 2008. Review of uranyl mineral solubility measurements *The Journal of Chemical Thermodynamics*, **40**, (3), 335-352 .

Grenthe, I., Fuger, J., Konings, R. J. M., Lemire, R. J., Muller, A. B., Nguyen-Trung, C. and Wanner, H., 1992. Chemical thermodynamics of uranium. 714p.

Grenthe, I., Sandino, M. C. A., Puigdomenech, I. and Rand, M. H., 1995. Corrections to the Uranium NEA-TDB review. Aendix D in Vol. 2. Chemical Thermodynamics of Americium. by R.J. Silva et al. Nuclear Energy Agency, OECD *Chemical Thermodynamics of Americium*. R. J. e. a. A. Silva (ed). Amsterdam., Elsevier,. 2, 347-374.

Gross, E. B., 1956. Mineralogy and paragenesis of the uranium ore, Mi Vida Mine, San Juan County, Utah. *Economic Geology*, **51**, Gross, 1956 E.B. Gross, Mineralogy and paragenesis of the uranium ore, Mi Vida Mine, San Juan County, Utah, Economic Geology 51 (1956), . 632–648. Full Text via CrossRef.

Guillaumont, R., Fanghänel, T., Fuger, J., Grenthe, I., Neck, V., Palmer, D. A. and Rand, M. H., 2003. Update on the chemical thermodynamics of uranium, neptunium, plutonium, americium and technetium. 970p.

Hanor, J. S., 1994. Physical and chemical controls on the composition of waters in sedimentary basins. *Marine and Petroleum Geology*, 11, (1), 31-45.

Hemingway, B. S., 1982. Thermodynamic properties of selected uranium compounds and aqueous species at 298.15 K and I bar and at higher temperatures -- Preliminary models for the origin of coffinite deposits. U.S. Geological Survey Open-File Report 82-619 U.S. Geological Survey. 90p.

Hills, J. H., 1973. Lead isotopes and the regional geochemistry of North Australian uranium deposits. Sydney, Macquarie University, PhD, p.

Hitzman, M., Kirkham, R., Broughton, D., Thorson, J. and Selley, D., 2005. The sediment-hosted stratiform copper ore system. *Economic Geology 100th Anniversay Volume*, 609-642.

Horstmann, U. E., and Halbich, I. W., 1995. Chemical composition of banded iron-formations of the Griqualand West Sequence, Northern Cape Province, South Africa, in comparison with other Precambrian iron formations. *Precambrian Research*, 72, 109-145.

Jefferson, C. W. and Delaney, G., 2007. EXTECH IV : geology and uranium EXploration TECHnology of the Proterozoic Athabasca Basin, Saskatchewan and Alberta. 644.

Kimberley, M. M., 1979. High-temperature uranium geochemistry. *Short course in uranium deposits: their mineralogy and origin*. S. J. Kimberley and M. M. Kimberley (ed). Toronto, Mineralogical Association of Canada. 3, 101 - 104.

Komninou, A. and Sverjensky, D. A., 1996. Geochemical modeling of the formation of an unconformity-type uranium deposit. *Economic Geology and the Bulletin of the Society of Economic Geologists*, **91**, (3), 590-606.

Landais, P., 1993. Bitumens in uranium deposits. *Bitumens in ore deposits*. J. Parnell, Kucha, H., Landais, P. (ed). Berlin, Springer-Verlag. 213 - 238.

Langmuir, D., 1978. Uranium solution-mineral equilibria at low temperatures with alications to sedimentary ore deposits. *Geochimica et Cosmochimica Acta*, **42**, 547 - 569.

Langmuir, D., 1979. Uranium solution-mineral equilibria at low temperatures with alications to sedimentary ore deposits. *Short Course in uranium deposits: their mineralogy and origin*. S. S. Kimberley and M. M. Kimberley (ed). Toronto, Mineralogical Association of Canada. 3, 17 - 56.

Langmuir, D., 2001. Book review: Uranium: mineralogy, geochemistry and the environment. *American Mineralogist*, **86**, 585-587.

Larsen, E., S. and Gottfried, D., 1961. Dsitribution of uranium in rocks and minerals of Mesozoic Batholiths in Western United States. Washington D. C., United States Department of the Interior, Geological Survey, 103p.

Leventhal, J. S., Grauch, R. I., Threlkeld, C. N., Lichte, F. E. and Harper, C. T., 1987. Unusual organic matter associated with uranium from the Claude Deposit, Cluff Lake, Canada. *Economic Geology*, **82**, (5), 1169-1176.

Ludwig, K. R. and Grauch, R. I., 1980. Coexisting coffinite and uraninite in some sandstone-host uranium ores of Wyoming. *Economic Geology*, **75**, 296-802.

Mann, A. W. and Deutscher, R. L., 1978. Genesis principles for the precipitation of carnotite in calcrete drainages in Western Australia. *Economic Geology*, **73**, (8), 1724-1737.

Marshall, W. L. and Franck, E. U., 1981. Ion product of water substance, 0-1000°C, 1-10000 bars new international formulation and its background. *J. Phys. Chem. Ref. Data*, **10**, (2), 295-304.

Murphy, W. M. and Shock, E. L., 1999. Environmental aqueous geochemistry of actinides. In Burns, P.C., and Finch, R. (eds.) Uranium: Mineralogy, Geochemistry and the Environment. Mineralogical Society of America Reviews in Mineralogy, 38, 221 - 253.

Parks, G. A. and Pohl, D. C., 1988. Hydrothermal solubility of uraninite. *Geochimica et Cosmochimica Acta*, **52**, 836–875.

Pearson, R. G., 1963. Hard and soft acids and bases. *Journal of the American Chemical Society*, **85**, 3533 - 3539.

Peiffert, C., Cuney, M. and Nguyen-Trung, C., 1994. Uranium in granitic magmas. Part I: Experimental determination of uranium solubility and fluid-melt partition coefficients in the uranium ox-ide-haplogranite-H2O-Na2CO3 system at 770°C, 2 kbar,. *Geochimica et Cosmochimica Acta*, **58**, 2495–2507.

Peiffert, C., Nguyen-Trung, C. and Cuney, M., 1996. Uranium in granitic magmas: Part 2. Experimental determination of uranium solubility and fluid-melt partition coefficients in the uranium oxide-haplogranite-H2O-NaX (X = Cl, F) system at 770°C, 2 kbar. *Geochimica et Cosmochimica Acta*, **60**, (9), 1515-1529.

Plyasunov, A. V. and Grenthe, I., 1994. The temperature dependence of stability constants for the formation of polynuclear cationic complexes. *Geochimica et Cosmochimica Acta*, **58**, (17), 3561-3582.

Polito, P. A., Kyser, T. K., Rheinberger, G. and Southgate, P. N., 2005. A Paragenetic and Isotopic Study of the Proterozoic Westmoreland Uranium Deposits, Southern McArthur Basin, Northern Territory, Australia. *Economic Geology*, **100**, 1243-1260.

Rafalsky, R. P. and Sidorov, 1958. NOT READY. .

Rawlings, D. J., 2001. Sedimentology, volcanology and geodynamics of the Redbank package, McArthur basin, northern Australia. Hobart, University of Tasmania, 439 p.p.

Rich, R. A., Holland, H. D. and Petersen, U., 1977. Hydrothermal uranium deposits. Amsterdam, Elsevier Scientific Publishing Company, 264p.

Robie, R. A. and Hemingway, B. S., 1995. Thermodynamic properties of minerals and related substances at 298.15°K and 1 bar (10^5 Pascals) pressure and higher temperatures. *U.S. Geological survey bulletin*, **2131**, .

Robie, R. A., Hemingway, B. S. and Fisher, J. R., 1979. Thermodynamic properties of minerals and related substances at 298.15 K and 1 bar (105 pascals) pressure and at higher temperatures. *U.S. Geological survey bulletin*, **1452**, 456 p.

Romberger, S. B., 1984. Transport and deposition of uranium in hydrothermal systems at temperatures up to 300oC: geological implications. *Uranium geochemistry, mineralogy, geology, exploration and resources*. B. De Vivo, Iolito, F., Capaldi, G., Simpson, P. R. (ed). London, The Institution of mining and metallurgy. 12 - 17.

Rozhkova, E. V., Razumnaya, E. G., Serebrykova, M. B. and Scherbak, D. V., 1958. The role of sorption in the process of uranium concentration in sedimentary rocks. *UN 2nd International conference on the peaceful use of Atomic Energy, v2, Geneva*, 420 - 431.

Scott, D. L., Rawlings, D. J., Page, R. W., Tarlowski, C. Z., Idnurm, M., Jackson, M. J. and Southgate, P. N., 2000. Basement framework and geodynamic evolution of the Palaeoproterozoic superbasins of north-central Australia: an integrated review of geochemical, geochronological and geophysical data. *Australian Journal of Earth Sciences*, **47**, 341-380.

Shock, E. L. and Helgeson, H. C., 1988. Calculation of the thermodynamic and transport properties of aqueous species at high pressures and temperatures: correlation algorithms for ionic species and equation of state predictions to 5 kb and 1000°C. *Geochimica et Cosmochimica Acta*, **52**, (8), 2009-2036.

Shock, E. L., Helgeson, H. C. and Sverjensky, D. A., 1989. Calculation of the thermodynamic and transport properties of aqueous species at high pressures and temperatures: Standard partial molal properties of inorganic neutral species. *Geochimica et Cosmochimica Acta*, **53**, 2157-2183.

Shock, E. L., Sassani, D. C. and Betz, H., 1997. Uranium in geologic fluids: Estimates of standard partial molal properties, oxidation potentials, and hydrolysis constants at high temperatures and pressures. *Geochimica et Cosmochimica Acta*, **61**, (20), 4245-4266.

Shvarov, Y. V., 1999. Algorithmization of the numerical equilibrium modelling of dynamic geochemical processes. *Geochemistry International*, **37**, (6), 571-576.

Shvarov, Y. V. and Bastrakov, E. N., 1999. HCh: a software package for geochemical equilibrium modelling. User's Guide. Australian Geological Survey Organisation, Record 1999/25. 61p.

Shvarov, Y. V., Borisov, M. V., Grichuk, D. V. and Bastrakov, E. N., 1999. Default UNITHERM database for the HCh package for geochemical modelling. Unpublished computer file.

Shvarov, Y. V., Zharikov, V. A. and Zhandarova, T. V., 2000. Calculation of an infiltrational metasomatic column on the basis of the local equilibrium principle. Geochemistry International, 38, (11), 1041-1049pp.

Skirrow, R. G., Jaireth, S., Huston, D., Bastrakov, E., Schofield, A., van der Wielen, S. E., Barnicoat., A., 2009. Uranium mineral systems: Processes, exploration criteria and a new deposit framework. Geoscience Australia, Record 2009/20. 38p.

Smith, D. K., 1984. Uranium Mineralogy. *Uranium Geochemistry, Mineralogy, Geology, Exploration and Resources*. F. Iolito, B. DeVero and G. Capaldi (ed). London, Institute of Mining and Metallurgy. 43-71.

Spirakis, C. S., 1996. The roles of organic matter in the formation of uranium deposits in sedimentary rocks. *Ore Geology Reviews*, **11**, 53–69.

Steacy, H. R. and Kiaman, S., 1978. Uranium minerals in Canada: Their description, identification and field guides. *Uranium deposits, their mineralogy and origin*. M. M. Kimberley (ed). Toronto, Mineralogical Association of Canada. 3, 107 - 140.

Sverjensky, D. A., Shock, E. L. and Helgeson, H. C., 1997. Prediction of the thermodynamic properties of aqueous metal complexes to 1000°C and 5kb. *Geochimica et Cosmochimica Acta*, **61**, (7), 1359-1412.

Thoenen, T. and Kulik, D., 2003. Nagra/PSI Chemical Thermodynamic Data Base 01/01 for the GEM-Selektor (V.2-PSI) Geochemical Modeling Code: Release 28-02-03. Unpublished report. Paul Scherrer Institut. 43p.

Unrug and R, 1988. Mineralization controls and source of metals in the Lufilian Fold Belt, Shaba (Zaire), Zambia, and Angola. *Economic Geology*, **83**, 1247 - 1258.

van der Lee, J. and Lomenech, C., 2003. Towards a common thermodynamic database for speciation models. *Radiochimica Acta*, **92**, (9-1), 811-818.

Walker, T. R., 1989. Application of diagenetic alterations in redbeds to the origin of stratiform copper deposits. Sediment-hosted Stratiform Copper Deposits, Boyle, R. W., Brown, A. C., Jefferson, C. W., Jowett, E. C., Kirkham, R. V. (eds). Geological Association of Canada. Special Paper, vol. 36, 85-96.

Zharikov, V. A., Ivanov, I. P., Omel'yanenko, B. I., Red'kin, A. F. and Yudintsev, S. V., 1987. Experimental study of the solubility of uraninite in granitic melts and fluid solutions at high pressures and temperatures. *International Geology Reviews*, **29**, 997-1004.